The Company of Biologists

RESEARCH ARTICLE

Single-cell imaging of the cell cycle reveals CDC25B-induced heterogeneity of G1 phase length in neural progenitor cells

Angie Molina[1], Frédéric Bonnet[1], Julie Pignolet[1], Valerie Lobjois[1], Sophie Bel-Vialar[1], Jacques Gautrais[2,*], Fabienne Pituello[1,*] and Eric Agius[1,*]

ABSTRACT

Although lengthening of the cell cycle and G1 phase is a generic feature of tissue maturation during development, the underlying mechanism remains poorly understood. Here, we develop a time-lapse imaging strategy to measure the four cell cycle phases in single chick neural progenitor cells in their endogenous environment. We show that neural progenitors are widely heterogeneous with respect to cell cycle length. This variability in duration is distributed over all phases of the cell cycle, with the G1 phase contributing the most. Within one cell cycle, each phase duration appears stochastic and independent except for a correlation between S and M phase duration. Lineage analysis indicates that the majority of daughter cells may have a longer G1 phase than mother cells, suggesting that, at each cell cycle, a mechanism lengthens the G1 phase. We identify that the CDC25B phosphatase known to regulate the G2/M transition indirectly increases the duration of the G1 phase, partly through delaying passage through the restriction point. We propose that CDC25B increases the heterogeneity of G1 phase length, revealing a previously undescribed mechanism of G1 lengthening that is associated with tissue development.

KEY WORDS: Neural stem cells, Neurogenesis, Proliferation, Differentiation, Single-cell imaging, Cell cycle kinetics, G1 phase, Retinoblastoma protein, CDC25 phosphatase, Neural tube, Vertebrate embryo, Chick

INTRODUCTION

Building a multicellular functional organ requires tight coordination between cell proliferation, cell fate specification and differentiation. In the developing nervous system, the spatiotemporal regulation of these processes is of key importance for the construction of functional neuronal circuits.

The cell cycle and components of the core cell cycle machinery have been shown to play a major role in the decision to proliferate or differentiate in embryonic stem cells, pluripotent stem cells and neural stem/progenitor cells (for reviews, see Hardwick et al., 2015; Liu et al., 2019). In numerous cell types, including neural

stem/progenitor cells, cell cycle and G1 phase lengthening is a general feature accompanying cell maturation and differentiation. During mammalian corticogenesis, in which consecutive types of progenitors have been described, lengthening of the G1 phase is associated with the transition from neural-stem-like apical progenitors (APs) to fate-restricted basal progenitors (BPs), and a shortening of the S phase with the transition from proliferative to neurogenic divisions (Arai et al., 2011). Reducing G1 phase length results in an inhibition of neurogenesis, whereas lengthening G1 duration promotes neurogenesis (Artegiani et al., 2011; Lange et al., 2009; Lim and Kaldis, 2012; Pilaz et al., 2009). In the developing spinal cord, different cell cycle kinetics are observed in discrete domains of neural progenitors (Molina and Pituello, 2017). Differentiation in the neural tube progresses from ventral to dorsal with time. When the maximum differentiation rate is reached in the ventral domain, neural progenitor cells (NPCs) exhibit a long G1 phase and short S and G2 phases (Kicheva et al., 2014; Peco et al., 2012; Saade et al., 2013). In contrast, at the same developmental stage, the dorsal domain is mainly composed of proliferative NPCs, which show a short G1 phase accompanied by long S and G2 phases (Kicheva et al., 2014; Peco et al., 2012; Saade et al., 2013). Overexpressing D-type cyclins in young neural tubes increases the pool of proliferating progenitors and induces a transient reduction of neuron production (Cao et al., 2008; Lacomme et al., 2012; Lobjois et al., 2008), whereas more mature NPCs will differentiate regardless of cyclin D overexpression and cell cycle exit (Lobjois et al., 2008). Shortening of the G2 phase associated with neurogenesis results from the upregulation of the phosphatase CDC25B, a regulator of the G2/M transition in NPCs. CDC25B promotes entry into mitosis by dephosphorylating its canonical substrates, the cyclin-dependent kinase (CDK) complexes. Surprisingly, for a positive regulator of the core cell cycle machinery, CDC25B has been shown to promote neurogenesis in mouse, chicken and *Xenopus* embryos (Gruber et al., 2011; Peco et al., 2012; Ueno et al., 2008). Gain- and loss-of-function experiments performed in chicken neural tubes show that CDC25B induces the conversion of proliferating NPCs into differentiating neurons by promoting neurogenic divisions (Bonnet et al., 2018). CDC25B acts using both CDK-independent and -dependent molecular mechanisms (Bonnet et al., 2018). A mathematical model has allowed us to hypothesize that CDC25B expression in neural progenitors progressively restricts the proliferative capacities of embryonic neural stem cells (Azaïs et al., 2019).

In all these studies, however, cell cycle analyses were performed at the population level. The durations of the cell cycle and individual phases were calculated from fixed tissues and correspond to estimated average lengths that consider the population of NPCs to be homogeneous (Nowakowski et al., 1989). Whether this neural progenitor population is homogeneous or heterogeneous relative to

[1]Unité de Biologie Moléculaire, Cellulaire et du Développement (MCD), Centre de Biologie Intégrative (CBI), Université de Toulouse, CNRS, Université Toulouse III – Paul Sabatier, Toulouse 31062 CEDEX 9, France. [2]Centre de Recherches sur la Cognition Animale (CRCA), Centre de Biologie Intégrative (CBI), Université de Toulouse, CNRS, Université Toulouse III – Paul Sabatier, Toulouse 31062 CEDEX 9, France.

*Authors for correspondence (jacques.gautrais@univ-tlse3.fr; fabienne.pituello@univ-tlse3.fr; eric.agius@univ-tlse3.fr)

F.B., 0000-0001-9334-8142; V.L., 0000-0003-2428-2084; J.G., 0000-0002-7002-9920; F.P., 0000-0002-6489-3886; E.A., 0000-0003-2123-9283

DEVELOPMENT

cell cycle kinetics is not well documented. An indication that the population of NPCs is indeed heterogeneous comes from a study where the total cell cycle (Tc) length was determined from the length of time measured between two cell divisions using time-lapse imaging in chick embryo slice cultures (Wilcock et al., 2007). These single-cell measurements reveal that the neural progenitor population displays a marked range of heterogeneity with respect to the Tc length, which ranges from 9 h to 28 h. Moreover, previous data indicate that the cell cycle lengths of cells dividing to produce two progenitors were shorter than that producing one neuron and one progenitor (Wilcock et al., 2007). However, how this Tc length heterogeneity translates into cell cycle kinetics and phase duration in single NPCs remains enigmatic.

The goal of this study was to determine the features of NPC cell cycle kinetics in their endogenous environment at the single-cell level and link these with tissue maturation and differentiation. We set up a methodology based on the use of fluorescent cell cycle reporters combined with high-resolution, single-cell, time-lapse imaging that allows single NPCs to be tracked within the developing neural tube over long periods to measure the duration of each phase of the cell cycle and to track the behavior of daughter cells after mitosis. We found that the lengths of the total cell cycle and all phases, except the M phase, are very heterogeneous. The duration of each phase can be described by a stochastic process in which the lengths of individual phases within a cell cycle are not coupled, except for a potential correlation between the M and S phases. The Tc length variation can be primarily explained by heterogeneity in the length of the G1 phase. Our analysis indicated that the majority of daughter cells may have a longer G1 phase than their mothers, suggesting that, gradually at each cell cycle, a mechanism lengthens the G1 phase. Finally, we showed that CDC25B increases cell-to-cell variability in G1 length, thereby increasing the G1 length in cells throughout the tissue, which is associated with tissue maturation and differentiation.

RESULTS
A single-cell, time-lapse imaging method to measure the four cell cycle phase lengths of NPCs within the neural tube
In order to determine the cell cycle kinetics of individual chick spinal NPCs, we developed a combination of biosensors to unambiguously detect the four phases of the cell cycle in living cells. We used the fluorescent ubiquitination-based cell cycle indicator (FUCCI) system, a set of fluorescent probes that enable visualization of cell cycle progression in living cells (Sakaue-Sawano et al., 2008) (see Materials and Methods for details). To visualize cells through the G1 phase, we used the zebrafish FUCCI G1 marker mKO2-zCdt1 (hereafter referred to as FUCCI G1) (Sugiyama et al., 2009). We verified its specificity in G1 by co-electroporating FUCCI G1 with FUCCI S/G2/M and quantifying, 24 h later, red, green and yellow cells corresponding to cells expressing FUCCI G1, FUCCI S/G2/M or both, respectively (Fig. 1A). We quantified 43.7% and 41.4% of cells expressing FUCCI G1 or FUCCI S/G2/M, respectively, and 14.9% expressing both markers, illustrating their transient overlap as already reported (Sakaue-Sawano et al., 2008). This result was comparable to previous quantifications performed by flow cytometry analysis (Bénazéraf et al., 2006). To time the G1/S transition more precisely and to identify the S/G2 transition, we used the NLS-eGFP-L2-PCNA protein (Leonhardt et al., 2000). Proliferating cell nuclear antigen (PCNA) is homogeneously distributed in the nucleus during the G1 and G2 phases. In early S phase, it is recruited at DNA replication sites that spread through the genome as the S phase

progresses. Indeed, the NLS-eGFP-L2-PCNA reporter allowed identification of S phase onset by its punctate distribution. A 30 min bromodeoxyuridine (BrdU) pulse confirmed that the punctate distribution observed with NLS-eGFP-L2-PCNA corresponded to S phase cells (Fig. 1B). As shown by flow cytometry analysis, electroporation of the NLS-eGFP-L2-PCNA or H2B-GFP constructs did not induce cell cycle disturbances (Fig. 1C). Moreover, the percentages (±s.e.m.) of cells that were positive for BrdU after a 30-min pulse were 41.44±0.043% after electroporation of the empty pCIG vector and 40.61±0.067% with the NLS-eGFP-L2-PCNA vector. Thus, our results showed that the PCNA reporter expression did not affect the percentage of cells in S phase. These results confirmed that NLS-eGFP-L2-PCNA overexpression does not interfere with cell cycle timing, as previously reported in zebrafish neuroepithelia (Leung et al., 2011) or the mouse cortex (Fousse et al., 2019). To perform proper mosaic expression through *in ovo* electroporation into two-day-old chick neural tubes, we constructed a plasmid allowing the co-expression of FUCCI G1 and NLS-eGFP-L2-PCNA (FUCCI G1-PCNA vector; Fig. 1D).

To analyze cell cycle parameters, embryonic day (E) 2 neural tubes were electroporated with the FUCCI G1-PCNA vector and sliced after 6 h of incubation. Thick slices of the brachial region of the embryos were placed in culture for 12 h prior to single-cell, real-time imaging experiments (Fig. 1E). This step of recovering was important to bypass the lengthening of the cell cycle and the delayed increase in the population of progenitors and neurons observed following slicing and culture (Fig. S1). Time-lapse imaging was performed for 48 h using a confocal microscope. It is important to stress that the use of 5% fetal calf serum in the culture medium and the use of spinning-disk confocal microscopy with attenuation of laser beam pulses to reduce phototoxicity (Boudreau et al., 2016) are essential for cell cycle measurements. Visualization of the FUCCI G1 and PCNA reporters by time-lapse imaging revealed that the different transitions in the cell cycle could be discriminated using nuclear expression and distribution of both proteins (Fig. 1F). The G1 phase was characterized by the co-expression of FUCCI G1 and NLS-eGFP-L2-PCNA with a uniform distribution in the nucleus. S-phase entry was detected by the appearance of the punctate pattern of the NLS-eGFP-L2-PCNA, which was associated with the gradual disappearance of the FUCCI G1 reporter. In the G2 phase, NLS-eGFP-L2-PCNA was evenly distributed inside the nucleus, and finally mitosis was detected by nuclear envelope breakdown that was accompanied by morphological changes in NPCs, which became rounded (Fig. 1F).

We thus designed a long-term, single-cell, time-lapse imaging methodology to measure the four cell cycle phase lengths accurately in individual cycling neural progenitors in their endogenous environment, the neural tube.

Neural progenitor nuclei display interkinetic nuclear movements in phase with the cell cycle and three distinct behaviors after mitosis
Imaging following electroporation of the FUCCI G1 and PCNA reporters in E2 [Hamburger–Hamilton stage (HH) 12] embryos showed cycling NPCs displaying G1 nuclei (orange) moving to the basal side, S-phase nuclei (green puncta) located in the basal half of the ventricular zone and G2 nuclei (green) moving back to the apical side where mitosis occurred (Fig. 2A; Movie 1). These characteristic positions indicate that in neuroepithelia the expression dynamics of the reporters is in accordance with the interkinetic nuclear movement occurring in phase with cell cycle progression (Fig. 2B) (Molina and Pituello, 2017). We also observed nuclei
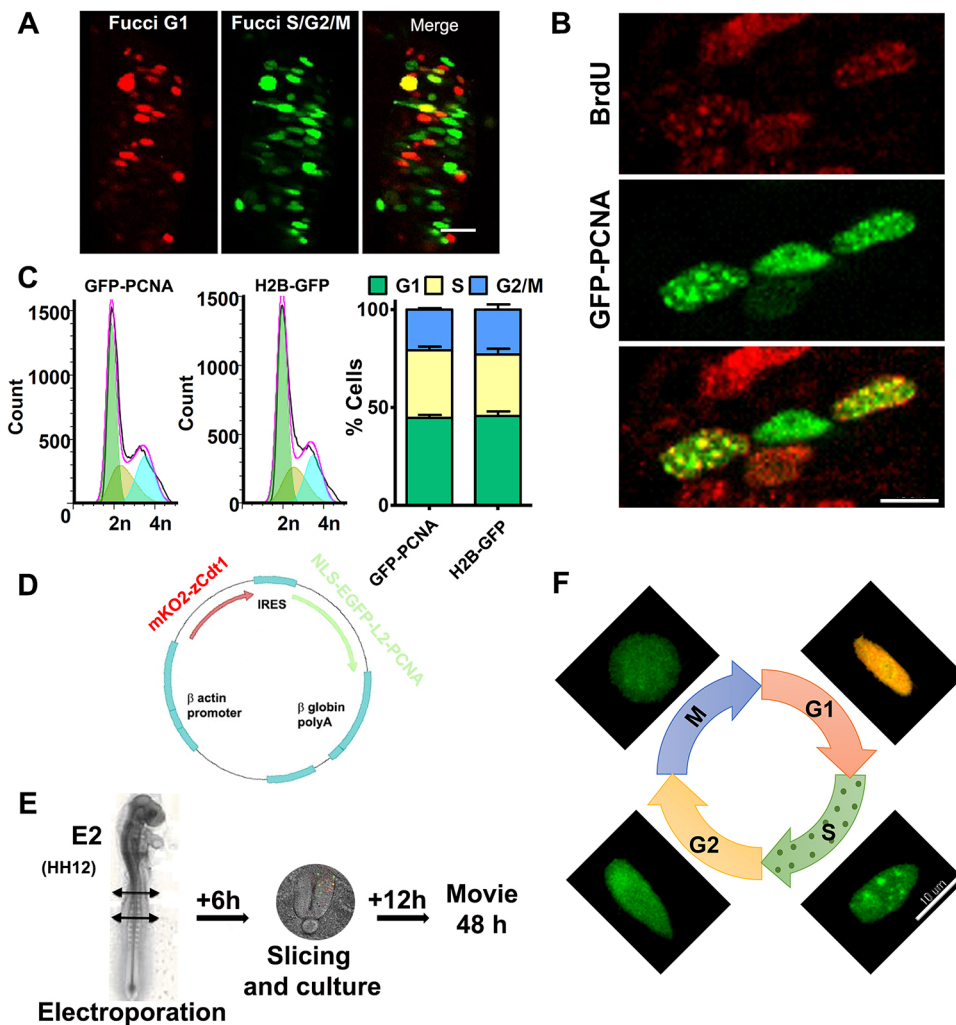
Fig. 1. FUCCI G1-PCNA biosensor marks the four cell cycle phases in chick neuroepithelia. (A) Representative cross-section of a chick neural tube expressing FUCCI G1 (red) and FUCCI S/G2/M (green) vectors. Scale bar: 50 μm. (B) Representative sections of chick embryonic spinal cord expressing GFP-PCNA (green) and stained after BrdU incorporation (red) to identify S phase cells. Scale bar: 10 μm. (C) Flow cytometry profiles of DNA content for NPCs electroporated with the GFP-PCNA- or H2B-GFP-expressing vectors (left panels). The histogram (right panel) corresponds to the deduced percentage of cells in G1 (44.7±1.4% compared with 45.7±2.4%, after GFP-PCNA or H2B-GFP vector electroporation, respectively), S (34.5±1.9% compared with 31.4±2.9%) and G2/M phases (20.8±0.7% compared with 22.9±2.6%). $n=3$, >30,000 cells per experiment. (D) Schematic representation of the mKO2-zCdt1-pIRES-NLS-EGFP-L2-PCNA reporter. (E) Scheme of the experimental protocol for time-lapse imaging. (F) Representative images of chick NPC nuclei through the cell cycle after electroporation of the FUCCI G1-PCNA vector. The four phases are identified by differential expression and distribution of FUCCI G1 (red) and GFP-PCNA (green) proteins. Scale bar: 10 μm. Images are representative of at least three experiments.

located on the basal side of the neural tube expressing brighter orange fluorescence (Fig. 2A), probably due to the accumulation of FUCCI G1 in differentiating G0 neurons after cell cycle exit, as previously described (Sakaue-Sawano et al., 2008).

Nuclear tracking after mitosis revealed three different behaviors in daughter cells (Fig. 2C): both daughter cells re-entered S phase (nuclei switch from FUCCI G1 expression to PCNA-punctate distribution), which clearly corresponded to the behavior of an NPC performing a proliferative division (PP) (with the progenitor cell P2 giving rise to P2.1 and P2.2, Fig. 2C); only one daughter cell re-entered the cell cycle, whereas the nucleus of the other remained orange and migrated to the basal side (P3 giving rise to P3.1 and N3.2); the nuclei of the two daughter cells remained orange and migrated to the basal side (P1 giving rise to N1.1 and N1.2). These orange nuclei that were located at the basal side and displayed a G1 phase longer than 1000 min (16 h 40 min) were never observed re-entering S phase. We thus assumed that these NPCs corresponded to cells primed to differentiate into neurons (Fig. 2A; Movie 1). To characterize these cells further, we performed immunostaining using an antibody against HuC/D, which marks differentiating neurons, after fixation of the sample at the end of the time-lapse experiment (Fig. 2D). Over the eight explants analyzed, we could identify 42 cells expressing the FUCCI G1 reporter that were located at the basal side, of which 35 were positive for the HuC/D markers (arrows in Fig. 2D). In addition, we could characterize long FUCCI G1 expression (more than

1000 min) for four cells located at the basal side, of which two were positive for HuC/D staining. Overall, these data suggest that the FUCCI G1-expressing cells that localized on the basal side of the explants and were characterized by a long FUCCI G1 expression (>1000 min) were probably differentiating neurons. The G1 lengths measured for these differentiating cells were excluded from our subsequent analyses. Hence, our strategy allowed us to track the nuclei of NPCs along the cell cycle and to determine, following mitosis, whether the daughter cells re-entered the cell cycle or not.

Cell cycle kinetics are highly heterogeneous in the population of NPCs

Using the methodology described previously, we measured the lengths of G1, S, G2 and M phases as well as Tc duration of individual NPCs within the neural tube of embryos electroporated at E2 (HH12) to ensure that we analyzed young proliferative progenitors (Fig. 3A). The mean durations measured using time lapse were 14 h 01 min for the Tc ($n=33$), 5 h 09 min for the G1 phase ($n=50$), 1 h 17 min ($n=54$) for the G2 phase and 31 min ($n=50$) for the M phase (Table 1). These data are in agreement with those determined from fixed embryos at equivalent developmental stages (Tc duration, 10 h and 16 h; G1, 4 h 30 min and 7 h; G2, 1 h 18 min and 2 h; M, 30 min) (Molina and Pituello, 2017). The S-phase length measured using time lapse (7 h 18 min±23 min, indicated as mean±s.e.m.) presented an average value higher than reported in fixed tissues [3 h 42 min (Peco et al., 2012)
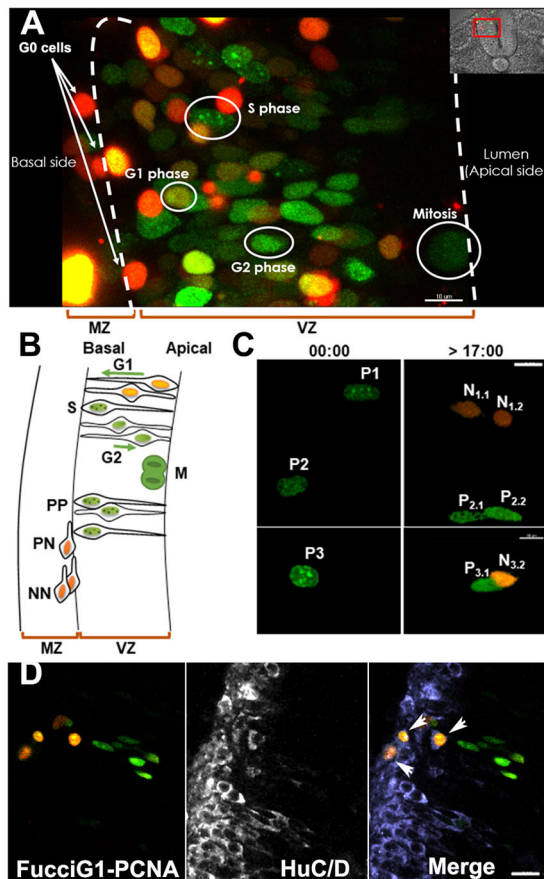
Fig. 2. Time-lapse observation of NPCs displaying three types of cell division after mitosis. (A) Still image from a time-lapse video showing the expression of the FUCCI G1-PCNA reporter in the nucleus of NPCs, which allows identification of the four cell cycle phases and the corresponding position within the neuroepithelium. The inset shows a bright-field image of the embryonic neural tube, and the red box indicates the approximate position of the main image. The dashed lines indicate the apical (right) and basal (left) limits of the neural tube. MZ, mantle zone. VZ, ventricular zone. Scale bar: 10 μm. (B) Schematic representation of the interkinetic nuclear movement and of the three modes of division (PP, PN and NN) occurring in the neural tube. (C) Still images from a time-lapse movie of a E2.25 culture showing the three modes of division observed in the spinal cord from progenitors P1 (NN), P2 (PP) and P3 (PN). Scale bars: 10 μm. (D) Images of an explant, immunostained for HuC/D after time-lapse imaging for 48 h. The FUCCI G1 expressing cells (orange) located at the basal side (arrows) are HuC/D positive. Scale bar: 20 μm. Images are representative of at least three experiments.

Fig. 3. Neural progenitor cell population is highly heterogeneous regarding the cell cycle. (A) Scatter dot-plot representing distributed lengths of the total cell cycle (Tc) and cell cycle phases for E2.25 embryonic spinal cord cells observed in live imaging (see numbers in Table 1). Each colored dot in the Tc column can be found in the cell cycle phase columns and corresponds to the same tracked nucleus. The empty dot corresponds to a cell with a G1 length of 1175 min (19 h 35 min) that did not enter S phase. (B-E) Survival curves to quantify absolute dispersion of G1 phase (B), G2 phase (C), S phase (D) and mitosis (E). The solid line corresponds to Kaplan–Meier estimates of survival and dashed lines to confidence intervals. (F) Variation partitioning showing how much variation of the Tc length is attributed to each phase. Asterisks represent values below 0.05. (G) Correlation analysis between S and M phases. Linear regression test. (H) Tc Survival curve. The black line corresponds to Kaplan–Meier estimate from data. The brown line corresponds to expected survival assuming a random sampling of cell cycle phase duration (see supplementary Materials and Methods). The red line corresponds to the survival curve obtained in Monte Carlo permutation of phase durations from the dataset. The blue curve corresponds to the case with G1 and S/G2/M phase lengths fully anti-correlated (see supplementary Materials and Methods).

and 5 h 54 min (Le Dreau et al., 2014)]. To test whether this increase in S-phase length was due to phototoxicity induced by time-lapse imaging, we analyzed expression of γH2AX, a marker for double-strand breaks induced by DNA damage (Fig. S2). No increase in γH2AX immunostaining was observed after time-lapse imaging, suggesting that S-phase lengthening did not primarily result from DNA damage. Thus, except for the S phase, which was slightly longer in our conditions, the mean duration determined from time-lapse experiments were consistent with those reported for fixed tissues at equivalent developmental stages.

At the single-cell level, our analyses showed a high degree of heterogeneity for Tc duration, as it ranged from 9 h55 min (595 min) to 24 h 45 min (1485 min) (Table 1; Fig. 3A), which was in accordance with previous time-lapse measurements reporting a total cell cycle length between 9 h and 28 h (see figure S2 in
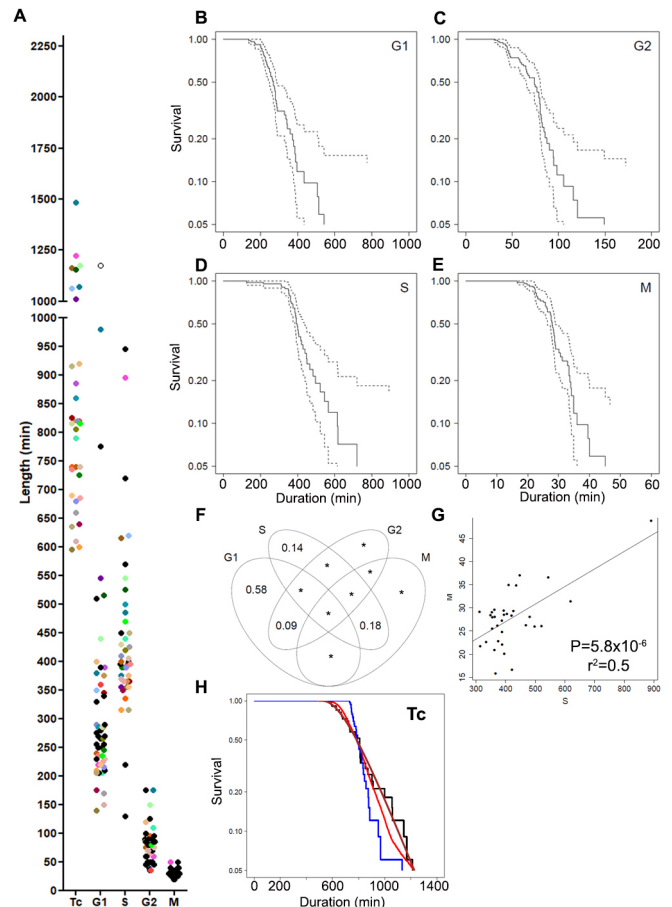
Wilcock et al., 2007). We tested whether NPCs undergoing very long cell cycles were also present in the neural tube of embryos developing *in ovo*. We performed cumulative 5-ethynyl-2′-deoxyuridine (EdU) experiments with EdU incorporation every 3 h for up to 27 h (Fig. S3). After 27 h of cumulative EdU incorporation, an average of 5±0.5% of NPCs containing EdU-negative nuclei were detected, indicative of NPCs displaying very long cell cycles or being quiescent. The use of the FUCCI G1 and PCNA reporters allowed us to determine how this heterogeneity was translated in relation to the different cell cycle phases (Table 1; Fig. 3A). G1-phase durations ranged from 2 h 20 min (140 min) to 16 h 20 min (980 min), S-phase durations from 2 h

Table 1. Column statistics of the cell cycle parameters

	Tc (min)	G1 (min)	S (min)	G2 (min)	M (min)
Control					
Mean	841	309	439	77	31
Median	815	268	395	75	30
Minimum	595	140	130	35	20
Maximum	1485	980	945	175	55
Minimal duration (D_m)	595	140	130	35	20
Exit time (τ)	246	169	309	42	11
Standard deviation	205	148	149	30	7
Number of values	33	50	41	54	50
Complete cycles					
Mean	841	307	423	80	30
Median	815	265	395	80	30
Minimum	595	140	315	35	20
Maximum	1485	980	895	175	50
Minimal duration (D_m)	584	139	311	33	20
Exit time (τ)	247	166	110	45	12
Standard deviation	205	156	108	29	6
Number of values	33	33	33	33	33
CDC25B					
Mean	1099	494	488	67	33
Median	1170	465	493	60	30
Minimum	595	160	120	10	20
Maximum	1585	930	855	170	45
Minimal duration (D_m)	595	160	120	10	20
Exit time (τ)	505	334	368	57	13
Standard deviation	266	202	147	34	6
Number of values	23	35	38	61	76
CDC25B$^{\Delta CDK}$					
Mean	809	310	416	79	31
Median	775	265	415	70	30
Minimum	515	130	105	30	20
Maximum	1200	840	930	170	45
Minimal duration (D_m)	509	130	105	30	20
Exit time (τ)	294	180	311	49	11
Standard deviation	170	144	116	33	5
Number of values	45	71	66	86	98

10 min (130 min) to 15 h 45 min (945 min), G2-phase durations from 35 min to 2 h 55 min (175 min) and mitosis durations from 20 min to 55 min. Since our data represented cell cycle phase durations before exiting the phase, we characterized the corresponding distributions using survival analysis (Fig. 3B-E). Each phase can be characterized by a minimal duration (D_{min}) and a mean exit time (τ), corresponding to the average duration spent in the phase after that minimal duration (Table 1; supplementary Materials and Methods, Section 1.2). The mean exit time reflects the slope of the survival function after minimal duration. The gentler the slope, the larger the mean exit time, and the more heterogeneous the distribution. Conversely, a very homogeneous population would display durations close to the minimal duration and a vanishing mean exit time. Hence, the mean exit time is a meaningful readout of the phase duration heterogeneity. The shapes of the survival curves and their mean exit times indicated that all the phases were heterogeneous (Table 1; Fig. 3B-D; supplementary Materials and Methods, Section 1.3). To exclude the possibility that this heterogeneity reflected the variation in cell cycle kinetics of NPCs depending on their position along the dorsoventral axis of the neural tube (see Introduction), we determined whether the range of heterogeneity observed for the G1 phase was linked with the position of the NPCs along the dorsoventral axis. Most of the cells that were analyzed for the G1 phase were located in the dorsal half of the spinal cord (Fig. S4A). In that domain, the range of heterogeneity was not dependent on the spatial localization of the

NPCs. Notably, the range of heterogeneity was also independent of the time elapsed since the beginning of the recording (Fig. S4B).

To identify the quantitative relationships between phases, we performed further analyses using the subset of 33 cells for which a complete cell cycle was monitored (Fig. 3F; Table 1; supplementary Materials and Methods, Section 2). In this sample, NPCs spent 37% of the cell cycle in G1, 52% in S phase, 9% in G2 and 4% in mitosis, in accordance with previous data obtained on fixed samples (Saade et al., 2013). Variation partitioning analysis showed that 58% of Tc length variation was due to the range of heterogeneity in G1 length alone (Fig. 3F; supplementary Materials and Methods, Section 2.2). We then tested correlations within each pair of phases (supplementary Materials and Methods, Section 2.3) and found no patterns, except for an unexpected significant positive correlation between S and M phase durations (Fig. 3G; supplementary Materials and Methods, Section 2.3). No significant correlation was identified between G1 length and S/G2/M lengths (supplementary Materials and Methods, Section 2.3.1), suggesting that phase durations are independent from each other within the same cell cycle.

To investigate further the likelihood of the hypothesis of the independent nature of phase durations, we examined how this hypothesis would correctly predict the observed distribution of Tc length. To build this prediction analytically, the survival curves of exit times for each phase in the subset were approximated by a simple exponential decay (red line in Fig. S5, supplementary Materials and Methods, Section 2.5.1), which would correspond to a model in which cell cycle phase exit is a stochastic process driven by a constant probability per unit time to exit once the minimal duration has passed for that phase. Under such a hypothesis, for each phase, the duration can be described by a stochastic exit process D defined as $D \sim D_{min} + E$, where $E \sim \text{Exp}(\tau)$ is an exponentially distributed variable with mean time τ.

Under this hypothesis, the complete cell cycle duration would then obey a stochastic process D_c defined simply as: $D_c = D_{G1} + D_S + D_{G2} + D_M$, i.e. the total duration would just result from the sum of four independent exit processes as defined above, each with its corresponding parameters for minimal duration and mean time before phase exit (see supplementary Materials and Methods, Section 2.4.1 for the analytical expression for D_c distribution under this hypothesis). We found that the predicted survival function for D_c under this hypothesis (brown curve in Fig. 3H) is actually compatible with the observed one (black line in Fig. 3H), suggesting that the phases are independent. This was confirmed using Monte Carlo permutation, a random sampling technique (red line in Fig. 3H; supplementary Materials and Methods, Sections 2.4.2 and 2.6). The experimental distribution appeared to be compatible with random mixing of phase durations ($P=0.84$, two-samples Kolmogorov–Smirnov goodness-of-fit test). The model shows that the phase lengths of the four phases can be considered to be independent. To challenge phase duration uncoupling, we considered the opposite hypothesis that the phases are fully anti-correlated, i.e. ascending ordered G1 lengths are paired with descending ordered S/G2/M lengths. The resulting Tc lengths are illustrated (blue line in Fig. 3H; supplementary Materials and Methods, Section 2.4.3). In this case, the range of heterogeneity of Tc length was greatly reduced compared with the experimental value, and not compatible with the experimental distribution ($P=0.0048$, two-sample Kolmogorov–Smirnov goodness-of-fit test).

Together, these data show that the spinal NPC population is highly heterogeneous with respect to the distribution of cycling time. The duration of each phase seems to be largely stochastic and

DEVELOPMENT

independent within one cell cycle, suggesting the absence of coupling between phase durations. The phase mostly responsible for Tc length variation was the G1 phase.

CDC25B activity increases the range of heterogeneity in G1 phase duration

As mentioned above, single-cell analysis revealed a high degree of heterogeneity in G1 phase length. One hypothesis is that a mechanism intrinsic to the cell cycle induces a lengthening of the G1 phase in individual proliferative NPCs. Recently, we showed that CDC25B is involved in NPC maturation (Bonnet et al., 2018; Peco et al., 2012). We then tested the impact of a gain of function of the CDC25B phosphatase on cell cycle kinetics using our time-lapse strategy. We used a vector that reproduces the iterated cell cycle-regulated expression of CDC25B during the S and G2 phases (Bonnet et al., 2018; Körner et al., 2001). As observed in the control condition, cell cycle kinetics were also highly heterogeneous after CDC25B gain of function (Fig. 4A; Table 1). As expected from its role in G2/M transition (Bonnet et al., 2018; Peco et al., 2012), CDC25B gain of function induced a significant decrease (12.7%) of the mean length of the G2 phase (P=0.029, Fig. 4C; Table 1). The mean Tc length increase of 32.8% (P=0.004 compared with control; Table 1) resulted from a slight increase in the mean lengths of the S and M phases (12.4% and 5.5%, respectively) and from a drastic

59.9% increase in the mean G1 phase length (P<0.0001 compared with control; Fig. 4C; Table 1). Survival curves and the corresponding frequency distribution histograms were then compared to analyze the dispersion of the data in various conditions (Fig. 4D-H). The 4 h 16 min (256 min) increase observed in mean Tc length induced by CDC25B was associated with an increase of the exit time (from 247 to 503 min), without modification of the minimal duration (583 min versus 586 min, Table 1). This clearly indicated that CDC25B increased the dispersion of the dataset. The pace at which CDC25B-expressing cells exit the cell cycle was about three times slower (hazard ratio of 0.35) than that of control cells (red curve compared with black curve in Fig. 4D; supplementary Materials and Methods, Section 3.1). Phase-by-phase comparison showed that CDC25B induced a significant increase in both G1 and S phase distributions compared with those in the control (compare red and black curves in Fig. 4E-H). Variation partitioning revealed that about 50% of Tc length variation was explained by the heterogeneity in G1 length alone, and 20% by S phase alone (Fig. S6A, supplementary Materials and Methods, Section 2.2). Minimal durations did not appear altered, but rather exit times were affected, with a mean lengthening of 2 h 45 min (165 min) and 1 h 02 min (62 min), and 0.41 and 0.65 hazard ratios for G1 and S phases, respectively (supplementary Materials and Methods, Sections 3.2 and 3.3).
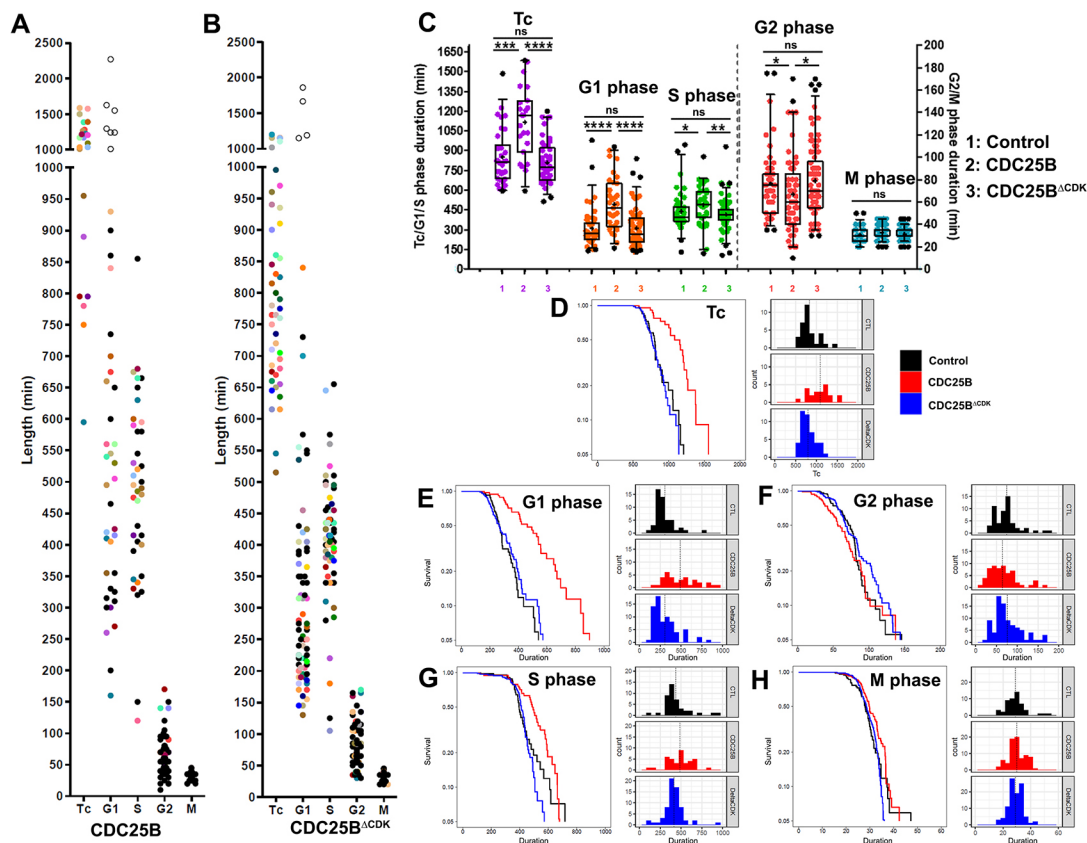

Fig. 4. CDC25B gain of function increases heterogeneity in G1 phase length. (A,B) Scatter dot plot representing distributed lengths of the total cell cycle (Tc) and cell cycle phases measured during live imaging of E2.25 cultures for cells electroporated with the CDC25B (A) or CDC25B^{ΔCDK} (B) constructs. Each colored dot in the Tc column can be found in the cell cycle phase columns and corresponds to the same tracked nucleus. Empty dots represent cells with a G1 length longer than 1000 min (16 h 40 min). (C) Box and whisker plots (5th-95th percentiles) illustrating the comparison of Tc and cell cycle phase lengths for the control condition (1) and CDC25B (2) and CDC25B^{ΔCDK} (3) gain of function. The top and the bottom of each box indicate upper and lower quartiles, respectively; the horizontal line represents the median and the cross indicates the mean value. ns, not significant; *P<0.05; **P<0.01; ***P<0.001; ****P<0.0001; Mann–Whitney test. (D-H) Survival curves and histograms comparing control (CTL, black), CDC25B (red) and CDC25B^{ΔCDK} (DeltaCDK, blue) conditions for the Tc (D), G1 (E), G2 (F), S (G) and M (H) phases. The vertical dotted line in histograms reports the average of the distribution.

No significant effect was found on the survival distributions for the G2 or M phases (Fig. 4F-H; Table 1; supplementary Materials and Methods, Sections 3.4 and 3.5). We note that the mean G2 length shortening appeared to be associated with a shorter minimal duration, with no effect upon its heterogeneity (shape of the curve in Fig. 4F; Table 1). Correlation analysis between phase lengths showed that the phases were uncoupled (supplementary Materials and Methods, Section 2.3.2). Monte Carlo permutations of the dataset (10^4 samples) suggest that the distribution of Tc length was compatible with independent cell cycle phase durations (compare red and black curves in Fig. S6B; supplementary Materials and Methods, Section 2.6.2). However, no heritable correlation between the G2 phase lengths in mother cells and the G1 phase lengths in daughter cells could be detected (Fig. S6C,D).

All these results show that in a context in which each cell cycle phase duration is stochastic and independent, CDC25B enhanced the range of heterogeneity in G1 phase duration, leading to an increase in the mean values of G1 and Tc durations at the population level.

CDC25B gain of function in G2 phase delays the passage through the restriction point in NPCs

We previously showed that part of CDC25B function in neurogenesis does not require interaction with its canonical substrate CDK1 (Bonnet et al., 2018). We then tested whether the CDC25B-CDK1 interaction played a role in regulating G1 phase length. Electroporation of the CDC25B$^{\Delta CDK}$ construct, generating a CDC25B mutant that is unable to interact with CDK, resulted in four cells with a G1>1000 min (open circles in Fig. 4B) in line with its neurogenic effect. In our experiments, the expression of CDC25B$^{\Delta CDK}$ did not significantly change cell cycle phase lengths and dispersion compared with the control conditions (Fig. 4B-H; Table 1; supplementary Materials and Methods, Section 3). Thus, the G1 phase length modification induced by CDC25B is dependent on its interaction with CDK, indicating that it might be related to the function of CDC25B in the cell cycle.

The next question was then to determine whether CDC25B acts directly in G1. To mis-express CDC25B, we used the mouse cell cycle-dependent CDC25B cis-regulatory element (ccRE) that reproduces the cell cycle-regulated transcription of CDC25B (Bonnet et al., 2018; Körner et al., 2001). To determine the precise timing of expression of the ectopic CDC25B protein during the cell cycle, we co-electroporated an eGFP-CDC25B-expressing vector and the pCS2:H2B-RFP vector in NPCs. We showed that the eGFP-CDC25B fusion protein was detected in only 6.6±0.8% of the electroporated population, which was identified using H2B-RFP fluorescence (Fig. S7B,D). To determine whether some of the eGFP-CDC25B-positive cells were in G1, we co-electroporated the eGFP-CDC25B-expressing vector with FUCCI G1. We did not detect co-expression of the eGFP-CDC25B fusion protein with FUCCI G1 (Fig. S7C,D), suggesting that the chimeric protein is not present during the G1 phase, but rather in S/G2/M. The very limited periodic expression induced by the promoter and the intrinsic instability of CDC25B, which is actively degraded at the end of mitosis, probably precludes protein expression during the G1 phase. These data are in accordance with the absence of expression of CDC25B in G1, which has previously been described for synchronized cells in culture (Astuti et al., 2010). Thus, CDC25B expressed in S/G2/M indirectly increases G1 phase length in NPCs.

One crucial event during the G1 phase is the passage through the restriction point, following which cells are committed to enter S phase. The passage through the restriction point depends on the phosphorylation of the retinoblastoma protein (Rb), which is used

as a marker for cell cycle commitment. Recent studies involving epithelial cell lines have shown that, in some cells, Rb becomes dephosphorylated as they exit mitosis, and these cells can stay in the G1 state for variable durations before re-entering the cell cycle, whereas other cells exit mitosis with a hyperphosphorylated Rb and are immediately committed to the next cell cycle (Gookin et al., 2017; Spencer et al., 2013). Moreover, it has been suggested that the timing of restriction point crossing in G1 depends on the signaling history of the mother cell in the previous cell cycle, and particularly on the accumulation of regulators in the previous G2 phase (Min et al., 2020; Moser et al., 2018; Naetar et al., 2014). Considering that CDC25B is expressed in G2, we hypothesized that the G1 lengthening induced by CDC25B in proliferative NPCs could be the consequence of a delay of the restriction point passage. Immunostaining for phospho-Rb (S807/S811) is classically used to analyze crossing of the restriction point (Moser et al., 2018; Spencer et al., 2013). Our goal was then to identify NPCs containing dephosphorylated Rb in G1 (phospho-Rb-negative cells) as a readout of the nuclei that are in the G1 phase before restriction point passage. To restrict quantification to NPCs and avoid counting young neurons, which are expected to be phospho-Rb-negative, we combined immunostaining for phospho-Rb with markers of young neurons (Tuj1/Tubb3 or HuC/D). We clearly identified phospho-Rb- and Tuj1- or HuC/D-negative cells in the ventricular zone (Fig. 5). We also verified that phospho-Rb- and HuC/D-negative cells were in G1 by using our FUCCI G1 and PCNA reporters. We then quantified the percentage of phospho-Rb-negative NPCs after electroporation of the CDC25B construct (Fig. 5). In the dorsal spinal cord, 12.2±0.8% of control electroporated cells were phospho-Rb and Tuj1 negative. This percentage increased to 19.9±1.3% for cells electroporated with the CDC25B construct, but was not affected in cells electroporated with the CDC25B$^{\Delta CDK}$ construct (10.9±0.7%). These data showing that CDC25B increases the proportion of NPCs displaying dephosphorylated Rb in G1 suggest that it could thereby delay the passage through the restriction point and lengthen the G1 phase.

G1 phase lengthening occurs within the NPC lineage

We then wanted to determine whether there was a link between the mode of division of NPCs and the length of the G1 phase. Three modes of division are observed in the developing spinal cord: proliferative, in which a progenitor (P) gives rise to two progenitors (PP), and neurogenic, in which a progenitor gives rise to either one progenitor and one neuron (PN) or to two neurons (NN) (Saade et al., 2013). In our analysis, daughter cells were considered to be proliferative progenitors (P) when, after mitosis, they entered S phase (i.e. they displayed the punctate distribution of the PCNA reporter). A cell that stopped cycling (i.e. in which FUCCI G1 expression was longer than 1000 min) was considered to be a committed neuron and referred to as N. We characterized 32, 27 and 48 divisions of progenitors in control, CDC25B and CDC25B$^{\Delta CDK}$ conditions, respectively (Table 2). In these dividing cells, the G1 phase lengths of 14 out of 20 mother cells undergoing PP divisions were below 4 h (240 min) (Fig. S8A). Notably, six out of 20 cells undergoing PP division with G1 phase lengths above 5 h (300 min) could still be observed (Fig. S8A), suggesting that a long G1 phase does not preclude proliferative division. Heterogeneity in G1 phase length was also observed for the few neurogenic divisions that we were able to analyze (green points in Fig. S8A). In these conditions, no clear correlation was observed between S-phase duration and the mode of division (Fig. S8B). However, the small amounts of data were only indicative and do not allow us to draw a clear conclusion.
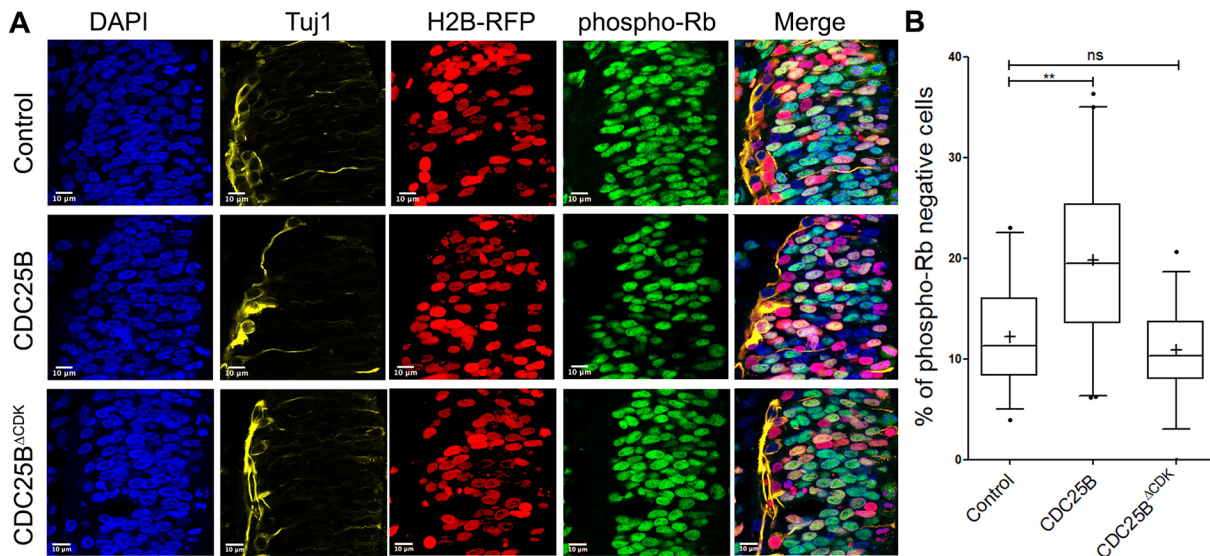
Fig. 5. CDC25B but not CDC25B$^{\Delta CDK}$ gain of function reduces the percentage of phosphorylated retinoblastoma protein. (A) Representative cross-sections of HH17 chick spinal cord, 24 h after co-electroporating pCS:H2B-RFP and control, CDC25B or CDC25B$^{\Delta CDK}$ vectors. Sections are stained with a DNA marker (DAPI), a neuronal marker (Tuj1) and the phospho-Rb marker. Images are representative of three experiments. Scale bars: 10 µm. (B) Box and whisker plots (5th-95th percentiles) illustrating the comparison of the proportion of phospho-Rb-negative cells in the electroporated population. The top and the bottom of each box indicate upper and lower quartiles, respectively; the horizontal line represents the median and the cross indicates the mean value. **$P \leq 0.001$, ns, non-significant; Mann–Whitney test. Data are from three independent experiments.

We then took advantage of our single-cell tracking method to decipher how cell cycle dynamics evolve with time within a cell lineage. One example is shown in Fig. 6A and an explicative scheme shown in Fig. 6B. We characterized the entire cell cycle of a mother cell and followed the cell cycles of the daughter cells. Cell-by-cell lineage analyses revealed that mother cells (MCs) and daughter cells (DCs) displayed differential behaviors in terms of G1 phase lengths. In control conditions, 12 out of 16 DCs presented a longer G1 phase than their MCs. To strengthen these data, and given the difficulty of carrying out cell lineages, we performed the same type of analyses in the CDC25B$^{\Delta CDK}$ gain-of-function experiments, since there were no modifications of the cell cycle phases in the CDC25B$^{\Delta CDK}$ condition compared with the control condition (Fig. 4C). In the CDC25B$^{\Delta CDK}$ condition, 25 out of 33 DCs exhibited a longer G1 phase (Fig. 6C). The average G1 phase length increased from 257 ± 28 min to 309 ± 38 min and from 249 ± 28 min to 315 ± 29 min in control and CDC25B$^{\Delta CDK}$ conditions, respectively. Among these DCs, few exhibited FUCCI G1 expression longer than 1000 min, corresponding to cells committed to neuronal differentiation (one and three cells in control and CDC25B$^{\Delta CDK}$ conditions, respectively; Fig. 6C). To analyze further the evolution of G1 phase length, we plotted the G1 phase lengths for mother and daughter cells (Fig. 6D). The datapoints were mostly located above the bisector between the axes (dotted line, Fig. 6D), suggesting that the G1 length of a DC was often longer than the G1 length of its

MC. We tested the hypothesis that the probability of finding a DC with G1 length longer than its MC was greater than 0.5 using binomial tests. We obtained the following 95% confidence interval (CI) and P-values: control, [0.52; 1.00], $P=0.04$; CDC25B, [0.19; 1.00], $P=0.5$ (not significant, sample too small); and CDC25B$^{\Delta CDK}$, [0.60; 1.00], $P=0.0023$. This reinforced the hypothesis that DCs might display longer G1 phases more often than their MCs. Interestingly, this effect did not appear to depend upon the MC G1 length.

DISCUSSION
In this study, we established a live-imaging strategy that allowed us to follow the behavior of single NPCs over a duration of 48 h in their endogenous environment. We showed that the cell cycle duration and, more interestingly, the lengths of each phase were very heterogeneous, and with no apparent links between phase lengths within one cell cycle or between the G2 phase lengths of mother cells and the G1 phase lengths of daughter cells. However, we found that G1 phase length increased with cell generations and was the phase that contributed mainly to total cell cycle lengthening. Furthermore, we showed that expression of the G2/M regulator CDC25B enhanced the percentage of non-phosphorylated Rb nuclei and the range of heterogeneity in G1 length in NPCs, contributing to neural tissue maturation (Fig. 7).

The lengthening of the cell cycle results from an enhanced range of heterogeneity
We showed that the total cell cycle length exhibited a high degree of heterogeneity, ranging from 9 h 55 min to 24 h 45 min without apparent patterns or coupling between the phase length, except for a link between the S- and M-phase durations. Such a heterogeneity of the total cell cycle length has already been observed using time-lapse imaging in neural stem/progenitor cells, including spinal NPCs (Wilcock et al., 2007), mouse neural stem cells in culture (Roccio et al., 2013) and human nervous system primary tissues and organoids (Subramanian et al., 2017). We demonstrate here that the

Table 2. Percentage of the modes of division observed during time lapse under various conditions

Mode of division	Control (32)	CDC25B (27)	CDC25B$^{\Delta CDK}$ (48)
PP	59.4%	40.7%	58.3%
PN	3.1%	14.8%	2.1%
NN	3.1%	14.8%	8.3%
P?*	34.4%	25.9%	25.0%
N?*	0%	3.7%	6.3%

*P? and N? correspond to cells for which only one daughter cell could be identified.
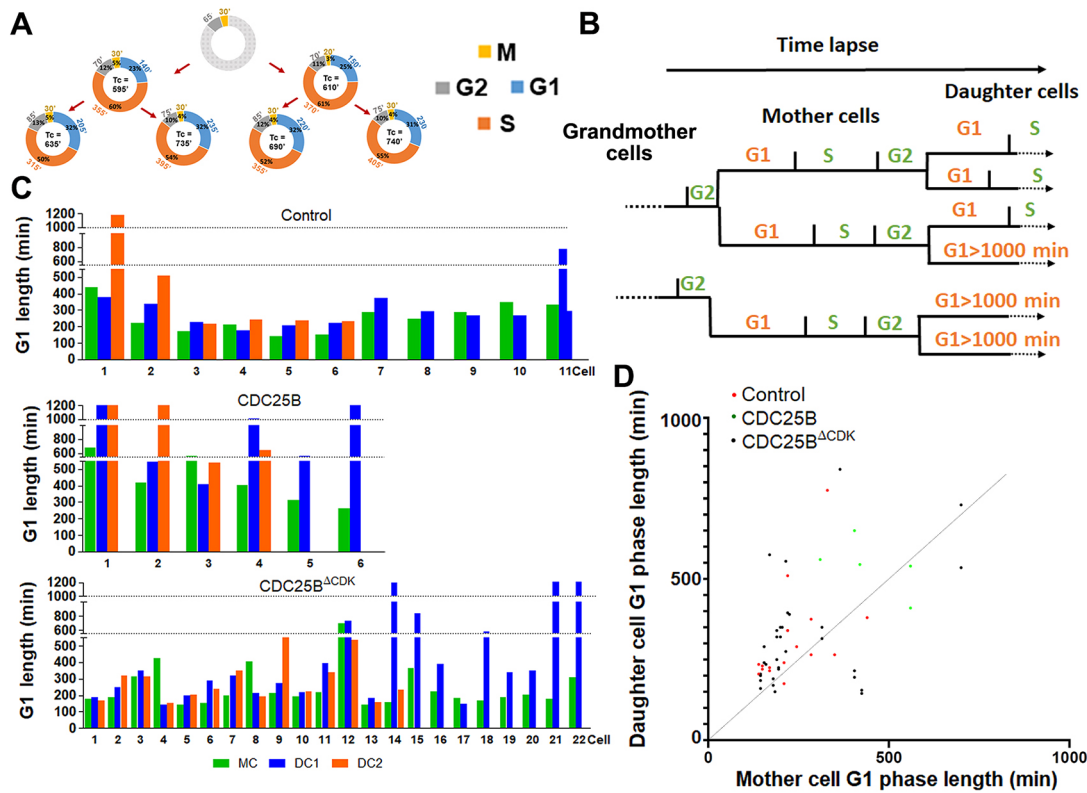
DEVELOPMENT

Fig. 6. G1 phase tends to lengthen in daughter cells. (A) Schematic representation of nuclei tracking over two generations of proliferating NPCs. Total cell cycle (Tc) and cell cycle phase lengths are calculated from time-lapse images. The proportion of each phase in the whole cell cycle is represented inside the circles. Light grey represents undetermined values. (B) Schematic representation of lineage tracking over two generations of proliferating NPCs. The entire cell cycle of mother and daughter cells was observed, and the cell cycle stages of the daughter cells allows the differentiation of cells re-entering the cycle from those stopping in G1 (G1>1000 min). (C) Bar graphs illustrating G1 phase lengths of mother cells (MC, green) and daughter cells (DC, visualized in blue and orange as DC1 and DC2, respectively) for NPCs in control (top), CDC25B (middle) or CDC25B$^{\Delta CDK}$ (bottom) conditions. (D) From data represented in C, only pairs of MCs and DCs where DC G1 length was <1000 min were analyzed. Each DC G1 length is reported in ordinates at abscissa of the corresponding MC G1 phase length. In 12 out of 16 cells for the control (red), three out of five for CDC25B (green) and 25 out of 33 for CDC25B$^{\Delta CDK}$ (black) conditions, DC G1 length is longer than its MC G1 length. Dotted line represents the bisector between the axes.

range of heterogeneity of the total cell cycle length is the result of cumulative heterogeneity observed for each phase of the cell cycle, the phase that contributes the most to the total cell cycle variability being the G1 phase. In our analysis, we observed a correlation

Fig. 7. Schematic representation of the evolution of neural progenitor cell cycle kinetics. Each cell cycle is represented by a colored line. The orange and blue cells represent proliferative progenitors and progenitors in a more mature state, respectively. In early stages, the population of neural progenitors display heterogeneous cell cycles. At the onset of neurogenesis, the cyclic expression of CDC25B (grey) leads to an increase in the heterogeneity in G1 phase length.

between the M and S phases. To our knowledge, no link has been made between M- and S-phase durations, but one between the duration of the M phase and total cell cycle length has been observed by Araujo et al. (2016), who showed that a modification of the CDK1-cyclin B1 positive feedback loop couples variability in cell cycle length to the duration of mitosis.

Previously, analyses of cell cycle parameters were performed using fixed tissues, with the assumption that neural stem cells are a homogenous population of asynchronous proliferating cells. Using this approximation, these analyses showed that, as the developmental time progressed, the proliferation rate of neural progenitors decreased and their cell cycle lengthened (Kicheva et al., 2014; Kicheva and Briscoe, 2015; Molina and Pituello, 2017). This evolution of the cell cycle length, which is most often associated with differentiation, was also observed in various stem cell types (Dalton, 2015; Julian et al., 2016). If the population of NPCs was homogeneous, an increase of the mean cell cycle duration with time would correspond to an increase of the cell cycle duration in each individual NPC. Instead, we observed that the population of NPCs was heterogeneous in terms of cell cycle length and, in this case, the increase in the mean cell cycle duration occurring with time correlated with an increase in the range of heterogeneity. To test possible relationships between the four phase lengths, we developed a mathematical model in which the durations of individual cell cycle phases were stochastic and independent of

9

each other. The experimental and theoretical Tc survival curves displayed a very similar pattern, suggesting that, indeed, cell cycle phase durations were stochastic and independent. It did not mean that the phases were independent, as cell divisions should not occur unless DNA is properly replicated, for example, but that their duration was independent. One hypothesis is that allowing such stochastic variations at the single-cell level is cost efficient for the population, which does not need to control strictly the cell cycle kinetics of each single cell and, thereby, is probably more robust. To our knowledge, it is the first time that this has been observed for progenitors within their endogenous environment. These results are reminiscent of experimental data and modeling obtained using various cell lines in culture. In NIH3T3 cell cultures, lengthening one phase does not imply lengthening other phases, suggesting that the durations of cell cycle phases can be considered to be independent (Mura et al., 2019). This has also been observed for three independent human cell lines, in which the cell cycle corresponds to a series of uncoupled memoryless phases (Chao et al., 2019).

Identification of a mechanism to generate the CDC25B-dependent increase of heterogeneity in G1 and cell cycle length

Time-lapse analysis showed that even if all cell cycle phase lengths were heterogeneous, the S and G1 phases contributed the most to the range of heterogeneity in total cell cycle length, and that G1 was the most affected phase upon development. Heterogeneity in G1 phase length has already been observed in neuroepithelial cells in culture (Roccio et al., 2013), in human embryonic stem cells in culture (Jang et al., 2019) and in mouse epidermal stem cells *in vivo* (Xie and Skotheim, 2020). Here, we identified a previously unidentified actor that triggers cell-to-cell heterogeneity in G1 phase length in NPCs, the phosphatase CDC25B. Electroporation of any expression vector into chick neural tube led to mosaic expression. We therefore considered whether the heterogeneity in G1 length could be caused by the methods we used. If cells expressing different quantities of plasmid have different responses depending on the dose received, the variation observed should be similar in all phases. To address this, we used the exit time (τ) in Table 1 as a readout of the heterogeneity range. Comparison of the exit time in control versus CDC25B conditions showed an increase of 18% in M, 19% in S, 36% in G2 and 97% in G1 phase. Moreover, we did not detect the presence of the ectopic protein in G1. This strongly suggests that the increase in the range of heterogeneity in G1 length cannot be solely linked to the mosaic expression induced by electroporation, but that it was mainly caused by the activity of CDC25B.

We have shown that the expression of CDC25B in NPCs correlates spatially and temporally with neurogenesis (Agius et al., 2015; Bonnet et al., 2018; Peco et al., 2012). Gain- and loss-of-function experiments revealed that CDC25B promotes neurogenic divisions (Bonnet et al., 2018; Peco et al., 2012) and acts as a maturing factor, reducing the proliferative capacities of the NPCs (Azaïs et al., 2019; Bonnet et al., 2018). Both CDK-dependent and CDK-independent activities of CDC25B are required for its full neurogenic activity. Here, we show that CDC25B induces a lengthening of the G1 phase duration in a CDK-dependent manner. The effect on G1 is probably indirect, as we did not detect the GFP-CDC25B fusion protein in G1. CDC25B gain of function induced a CDK-dependent increase of the percentage of NPCs with the unphosphorylated retinoblastoma protein. This result suggests that CDC25B could, at least indirectly, have an impact on the timing of restriction point crossing in NPCs. Indeed, one of the major mechanisms controlling the progression in the G1 phase is the restriction point that divides the G1 phase into two parts, early G1 that lasts from mitosis to the restriction point and the late G1 period after passage through the restriction point and entry into S phase. Spencer and colleagues working on epithelial cells in culture have shown that restriction point crossing might occur after mitotic exit either directly or after a variable amount of time spent in G1 (Gookin et al., 2017; Spencer et al., 2013). Interestingly, the same group showed that the timing of restriction point crossing during G1 is associated with the level of cyclin D protein synthesis that occurs in G2 (Min et al., 2020). CDC25B shortens the G2 phase and could therefore hinder the synthesis of cyclin D, thereby delaying the restriction point crossing by reducing the level of Rb phosphorylation in daughter cells after mitosis. One possibility is that NPCs that do not express CDC25B display longer G2 phases and cross the restriction point early after mitotic exit, whereas those expressing CDC25B exhibit shorter G2 phases and have a variable restriction point crossing time. CDC25B-mediated control of restriction point crossing could therefore contribute, at least partly, to heterogeneity in G1 phase length. Deciphering this hypothesis in our model system is challenging and will require further investigations, including single-cell measurement of the time spent in G1 prior to restriction point crossing.

In CDC25B gain-of-function experiments, the total cell cycle duration was increased at least partly as a consequence of G1 phase lengthening. In our recent theoretical studies (Azaïs et al., 2019), we proposed that CDC25B expression in neural progenitors progressively restricts proliferative capacities of the cell. We propose that CDC25B reiteration at each cell cycle indirectly increases the range of heterogeneity of the G1 phase length, increasing the cell cycle duration, which is associated with differentiation and leading to tissue maturation (Fig. 7). Such a mechanism is likely to be applicable to other developing organs or tissues, as well as to stem cells, including human stem cells.

MATERIALS AND METHODS
Embryos
Fertile hens' eggs from *Gallus gallus* obtained from a local supplier (Couvoirs du Languedoc) were incubated at 38°C in a humidified incubator to yield embryos appropriately staged (Hamburger and Hamilton, 1992).

DNA constructs and *in ovo* electroporation
In ovo electroporation experiments were performed using 1.5- to 2-day-old chicken embryos as described previously (Peco et al., 2012). In the present study, we used FUCCI (Sakaue-Sawano et al., 2008), which utilizes the cell cycle phase-dependent degradation of the replication licensing factor Cdt1 (FUCCI G1), which is degraded during S/G2/M, and Geminin (FUCCI S/G2/M), which is degraded during G1. Both were cloned in fusion with distinct fluorescent proteins. A fusion protein consisting of Cdt1 and an orange fluorescent protein (mKO2) serves as an indicator of the G1 phase, and a fusion protein consisting of Geminin and a green fluorescent protein allows visualization of the S, G2 and M phases. Rapid degradation of both fluorescent chimeric proteins, mediated by the ubiquitin-proteasome system, provide a visual marker to distinguish cells in the G1 or S/G2/M phases of the cell cycle. To visualize cells through the G1 phase, we used the zebrafish FUCCI G1 marker mKO2-zCdt1 (a gift from Atsushi Miyawaki, RIKEN Center for Brain Science, Saitama, Japan) (Sugiyama et al., 2009) instead of the human Cdt1, which persists in all cell cycle phases in chick NPCs, suggesting that it is not properly degraded. To detect the four phases of the cell cycle, we developed the mKO2-zCdt1-pIRES-NLS-eGFP-L2-PCNA biosensor. In the pCAG plasmid (derived from pCAG-luciferase, Addgene #55764), we inserted the FUCCI G1 probe derived from zebrafish Cdt1 (Sugiyama et al., 2009) and, downstream of the internal ribosome

entry site (IRES) element, PCNA tagged with eGFP and a nuclear localization signal (NLS) (Leonhardt et al., 2000). This FUCCI G1-PCNA vector was transfected at 0.5 µg/µl by *in ovo* electroporation in chicken neural tubes to reproducibly obtain a high degree of mosaicism compatible with lineage tracing (Wilcock et al., 2007). The hCDC25B or hCDC25B$^{\Delta CDK}$ gain-of-function experiments were performed at 1.5 µg/µl as described by Bonnet et al. (2018). The FUCCI S/G2/M mAG-hGem (MBL Life Science; Sakaue-Sawano et al., 2008) and the FUCCI G1 mKO2-zCdt1 (Sugiyama et al., 2009) vectors were used at 0.5 µg/µl. The pCIG vector was obtained from Andrew P. McMahon (W.M. Keck School of Medicine of the University of Southern California, Los Angeles, CA, USA), pCS2:H2B-GFP was obtained from Xavier Morin (Institut de Biologie de l'Ecole Normale Superieure, Paris, France).

Immunohistochemistry
Embryos or neural tube explants were fixed in 3.7% formaldehyde for 2 h and sliced using a VT100S vibratome (Leica). Proteins were detected on 50 µm vibratome sections, as previously described (Peco et al., 2012). The antibodies used were: anti-Olig2 (1:1000, AB9610, Merck Millipore), anti-Islet1/2 (1:3, 3.39.4D5, Developmental Studies Hybridoma Bank), anti-HuC/D (1:1000, 16A11, Thermo Fisher Scientific), anti-MNR2 (1:500, 81.5C10, Developmental Studies Hybridoma Bank), anti-GFP (1:1000, R970-01, Invitrogen), anti-γH2AX (1:1000, NB100-384, Novus Biologicals), anti-active caspase 3 (1:500, C92-605, BD Biosciences) anti phospho-Rb (S807/811) (1:400, 8516, Cell Signaling Technology) and anti-Tuj1 (1:1000, T3952, Sigma-Aldrich).

Determination of S-phase length and Tc length were based on the relative numbers of cells that incorporated one or two thymidine analogs (Martynoga et al., 2005). For *in ovo* incorporation, 10 µl of BrdU (500 µM; Sigma-Aldrich) were injected into embryos and followed by EdU (500 µM, Invitrogen) incorporation after 90 min. Embryos were fixed 30 min later. EdU was detected first (Click-iT EdU Alexa Fluor 647 Imaging Kit, Invitrogen), followed by BrdU detection using the anti-BrdU antibody (1:400, G3G4, Developmental Studies Hybridoma Bank), which does not recognize EdU. For single BrdU incorporation, 10 µl of BrdU (500 µM) was injected into embryos, which were then re-incubated for 30 min before fixation. BrdU immunodetection was performed on vibratome sections using anti-BrdU, as described by Lobjois et al. (2004). For cumulative *in ovo* incorporation of EdU, 10 µl of EdU was injected into E2.5 embryos every 3 h for up to 27 h. Embryos were fixed and processed for vibratome sectioning and EdU detected according to the manufacturer's instructions (Click-iT EdU Alexa Fluor 488 Imaging Kit, Invitrogen). Cell death was analyzed by immunofluorescence, using the anti-active caspase 3 antibody.

Flow cytometry analysis
Chicken embryos (1.5 to 2 days old) were electroporated with the H2B-GFP or NLS-eGFP-L2-PCNA constructs. Neural tubes were dissected 24 h following electroporation, incubated at 37°C for 10 min in trypsin-EDTA to obtain a single-cell suspension, and fixed for 30 min in 4% formaldehyde. Cell suspensions were incubated for 30 min in 400 µl of propidium iodide (PI; 20 µg/ml) and RNase cocktail (100 µg/ml; Sigma-Aldrich). PI and GFP fluorescence were detected using a FACSCalibur cytometer (342975, Becton Dickinson), and DNA content analysis was performed using FlowJo software.

Embryonic neural tube culture and time-lapse imaging
Electroporated E2 embryos were collected in PBS and 100 µm slices were obtained using a McIlwain tissue chopper (WPI), from the brachial region corresponding to somites 12 to 17, which generate the greatest number of motoneurons (Oppenheim et al., 1989). Sections were collected in Medium 199 (Gibco) and were analyzed under a fluorescence microscope to visualize the tissues and identify the presence of isolated fluorescent cells along the dorsoventral axis. Each slice was embedded into 10 µl of rat type I collagen [Roche Diagnosis; diluted at 80% with 1× Minimum Essential Medium (MEM; Gibco), 1× GlutaMax (Gibco) and neutralizing bicarbonate (Gibco)]. Four neural tube-containing collagen drops (5 µl) were distributed on a 35 mm glass-bottom culture dish (ibidi) (procedure

modified from Das et al., 2012). Collagen polymerization was performed at 38°C for 30 min and 1.5 ml of complete culture medium was added [Medium 199 supplemented with 1× GlutaMax, 5% fetal calf serum (Thermo Fisher Scientific) and gentamicin (Gibco, 40 µg/ml)]. The culture dish was placed in a humid atmosphere incubator with 5% CO_2 for 12 h before time-lapse imaging. Alternatively, explants were cultured for 24 or 48 h, fixed in 3.7% formaldehyde and processed for immunostaining.

For time-lapse imaging, images were acquired on an inverted microscope (Leica inverted DMI8) equipped with a heating enclosure (set up at 39°C) in an atmosphere containing 5% CO_2, a spinning-disk confocal head (CSU-X1-M1N, Yokogawa), a SCMOS camera and a 63× oil immersion objective (NA 1.4-0.7). Attenuation of laser beam pulses was performed to reduce cell damage due to phototoxicity (Boudreau et al., 2016). We recorded 40 µm thick z-stacks (2 µm z-steps) at 5 min intervals for 48 h.

Imaging, data analysis and statistics
IMARIS® and ImageJ software (Schneider et al., 2012) were used for image processing and data analysis. Statistical analyses were performed using GraphPad Prism and R. The normality of the datasets was determined, and analyses of variance performed. Values shown are mean±s.e.m. Significance was assessed by performing the Mann–Whitney test. *$P<0.05$; **$P<0.01$; ***$P<0.001$. See also supplementary Materials and Methods.

References
Agius, E., Bel-Vialar, S., Bonnet, F. and Pituello, F. (2015). Cell cycle and cell fate in the developing nervous system: the role of CDC25B phosphatase. *Cell Tissue Res.* **359**, 201-213. doi:10.1007/s00441-014-1998-2

Arai, Y., Pulvers, J. N., Haffner, C., Schilling, B., Nüsslein, I., Calegari, F. and Huttner, W. B. (2011). Neural stem and progenitor cells shorten S-phase on commitment to neuron production. *Nat. Commun.* **2**, 154. doi:10.1038/ncomms1155

Araujo, A. R., Gelens, L., Sheriff, R. S. M. and Santos, S. D. M. (2016). Positive feedback keeps duration of mitosis temporally insulated from upstream cell-cycle events. *Mol. Cell* **64**, 362-375. doi:10.1016/j.molcel.2016.09.018

Artegiani, B., Lindemann, D. and Calegari, F. (2011). Overexpression of cdk4 and cyclinD1 triggers greater expansion of neural stem cells in the adult mouse brain. *J. Exp. Med.* **208**, 937-948. doi:10.1084/jem.20102167

Astuti, P., Boutros, R., Ducommun, B. and Gabrielli, B. (2010). Mitotic phosphorylation of Cdc25B Ser^{321} disrupts 14-3-3 binding to the high affinity Ser^{323} site. *J. Biol. Chem.* **285**, 34364-34370. doi:10.1074/jbc.M110.138412

DEVELOPMENT

Azaïs, M., Agius, E., Blanco, S., Molina, A., Pituello, F., Tregan, J.-M., Vallet, A. and Gautrais, J. (2019). Timing the spinal cord development with neural progenitor cells losing their proliferative capacity: a theoretical analysis. *Neural Dev* 14, 7. doi:10.1186/s13064-019-0131-3

Bénazéraf, B., Chen, Q., Peco, E., Lobjois, V., Médevielle, F., Ducommun, B. and Pituello, F. (2006). Identification of an unexpected link between the Shh pathway and a G2/M regulator, the phosphatase CDC25B. *Dev. Biol.* 294, 133-147. doi:10.1016/j.ydbio.2006.02.035

Bonnet, F., Molina, A., Roussat, M., Azais, M., Bel-Vialar, S., Gautrais, J., Pituello, F. and Agius, E. (2018). Neurogenic decisions require a cell cycle independent function of the CDC25B phosphatase. *eLife* 7, e32937. doi:10.7554/eLife.32937

Boudreau, C., Wee, T.-L. E., Duh, Y.-R. S., Couto, M. P., Ardakani, K. H. and Brown, C. M. (2016). Excitation Light Dose Engineering to Reduce Photobleaching and Photo-toxicity. *Sci. Rep.* 6, 30892. doi:10.1038/srep30892

Cao, X., Pfaff, S. L. and Gage, F. H. (2008). YAP regulates neural progenitor cell number via the TEA domain transcription factor. *Genes Dev.* 22, 3320-3334. doi:10.1101/gad.1726608

Chao, H. X., Fakhreddin, R. I., Shimerov, H. K., Kedziora, K. M., Kumar, R. J., Perez, J., Limas, J. C., Grant, G. D., Cook, J. G., Gupta, G. P. et al. (2019). Evidence that the human cell cycle is a series of uncoupled, memoryless phases. *Mol. Syst. Biol.* 15, e8604. doi:10.15252/msb.20188604

Dalton, S. (2015). Linking the cell cycle to cell fate decisions. *Trends Cell Biol.* 25, 592-600. doi:10.1016/j.tcb.2015.07.007

Das, R. M., Wilcock, A. C., Swedlow, J. R. and Storey, K. G. (2012). High-resolution live imaging of cell behavior in the developing neuroepithelium. *J. Vis. Exp.* 62, e3920. doi:10.3791/3920

Fousse, J., Gautier, E., Patti, D. and Dehay, C. (2019). Developmental changes in interkinetic nuclear migration dynamics with respect to cell-cycle progression in the mouse cerebral cortex ventricular zone. *J. Comp. Neurol.* 527, 1545-1557. doi:10.1002/cne.24641

Gookin, S., Min, M., Phadke, H., Chung, M., Moser, J., Miller, I., Carter, D. and Spencer, S. L. (2017). A map of protein dynamics during cell-cycle progression and cell-cycle exit. *PLoS Biol.* 15, e2003268. doi:10.1371/journal.pbio.2003268

Gruber, R., Zhou, Z., Sukchev, M., Joerss, T., Frappart, P.-O. and Wang, Z.-Q. (2011). MCPH1 regulates the neuroprogenitor division mode by coupling the centrosomal cycle with mitotic entry through the Chk1-Cdc25 pathway. *Nat. Cell Biol.* 13, 1325-1334. doi:10.1038/ncb2342

Hamburger, V. and Hamilton, H. L. (1992). A series of normal stages in the development of the chick embryo. *Dev. Dyn.* 195, 231-272. doi:10.1002/aja.1001950404

Hardwick, L. J. A., Ali, F. R., Azzarelli, R. and Philpott, A. (2015). Cell cycle regulation of proliferation versus differentiation in the central nervous system. *Cell Tissue Res.* 359, 187-200. doi:10.1007/s00441-014-1895-8

Jang, J., Han, D., Golkaram, M., Audouard, M., Liu, G., Bridges, D., Hellander, S., Chialastri, A., Dey, S. S., Petzold, L. R. et al. (2019). Control over single-cell distribution of G1 lengths by WNT governs pluripotency. *PLoS Biol.* 17, e3000453. doi:10.1371/journal.pbio.3000453

Julian, L. M., Carpenedo, R. L., Rothberg, J. L. M. and Stanford, W. L. (2016). Formula G1: cell cycle in the driver's seat of stem cell fate determination. *BioEssays* 38, 325-332. doi:10.1002/bies.201500187

Kicheva, A. and Briscoe, J. (2015). Developmental pattern formation in phases. *Trends Cell Biol.* 25, 579-591. doi:10.1016/j.tcb.2015.07.006

Kicheva, A., Bollenbach, T., Ribeiro, A., Valle, H. P., Lovell-Badge, R., Episkopou, V. and Briscoe, J. (2014). Coordination of progenitor specification and growth in mouse and chick spinal cord. *Science* 345, 1254927. doi:10.1126/science.1254927

Körner, K., Jérôme, V., Schmidt, T. and Müller, R. (2001). Cell cycle regulation of the murine cdc25B promoter: essential role for nuclear factor-Y and a proximal repressor element. *J. Biol. Chem.* 276, 9662-9669. doi:10.1074/jbc.M008696200

Lacomme, M., Liaubet, L., Pituello, F. and Bel-Vialar, S. (2012). NEUROG2 drives cell cycle exit of neuronal precursors by specifically repressing a subset of cyclins acting at the G1 and S phases of the cell cycle. *Mol. Cell. Biol.* 32, 2596-2607. doi:10.1128/MCB.06745-11

Lange, C., Huttner, W. B. and Calegari, F. (2009). Cdk4/cyclinD1 overexpression in neural stem cells shortens G1, delays neurogenesis, and promotes the generation and expansion of basal progenitors. *Cell Stem Cell* 5, 320-331. doi:10.1016/j.stem.2009.05.026

Le Dreau, G., Saade, M., Gutierrez-Vallejo, I. and Marti, E. (2014). The strength of SMAD1/5 activity determines the mode of stem cell division in the developing spinal cord. *J. Cell Biol.* 204, 591-605. doi:10.1083/jcb.201307031

Leonhardt, H., Rahn, H.-P., Weinzierl, P., Sporbert, A., Cremer, T., Zink, D. and Cardoso, M. C. (2000). Dynamics of DNA replication factories in living cells. *J. Cell Biol.* 149, 271-280. doi:10.1083/jcb.149.2.271

Leung, L., Klopper, A. V., Grill, S. W., Harris, W. A. and Norden, C. (2011). Apical migration of nuclei during G2 is a prerequisite for all nuclear motion in zebrafish neuroepithelia. *Development* 138, 5003-5013. doi:10.1242/dev.071522

Lim, S. and Kaldis, P. (2012). Loss of Cdk2 and Cdk4 induces a switch from proliferation to differentiation in neural stem cells. *Stem Cells* 30, 1509-1520. doi:10.1002/stem.1114

Liu, L., Michowski, W., Kolodziejczyk, A. and Sicinski, P. (2019). The cell cycle in stem cell proliferation, pluripotency and differentiation. *Nat. Cell Biol.* 21, 1060-1067. doi:10.1038/s41556-019-0384-4

Lobjois, V., Benazeraf, B., Bertrand, N., Medevielle, F. and Pituello, F. (2004). Specific regulation of cyclins D1 and D2 by FGF and Shh signaling coordinates cell cycle progression, patterning, and differentiation during early steps of spinal cord development. *Dev. Biol.* 273, 195-209. doi:10.1016/j.ydbio.2004.05.031

Lobjois, V., Bel-Vialar, S., Trousse, F. and Pituello, F. (2008). Forcing neural progenitor cells to cycle is insufficient to alter cell-fate decision and timing of neuronal differentiation in the spinal cord. *Neural Dev.* 3, 4. doi:10.1186/1749-8104-3-4

Martynoga, B., Morrison, H., Price, D. J. and Mason, J. O. (2005). Foxg1 is required for specification of ventral telencephalon and region-specific regulation of dorsal telencephalic precursor proliferation and apoptosis. *Dev. Biol.* 283, 113-127. doi:10.1016/j.ydbio.2005.04.005

Min, M., Rong, Y., Tian, C. and Spencer, S. L. (2020). Temporal integration of mitogen history in mother cells controls proliferation of daughter cells. *Science* 368, 1261-1265. doi:10.1126/science.aay8241

Molina, A. and Pituello, F. (2017). Playing with the cell cycle to build the spinal cord. *Dev. Biol.* 432, 14-23. doi:10.1016/j.ydbio.2016.12.022

Moser, J., Miller, I., Carter, D. and Spencer, S. L. (2018). Control of the restriction point by Rb and p21. *Proc. Natl. Acad. Sci. USA* 115, E8219-E8227. doi:10.1073/pnas.1722446115

Mura, M., Feillet, C., Bertolusso, R., Delaunay, F. and Kimmel, M. (2019). Mathematical modelling reveals unexpected inheritance and variability patterns of cell cycle parameters in mammalian cells. *PLoS Comput. Biol.* 15, e1007054. doi:10.1371/journal.pcbi.1007054

Naetar, N., Soundarapandian, V., Litovchick, L., Goguen, K. L., Sablina, A. A., Bowman-Colin, C., Sicinski, P., Hahn, W. C., DeCaprio, J. A. and Livingston, D. M. (2014). PP2A-mediated regulation of Ras signaling in G2 is essential for stable quiescence and normal G1 length. *Mol. Cell* 54, 932-945. doi:10.1016/j.molcel.2014.04.023

Nowakowski, R. S., Lewin, S. B. and Miller, M. W. (1989). Bromodeoxyuridine immunohistochemical determination of the lengths of the cell cycle and the DNA-synthetic phase for an anatomically defined population. *J. Neurocytol.* 18, 311-318. doi:10.1007/BF01190834

Oppenheim, R. W., Cole, T. and Prevette, D. (1989). Early regional variations in motoneuron numbers arise by differential proliferation in the chick embryo spinal cord. *Dev. Biol.* 133, 468-474. doi:10.1016/0012-1606(89)90050-X

Peco, E., Escude, T., Agius, E., Sabado, V., Medevielle, F., Ducommun, B. and Pituello, F. (2012). The CDC25B phosphatase shortens the G2 phase of neural progenitors and promotes efficient neuron production. *Development* 139, 1095-1104. doi:10.1242/dev.068569

Pilaz, L.-J., Patti, D., Marcy, G., Ollier, E., Pfister, S., Douglas, R. J., Betizeau, M., Gautier, E., Cortay, V., Doerflinger, N. et al. (2009). Forced G1-phase reduction alters mode of division, neuron number, and laminar phenotype in the cerebral cortex. *Proc. Natl. Acad. Sci. USA* 106, 21924-21929. doi:10.1073/pnas.0909894106

Roccio, M., Schmitter, D., Knobloch, M., Okawa, Y., Sage, D. and Lutolf, M. P. (2013). Predicting stem cell fate changes by differential cell cycle progression patterns. *Development* 140, 459-470. doi:10.1242/dev.086215

Saade, M., Gutiérrez-Vallejo, I., Le Dréau, G., Rabadán, M. A., Miguez, D. G., Buceta, J. and Martí, E. (2013). Sonic hedgehog signaling switches the mode of division in the developing nervous system. *Cell Rep.* 4, 492-503. doi:10.1016/j.celrep.2013.06.038

Sakaue-Sawano, A., Kurokawa, H., Morimura, T., Hanyu, A., Hama, H., Osawa, H., Kashiwagi, S., Fukami, K., Miyata, T., Miyoshi, H. et al. (2008). Visualizing spatiotemporal dynamics of multicellular cell-cycle progression. *Cell* 132, 487-498. doi:10.1016/j.cell.2007.12.033

Schneider, C. A., Rasband, W. S. and Eliceiri, K. W. (2012). NIH Image to ImageJ: 25 years of image analysis. *Nat. Methods* 9, 671-675. doi:10.1038/nmeth.2089

Spencer, S. L., Cappell, S. D., Tsai, F.-C., Overton, K. W., Wang, C. L. and Meyer, T. (2013). The proliferation-quiescence decision is controlled by a bifurcation in CDK2 activity at mitotic exit. *Cell* 155, 369-383. doi:10.1016/j.cell.2013.08.062

Subramanian, L., Bershteyn, M., Paredes, M. F. and Kriegstein, A. R. (2017). Dynamic behaviour of human neuroepithelial cells in the developing forebrain. *Nat. Commun.* 8, 14167. doi:10.1038/ncomms14167

Sugiyama, M., Sakaue-Sawano, A., Iimura, T., Fukami, K., Kitaguchi, T., Kawakami, K., Okamoto, H., Higashijima, S. and Miyawaki, A. (2009). Illuminating cell-cycle progression in the developing zebrafish embryo. *Proc. Natl. Acad. Sci. USA* 106, 20812-20817. doi:10.1073/pnas.0906464106

Ueno, H., Nakajo, N., Watanabe, M., Isoda, M. and Sagata, N. (2008). FoxM1-driven cell division is required for neuronal differentiation in early Xenopus embryos. *Development* 135, 2023-2030. doi:10.1242/dev.019893

Wilcock, A. C., Swedlow, J. R. and Storey, K. G. (2007). Mitotic spindle orientation distinguishes stem cell and terminal modes of neuron production in the early spinal cord. *Development* 134, 1943-1954. doi:10.1242/dev.002519

Xie, S. and Skotheim, J. M. (2020). A G1 sizer coordinates growth and division in the mouse epidermis. *Curr. Biol.* 30, 916-924.e12. doi:10.1016/j.cub.2019.12.062
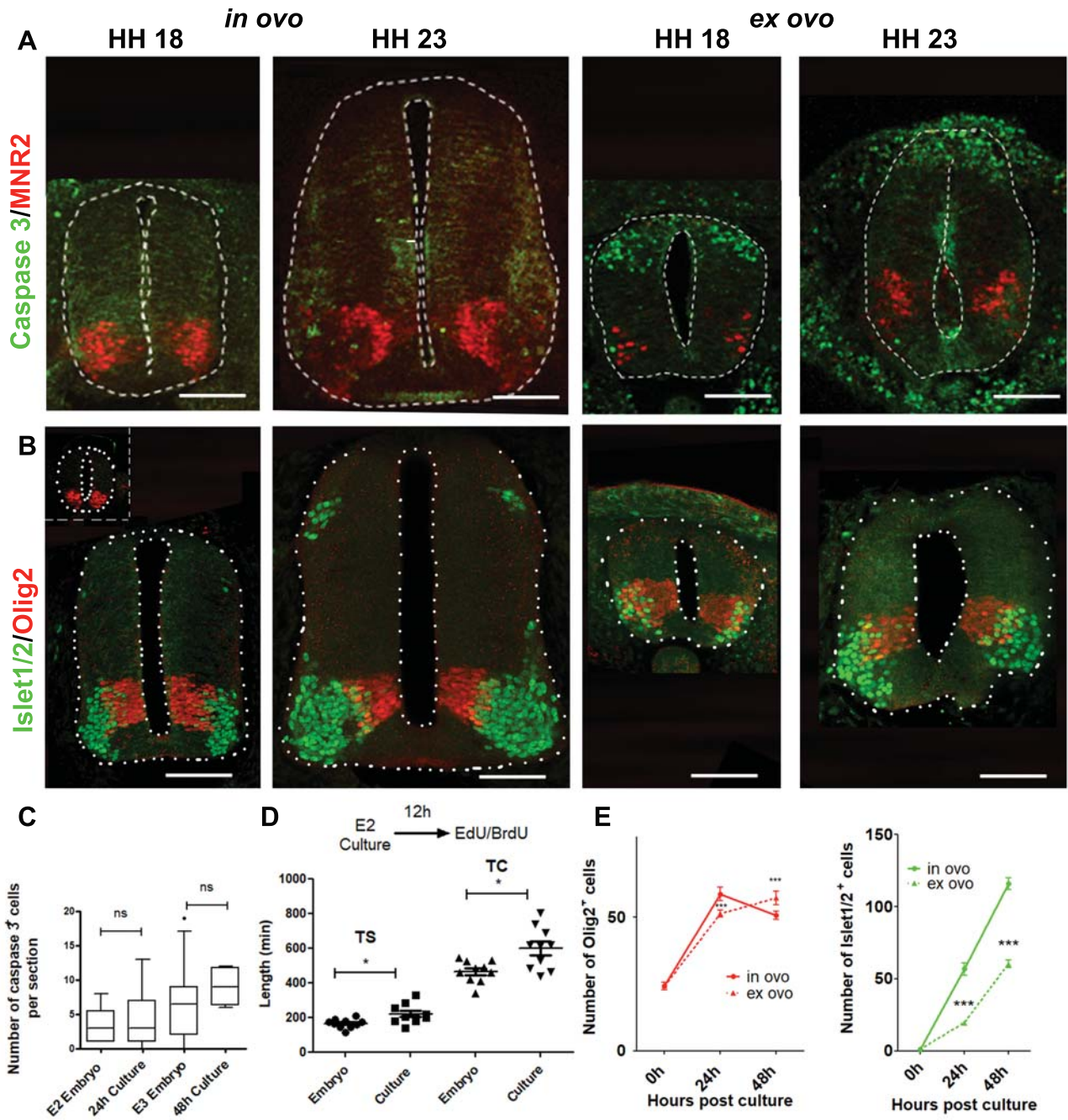
DEVELOPMENT

Fig. S1. Characterization of *ex vivo* culture of chick embryonic neural tube explants. A, B: Cross-sections of E2.5 and E3.5 (stage HH18, HH23) chick embryo spinal cord (in ovo), and explants dissected at E1.5 and cultivated for 24 hours and 48h hours (ex ovo). Sections processed for anti-caspase3 (green) and anti-MNR2 (red) immunostaining (**A**) or anti-Olig2 (red) and anti-Islet1/2 (green) immunostaining (**B**). Inset in B, E1.5 (HH13) embryo section. **C:** Bar plots representing the number activated caspase 3 positive cells per optical section under various conditions. Means +/- sem of 3 different experiments with at least 4 embryos. **D:** Scatter dot plot representing S phase duration (Ts) and total cell cycle duration (Tc) calculated using Dual Pulse Labeling using EdU and BrdU incorporation paradigm in embryos and in cultures, revealing a transient lengthening of the cell cycle in progenitors at 12 hours after dissection that is recovered at 24 hours (not shown). **E:** Curves representing kinetics of the number of cells expressing Olig2 and Islet1/2 per section in the spinal cord (in ovo) or in explants (ex vivo) starting at E1.5 (t = 0h), 24 hours or 48 hours later. The increase in the population of progenitors and neurons in our culture conditions indicates that progenitors are performing both proliferative and neurogenic divisions. Data from three different experiments with at least four embryos for in ovo condition, and six sections from three embryos for the ex ovo condition. Scale bars represent 100 µm.
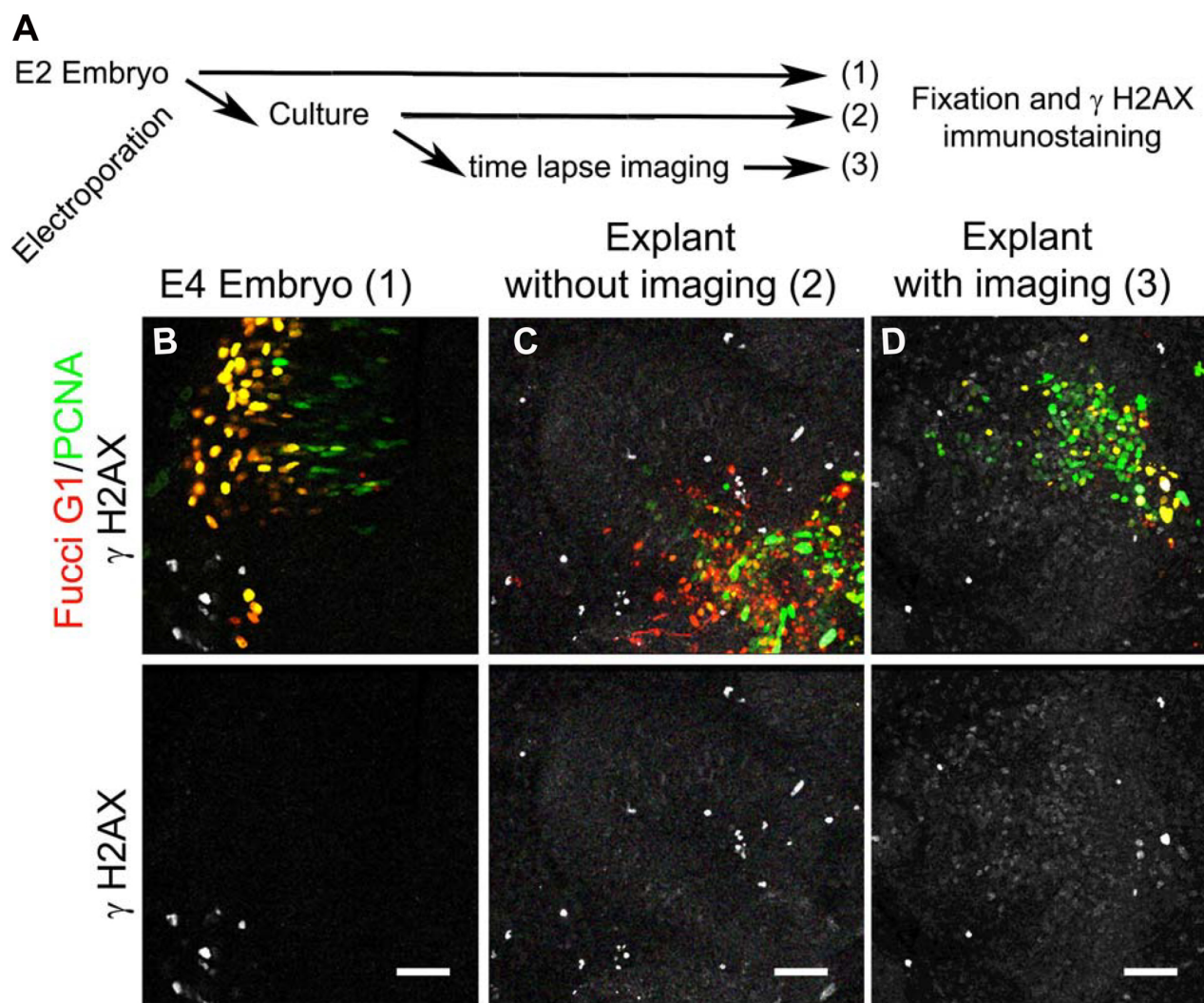
Fig. S2. γH2AX immunostaining after time lapse experiments. **A:** scheme of the protocol. **B:** Representative spinal cord section of an electroporated embryo with the FUCCI G1/PCNA plasmid and allowed to develop for 2.5 days. The γH2AX positive cells are apoptotic motoneurons. **C:** Spinal cord explant of an electroporated embryo with the FUCCI G1/PCNA plasmid and allowed to develop for 2.5 days in culture without imaging. **D:** Spinal cord explant of an electroporated embryo with the FUCCI G1/PCNA plasmid and imaged for 48 hours. Scale bars represent 50µm.
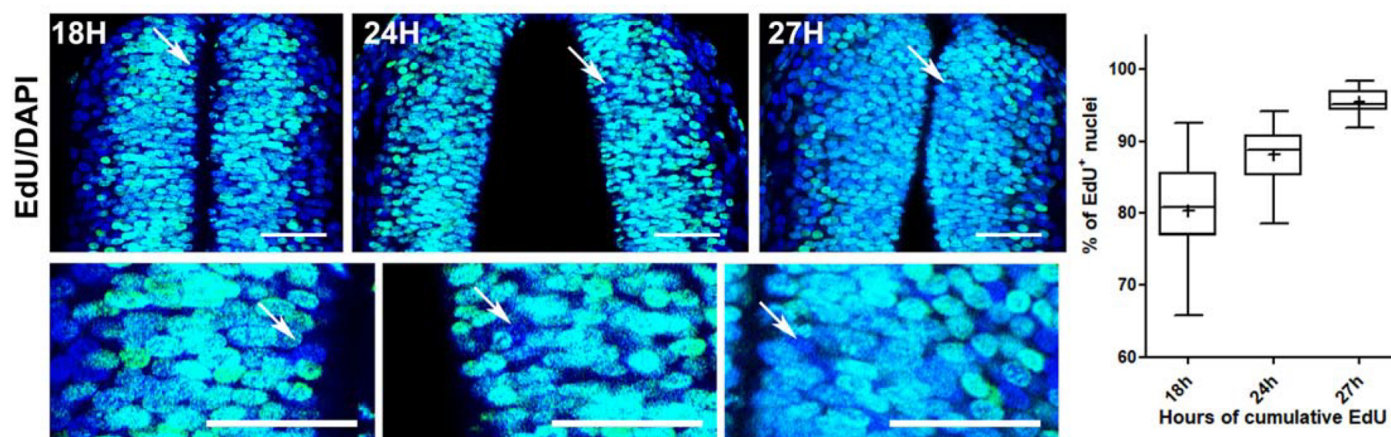
Fig. S3. Cumulative EdU experiment. **A:** E2.5 embryos received 10µl of 4µM EdU on the heart every 3 hours for 27 hours. Embryos were fixed at 6 hours, 12 hours, 18 hours, 24 hours and 27 hours, 30 min after the last EdU treatment. EdU (green) was revealed according to manufacturer's protocol (Invitrogen) and sections were counterstained using DAPI (blue). The figure shows spinal cord sections at 18, 24 or 27 hours. The arrows point to progenitor nuclei without EdU. Scale bars represent 50µm. **B:** Box and whiskers plots (5-95 percentile) illustrating the quantification of the percentage of EdU$^+$ nuclei in the dorsal spinal cord. At least 2 sections were counted on three embryos for each time points.
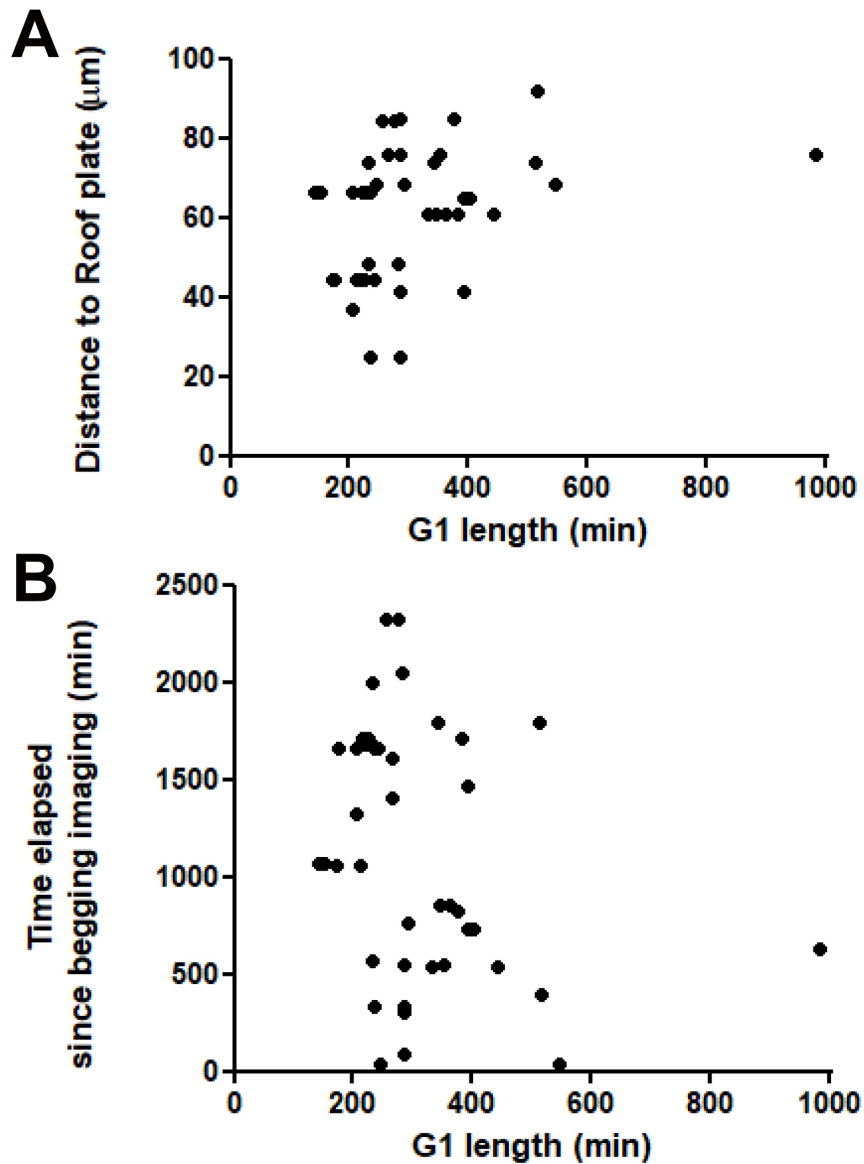
Fig. S4. The G1 phase length variation is independent of the clone position or of the time of analysis. A: Dot plot analysis of the G1 phase length plotted compared to the distance of the cell to the roof plate. **B:** Dot plot analysis of the G1 phase length plotted compared to the time elapsed since then beginning of the video.
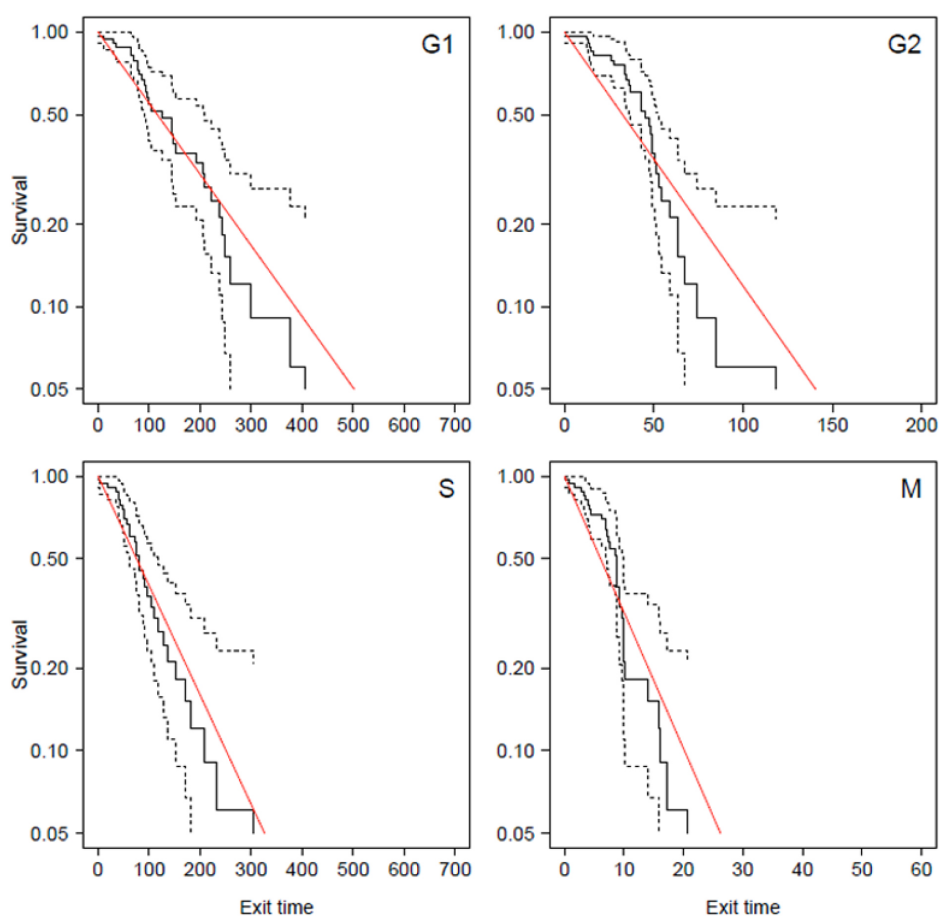
Fig. S5. **Survival curves for exit times for the four cell cycle phases**. Survival curves were obtained from the data subset of complete cell cycle tracked cells in control conditions. Exit times are obtained by subtracting minimal time from observed times. Black curves are Kaplan-Meier estimates of survival, with confidence interval. For this subset, survival curves appear to be about compatible with simple exponential decay (red curves), corresponding to a simple memoryless process.
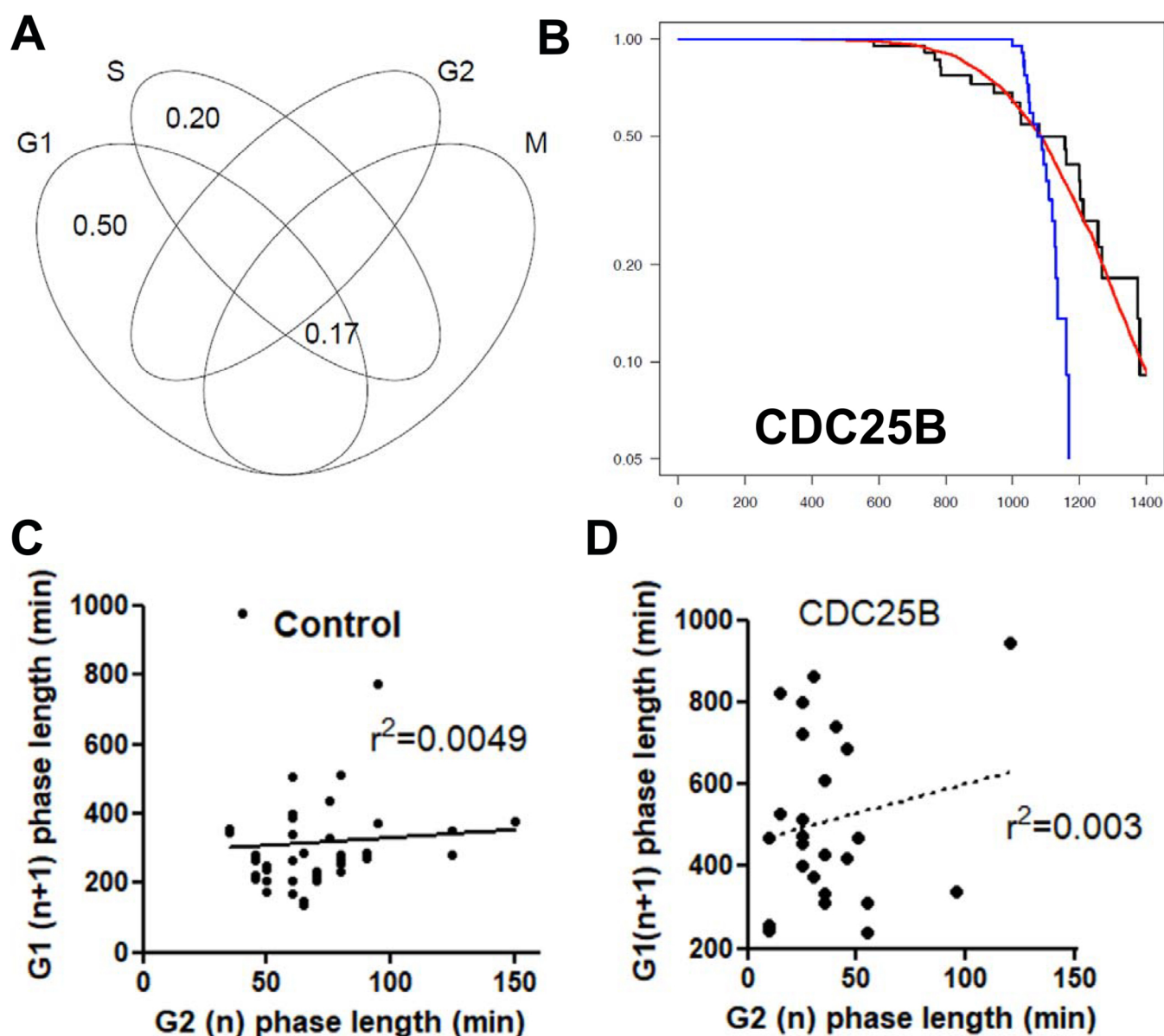
Fig. S6. CDC25B effects on cell cycle heterogeneity A: Variation partitioning (Venn Diagrams) in CDC25B gain of function showing how much variation is attributed to each phase. **B:** Survival curve of Tc phase length data in the CDC25B condition. Black line corresponds to Kaplan-Meier estimate from data. Red line corresponds to the survival curve obtained in Monte Carlo permutation of phase durations from the data set and the blue curve corresponds to the case with G1 and S/G2/M phases lengths fully anti-correlated (see SI-sect). **C, D:** Correlation analysis between G2 phase lengths of the mother cell and G1 phase lengths of the daughter cell in control (**C**) and CDC25B (**D**) conditions.
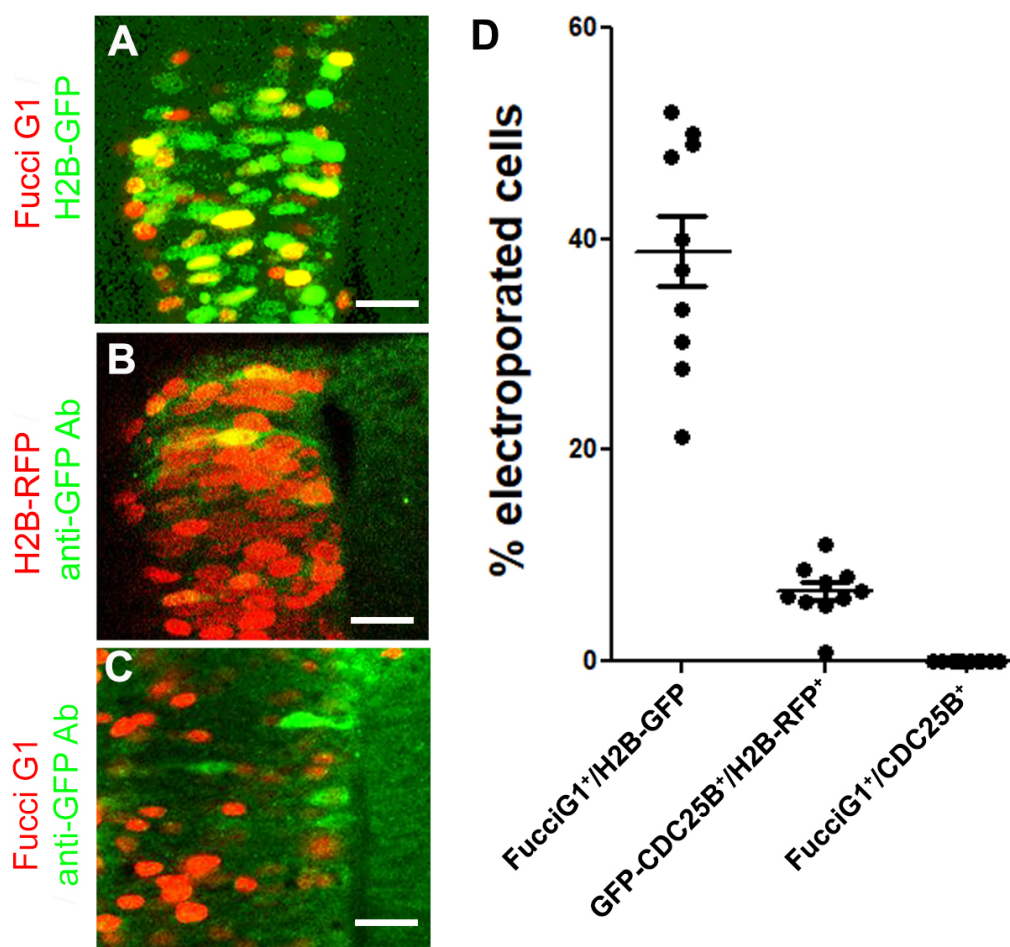
Fig. S7. CDC25B-GFP protein is not detected during the G1 phase. **A**: Co electroporation of pCS::H2B-GFP and mKO-zFucci-G1 to quantify the number of cells co-expressing the FUCCI G1-RFP and the H2B-GFP proteins (38.8+/-3.4%). **B**: immunodetection using an anti GFP antibody after co-electroporation of the ccRE::GFP-CDC25B (green) with pCS::H2B-RFP (red) to quantify the number of electroporated cells expressing CDC25B protein (6.6+/-0.8%). **C**: Immunodetection using an anti GFP antibody after co-electroporation of ccRE::GFP-CDC25B with mKO-zFucci-G1. CDC25B-GFP expressing cells are not expressing the G1 marker. **D:** The graph shows the percentage of co-electroporated cells in the indicated conditions. Dots correspond to sections from 3 embryos and 2 experiments. Mean+/- sem is shown for each condition.
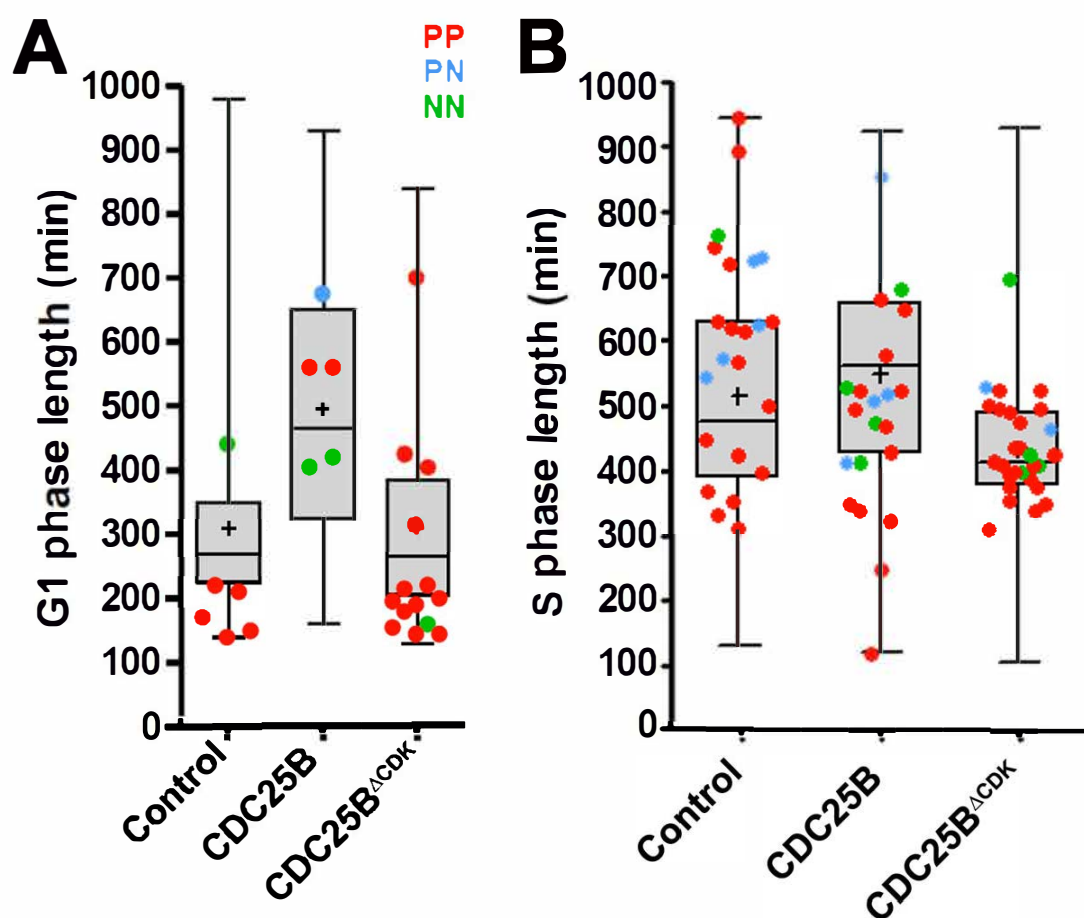
Fig. S8. Modes of division and G1 phase length. Box and whiskers plot representing the distribution of lengths of G1 phase (**A**) or S phase (**B**) in Control, CDC25B, CDC25B$^{\Delta CDK}$ associated with scatter dot-plot representing the G1 lengths of individual NPCs performing PP divisions in the following cell cycle (red dots), NPCs giving rise to a progenitor and a cell with a long G1 (asymmetric division, green dots) and NPCs generating 2 daughter cells with long G1s (blue dots).
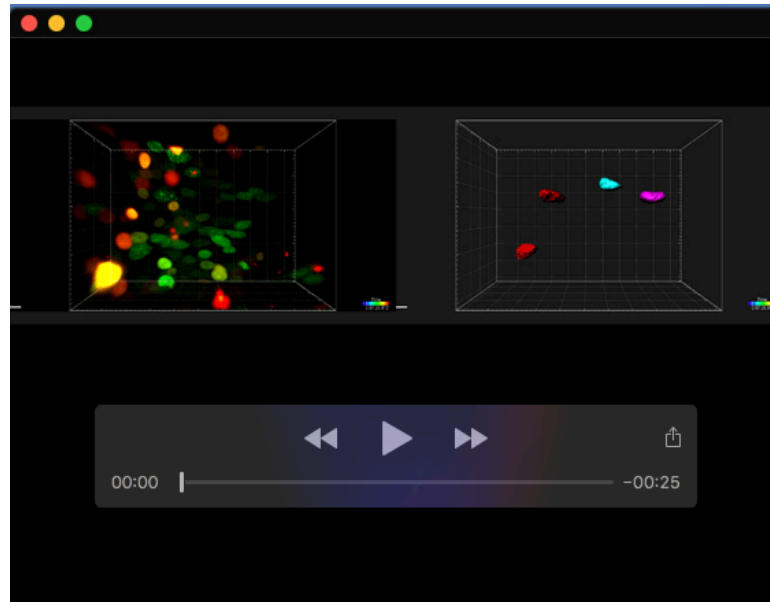
Movie 1. Expression of the cell cycle biosensor within the nucleus of NPCs allows the identification of the four cell cycle phases. Left panel- Live imaging movie. The four cell cycle phases are discriminated by the differential expression of the sensor, as well as the movements of nuclei inside the neural tube (Interkinetic Nuclear Movement, INM). Right panel - Segmentation of some analyzed nuclei. Time interval between frames = 5 min. Scale bar = 10 µm.

Supplementary Materials and Methods

1 Data Descriptions

We read durations data from 00-AllPhasesData.csv.

For complete cycles, we can compute Tc.

Note : in R outputs all along below, the condition is encoded as factor according to :

Condition	Code
CONTROL	CTL
CDC25B	CDC25B
CDC25B$^{\Delta\text{CDK}}$	DeltaCDK

1.1 Data summaries

1.1.1 CONTROL

```
  Condition         G1              S               G2               M               Tc
CTL    :54   Min.   :140.0   Min.   :130.0   Min.   : 35.00   Min.   :20.00   Min.   : 595.0
CDC25B : 0   1st Qu.:227.5   1st Qu.:365.0   1st Qu.: 52.50   1st Qu.:25.00   1st Qu.: 690.0
DeltaCDK: 0  Median :270.0   Median :397.5   Median : 75.00   Median :30.00   Median : 815.0
             Mean   :308.7   Mean   :438.6   Mean   : 76.57   Mean   :31.27   Mean   : 840.9
             3rd Qu.:347.5   3rd Qu.:465.0   3rd Qu.: 85.00   3rd Qu.:35.00   3rd Qu.: 915.0
             Max.   :980.0   Max.   :945.0   Max.   :175.00   Max.   :55.00   Max.   :1485.0
             NA's   :3       NA's   :12                       NA's   :3       NA's   :21
```

1.1.2 CDC25B

```
  Condition         G1              S               G2               M               Tc
CTL    : 0   Min.   :160.0   Min.   :120.0   Min.   : 10.00   Min.   :20.00   Min.   : 595.0
CDC25B :76   1st Qu.:327.5   1st Qu.:401.2   1st Qu.: 40.00   1st Qu.:30.00   1st Qu.: 906.2
DeltaCDK: 0  Median :465.0   Median :492.5   Median : 60.00   Median :30.00   Median :1130.0
             Mean   :494.4   Mean   :487.5   Mean   : 66.89   Mean   :32.76   Mean   :1099.8
             3rd Qu.:625.0   3rd Qu.:587.5   3rd Qu.: 80.00   3rd Qu.:35.00   3rd Qu.:1255.0
             Max.   :930.0   Max.   :855.0   Max.   :170.00   Max.   :45.00   Max.   :1585.0
             NA's   :41      NA's   :38      NA's   :15                       NA's   :54
```

1.1.3 CDC25B$^{\Delta\text{CDK}}$

```
  Condition         G1              S               G2               M               Tc
CTL    : 0   Min.   :130.0   Min.   :105.0   Min.   : 30.00   Min.   :20.00   Min.   : 515.0
CDC25B : 0   1st Qu.:207.5   1st Qu.:376.2   1st Qu.: 56.25   1st Qu.:30.00   1st Qu.: 680.0
DeltaCDK:98  Median :265.0   Median :415.0   Median : 70.00   Median :30.00   Median : 775.0
             Mean   :309.6   Mean   :416.4   Mean   : 79.13   Mean   :31.48   Mean   : 809.3
             3rd Qu.:377.5   3rd Qu.:455.0   3rd Qu.: 93.75   3rd Qu.:35.00   3rd Qu.: 910.0
             Max.   :840.0   Max.   :930.0   Max.   :170.00   Max.   :45.00   Max.   :1200.0
             NA's   :27      NA's   :32      NA's   :12                       NA's   :53
```

1.2 Statistics of durations

For each phase: minimal duration, standard deviations of phases duration and mean latency before exiting the phase starting from this minimum (hereafter denoted *Exit times*).

1.2.1 Minimal durations

Condition	G1	S	G2	M	Tc
CONTROL	140	130	35	20	595
CDC25B	160	120	10	20	595
CDC25B$^{\Delta\text{CDK}}$	130	105	30	20	515

1.2.2 Standard deviation of phase durations

Condition	G1	S	G2	M	Tc
CONTROL	148	149	30	7	205
CDC25B	202	147	34	6	266
CDC25B$^{\Delta\text{CDK}}$	144	116	33	5	170

1.2.3 Mean exit times

Condition	G1	S	G2	M	Tc
CONTROL	169	309	42	11	246
CDC25B	334	368	57	13	505
CDC25B$^{\Delta\text{CDK}}$	180	311	49	11	294

1.3 Survival curves for each condition.

We add noise to avoid ties. Actually, snaps were made every 5 min, so the event has occured within the last 5 minutes. Hence we distribube its date randomly within those last 5 minutes.

1.3.1 CONTROL
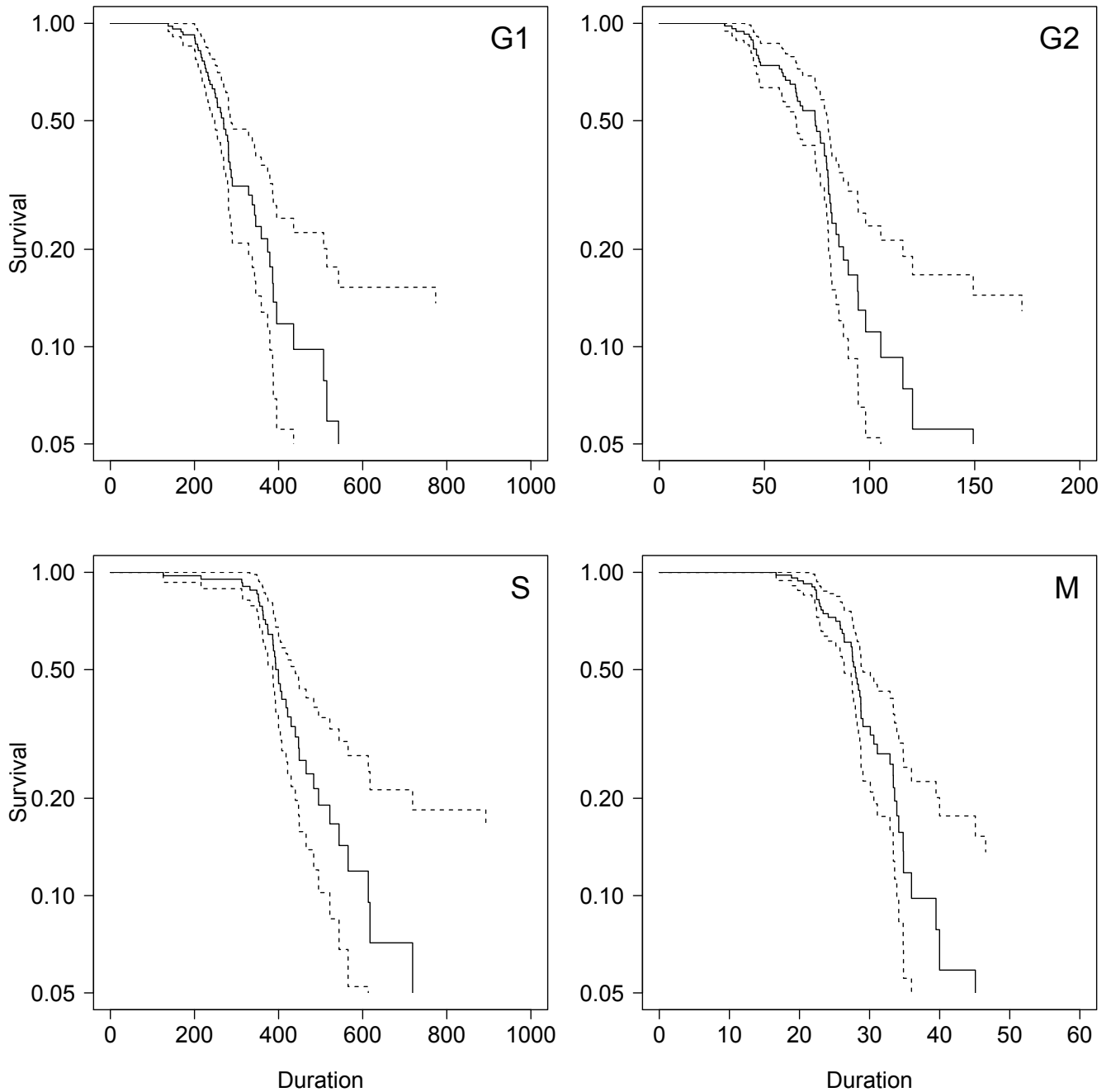
Fig. S1. Phases Survival curves

1.3.2 CDC25B
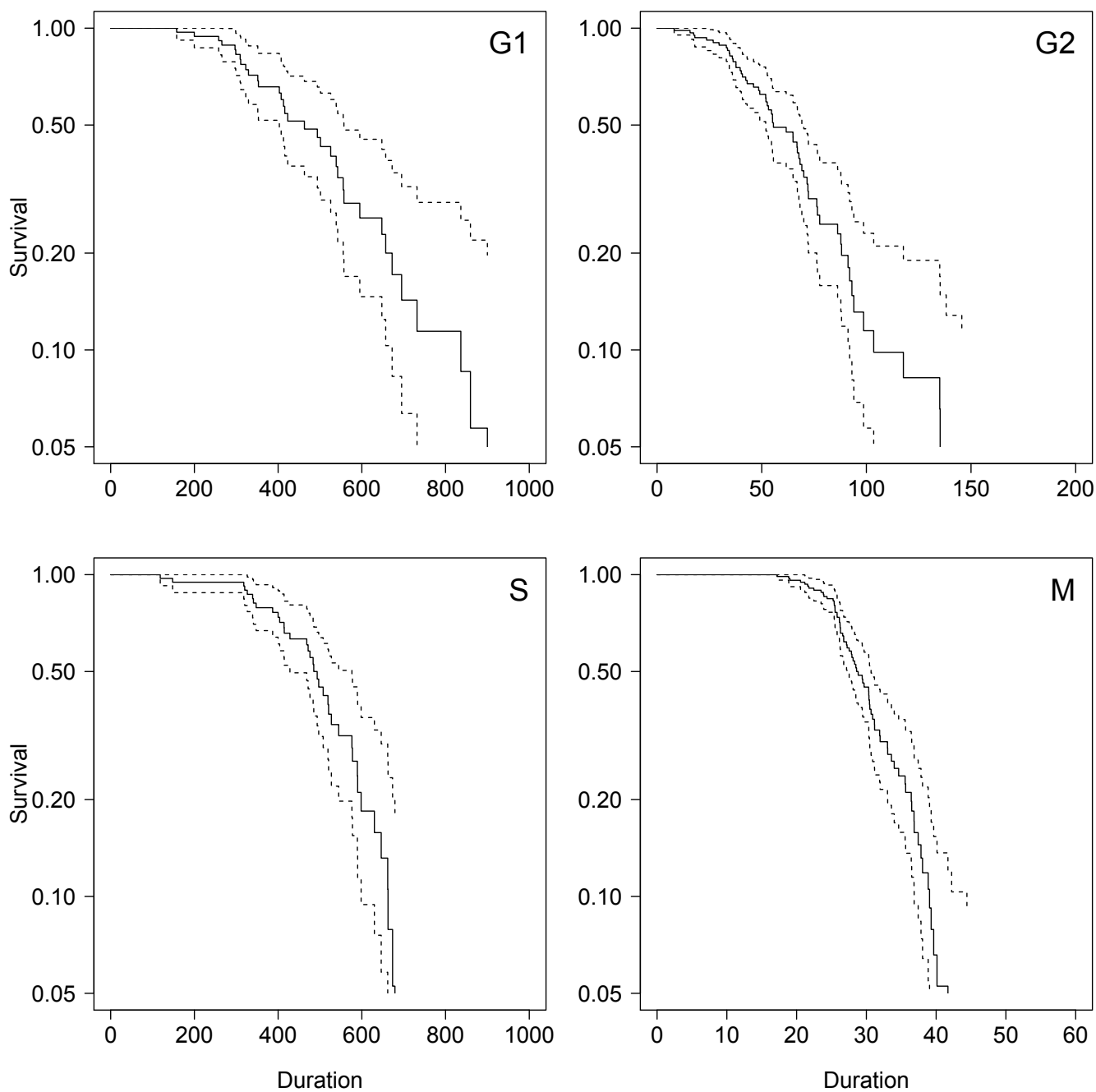
Fig. S2. Phases Survival curves

1.3.3 CDC25B$^{\Delta \text{CDK}}$
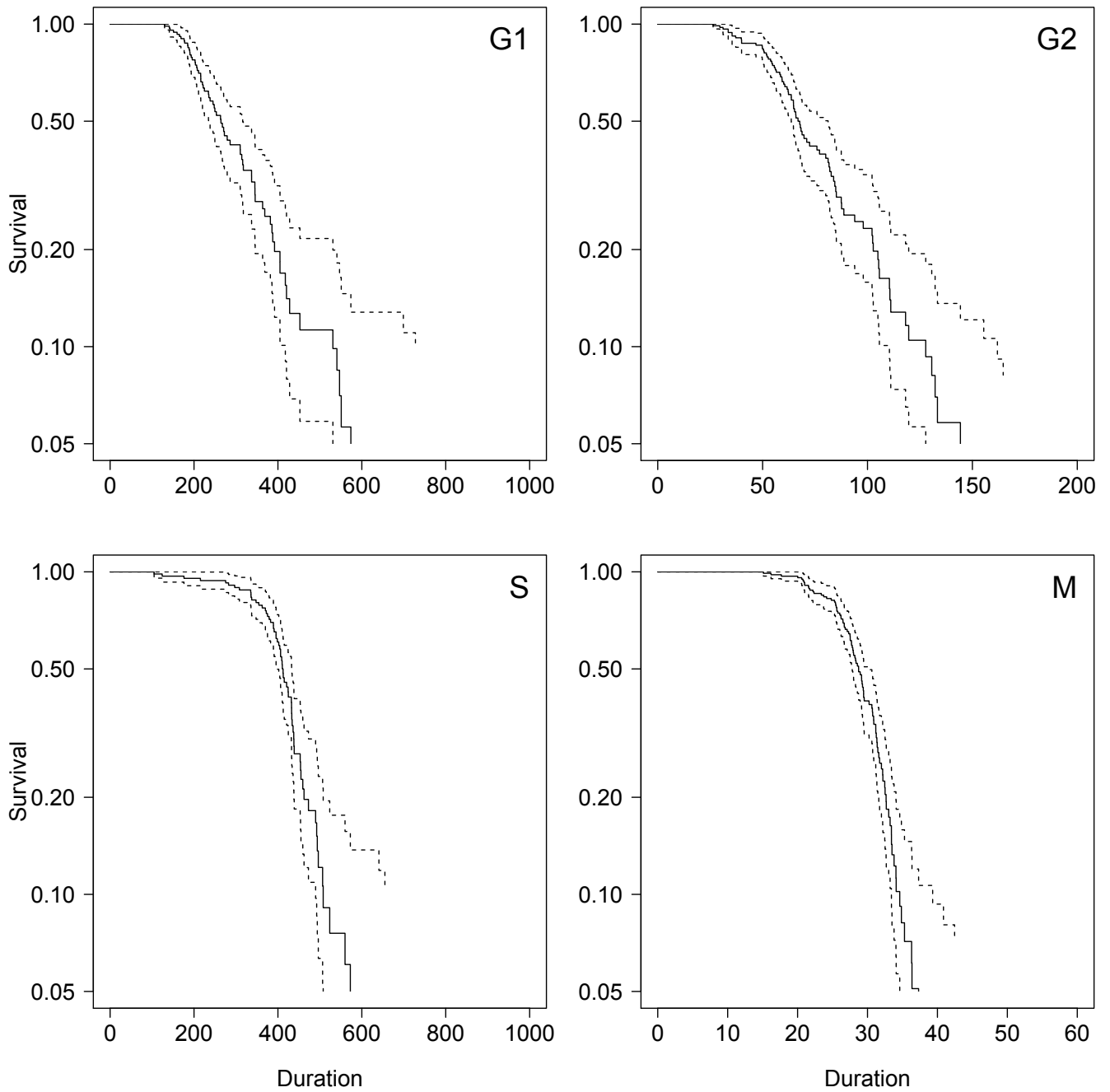
Fig. S3. Phases Survival curves

2 Subset with complete tracking of phases within the same cycle

In this section, we only use the subset of data with complete cell cycle measures.

2.1 Graphical summaries
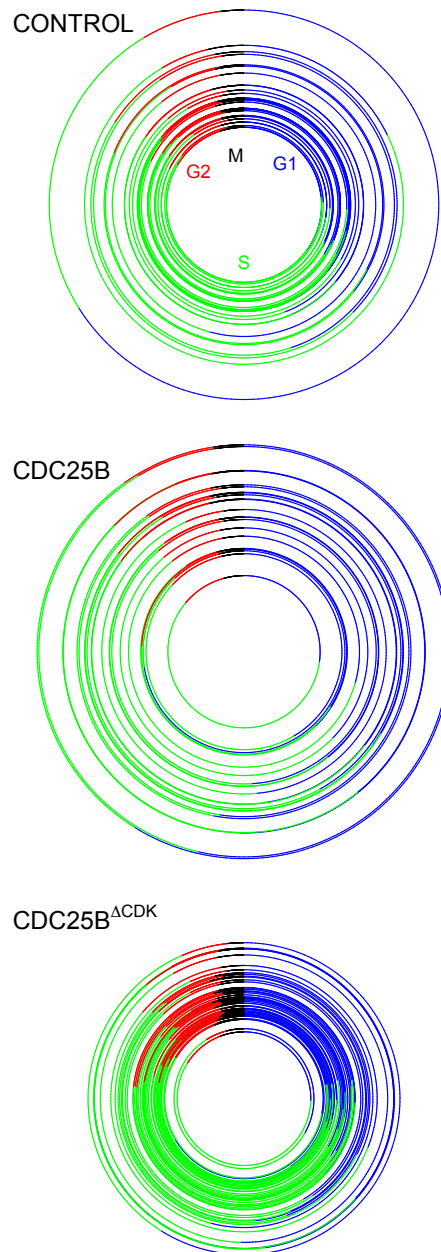
Fig. S4. Graphical summary of data

2.2 Variation Partitionning (Venn Diagrams)

The variation of cycle length is partionned in regards to phases to examine how much variation is explained by each phase.

See : Jari Oksanen, F. Guillaume Blanchet, Michael Friendly, Roeland Kindt, Pierre Legendre, Dan McGlinn, Peter R. Minchin, R. B. O'Hara, Gavin L. Simpson, Peter Solymos, M. Henry H. Stevens, Eduard Szoecs and Helene Wagner (2019). vegan: Community Ecology Package. R package version 2.5-6. https://CRAN.R-project.org/package=vegan

In Venn Diagrams, the number represent adjusted-Rsquare. For the sake of clarity, values below 0.05 are not reported.

In the three conditions, G1 phase duration explains the largest part of total length variations.
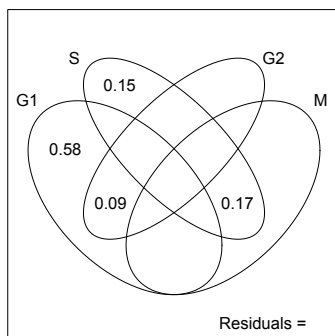
Fig. S5. Venn Diagrams for CONTROL condition.
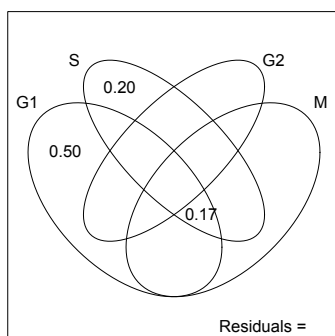
Fig. S6. Venn Diagrams for CDC25B gain of fonction
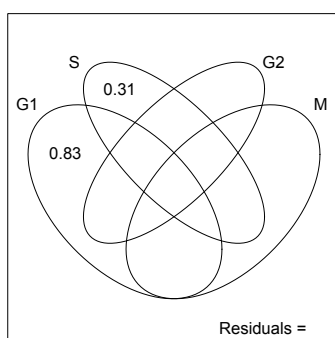
Fig. S7. Venn Diagrams for DeltaCDK condition.

2.3 Tests of correlation among phases

2.3.1 Statistical results

We test every pair of phases for linear regression. Tables below report R^2 values with their p-value, as well as correlation values with their associated p-value.

The symbol *SG2M* stands for S+G2+M

2.3.1.1 CONTROL

Phase	Phase	R^2	p-val	Pearson	p-val	Kendall	p-val	Spearman	p-val	Signif
G1	S	0.00	0.90	0.02	0.90	0.17	0.18	0.23	0.20	—
G1	G2	0.09	0.08	0.30	0.08	0.22	0.07	0.33	0.06	—
G1	M	0.01	0.57	0.10	0.57	0.09	0.45	0.17	0.35	—
S	G2	0.00	0.80	0.05	0.80	-0.00	0.99	-0.01	0.94	—
S	M	0.49	0.00	0.70	0.00	0.33	0.01	0.47	0.01	yes
G2	M	0.04	0.26	0.20	0.26	0.15	0.22	0.24	0.17	—
G1	SG2M	0.01	0.58	0.10	0.58	0.25	0.04	0.35	0.05	—

2.3.1.2 CDC25B

Phase	Phase	R^2	p-val	Pearson	p-val	Kendall	p-val	Spearman	p-val	Signif
G1	S	0.05	0.30	0.23	0.30	0.17	0.29	0.24	0.29	—
G1	G2	0.02	0.53	0.14	0.53	0.16	0.31	0.21	0.36	—
G1	M	0.16	0.07	0.40	0.07	0.31	0.05	0.43	0.05	—
S	G2	0.04	0.39	0.19	0.39	0.11	0.50	0.18	0.41	—
S	M	0.26	0.01	0.51	0.01	0.38	0.01	0.50	0.02	yes
G2	M	0.05	0.31	0.23	0.31	0.19	0.22	0.26	0.23	—
G1	SG2M	0.07	0.24	0.26	0.24	0.21	0.18	0.31	0.16	—

2.3.1.3 CDC25B$^{\Delta \text{CDK}}$

Phase	Phase	R^2	p-val	Pearson	p-val	Kendall	p-val	Spearman	p-val	Signif
G1	S	0.01	0.56	-0.09	0.56	0.13	0.22	0.18	0.24	—
G1	G2	0.03	0.28	-0.17	0.28	-0.10	0.33	-0.19	0.21	—
G1	M	0.01	0.48	-0.11	0.48	-0.05	0.65	-0.09	0.58	—
S	G2	0.00	0.98	-0.00	0.98	-0.00	0.98	0.01	0.97	—
S	M	0.03	0.27	0.17	0.27	0.18	0.09	0.26	0.09	—
G2	M	0.01	0.59	0.08	0.59	0.01	0.93	0.03	0.84	—
G1	SG2M	0.02	0.34	-0.14	0.34	0.02	0.85	0.02	0.92	—

2.3.2   Graphics for CONTROL
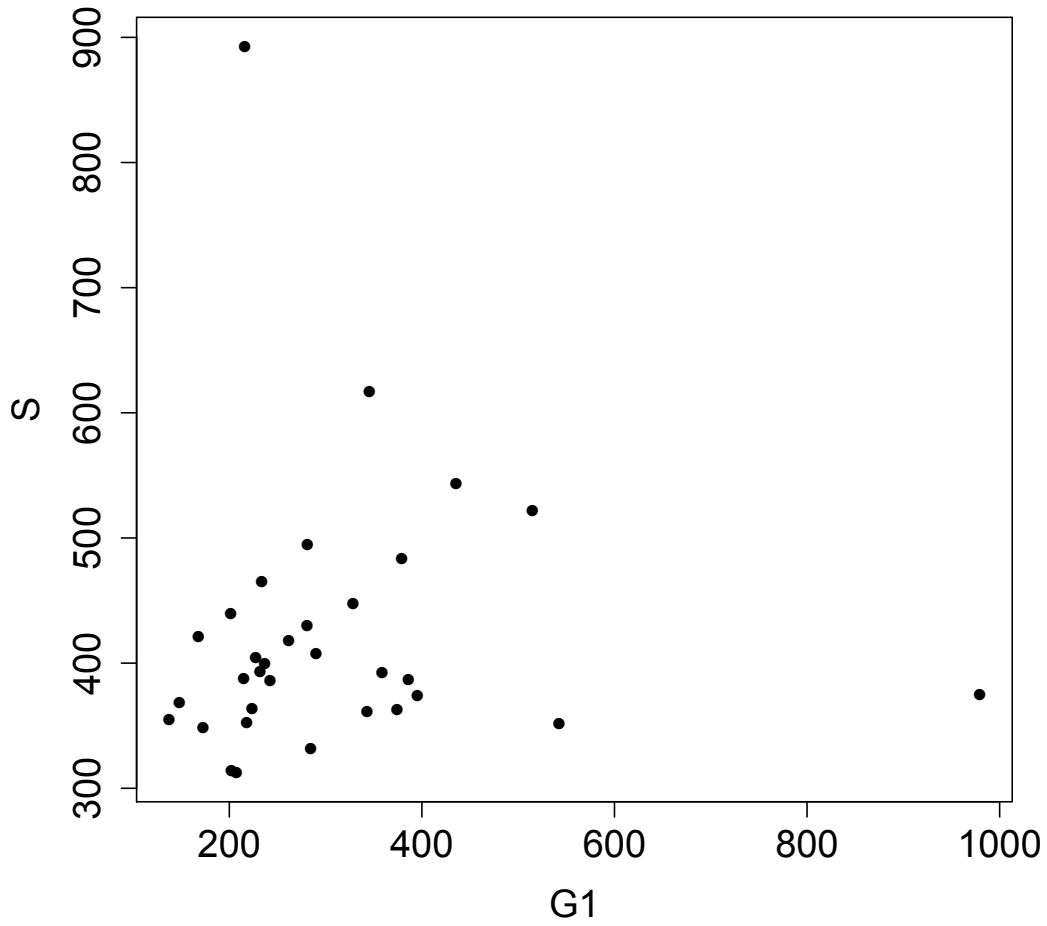
Fig. S8. CTL : S duration vs. G1 duration
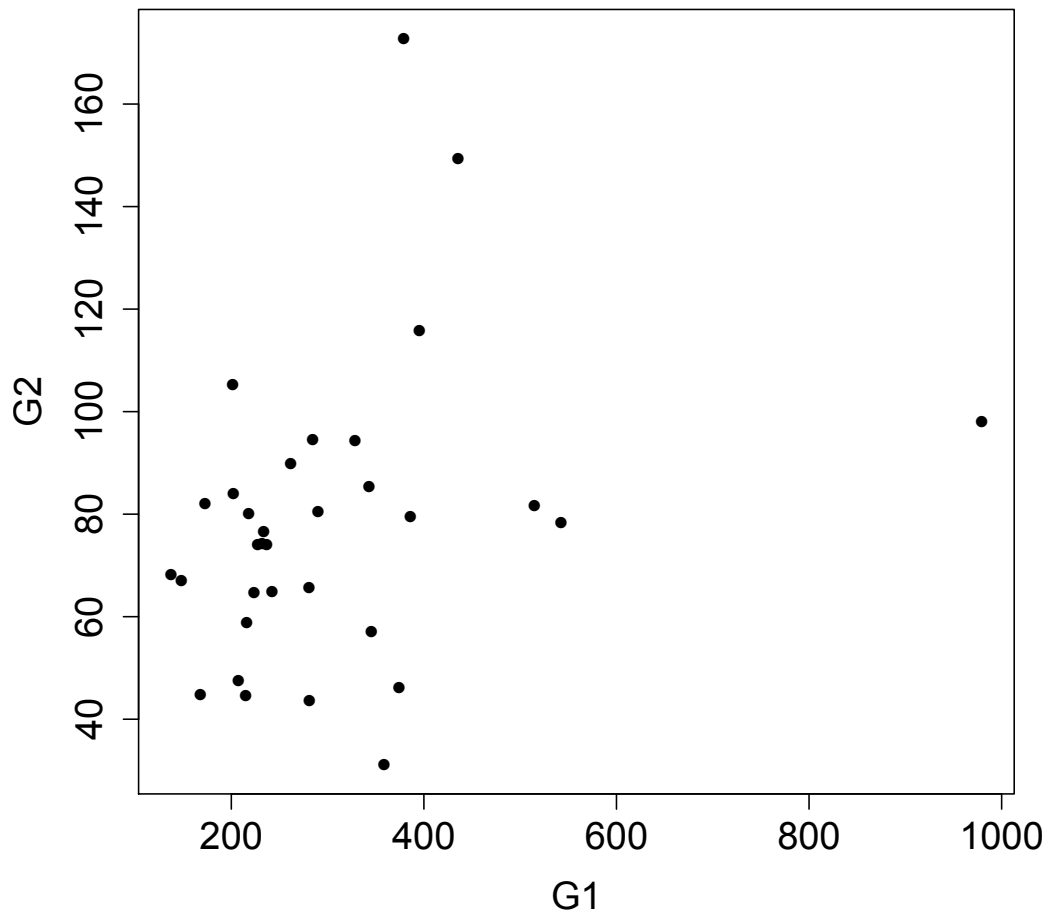
Fig. S9. CTL : G2 duration vs. G1 duration
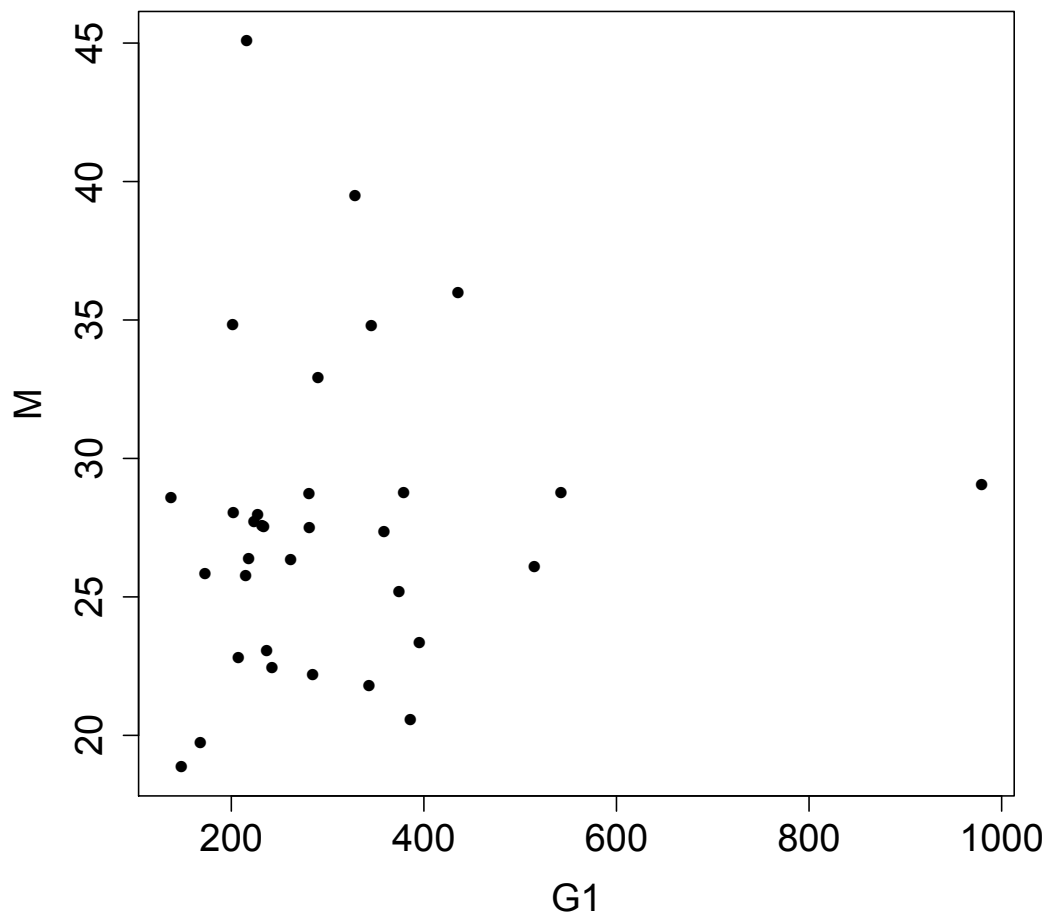
Fig. S10. CTL : M duration vs. G1 duration
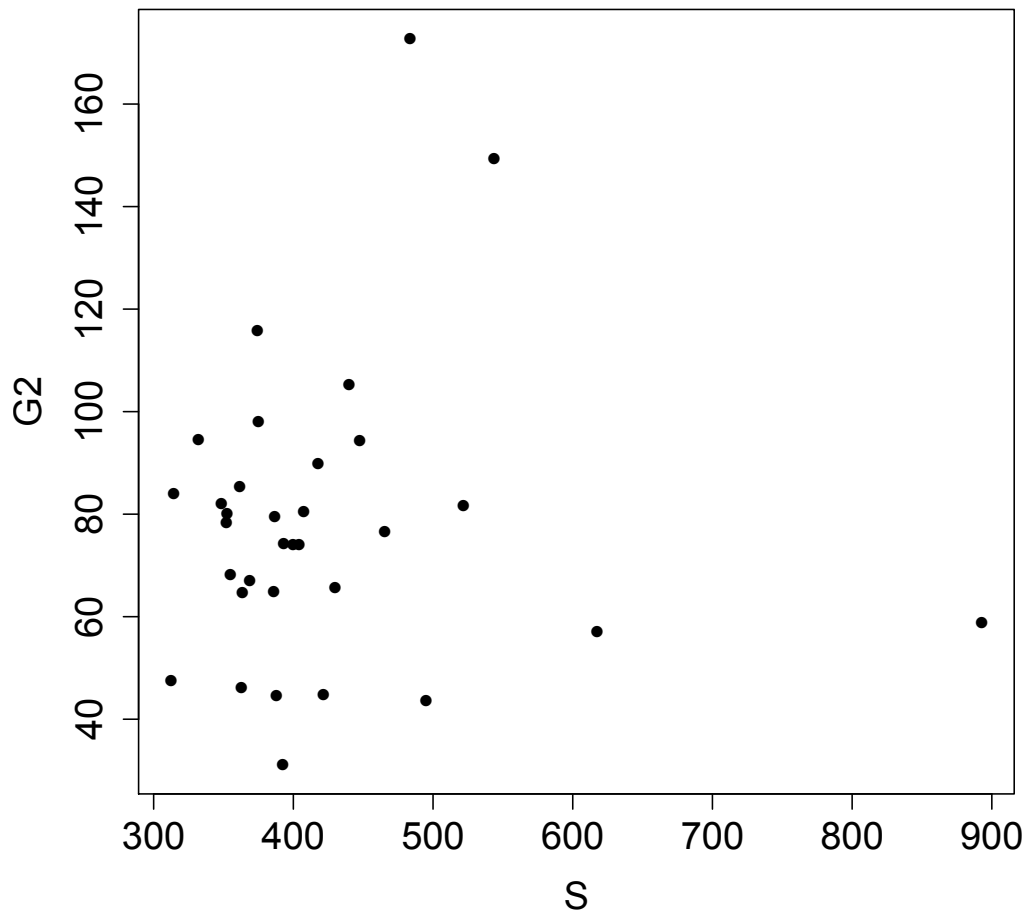
Fig. S11. CTL : G2 duration vs. S duration
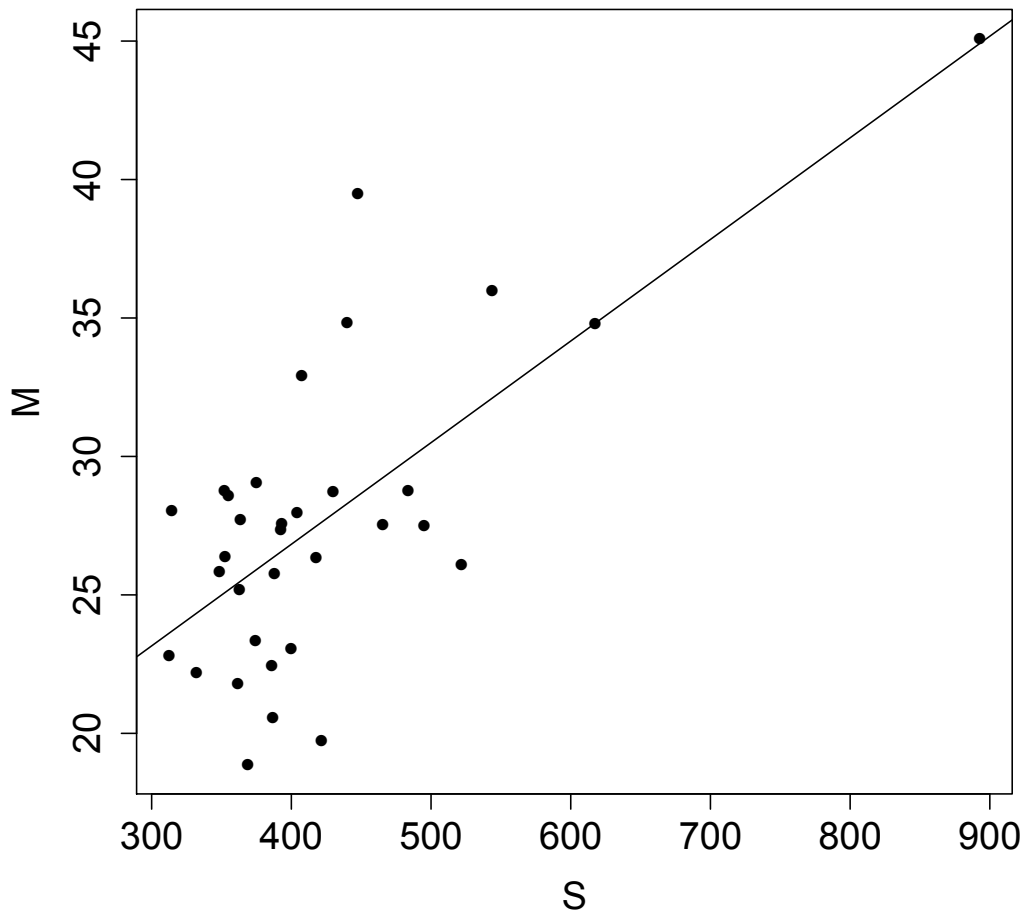
Fig. S12. CTL : M duration vs. S duration
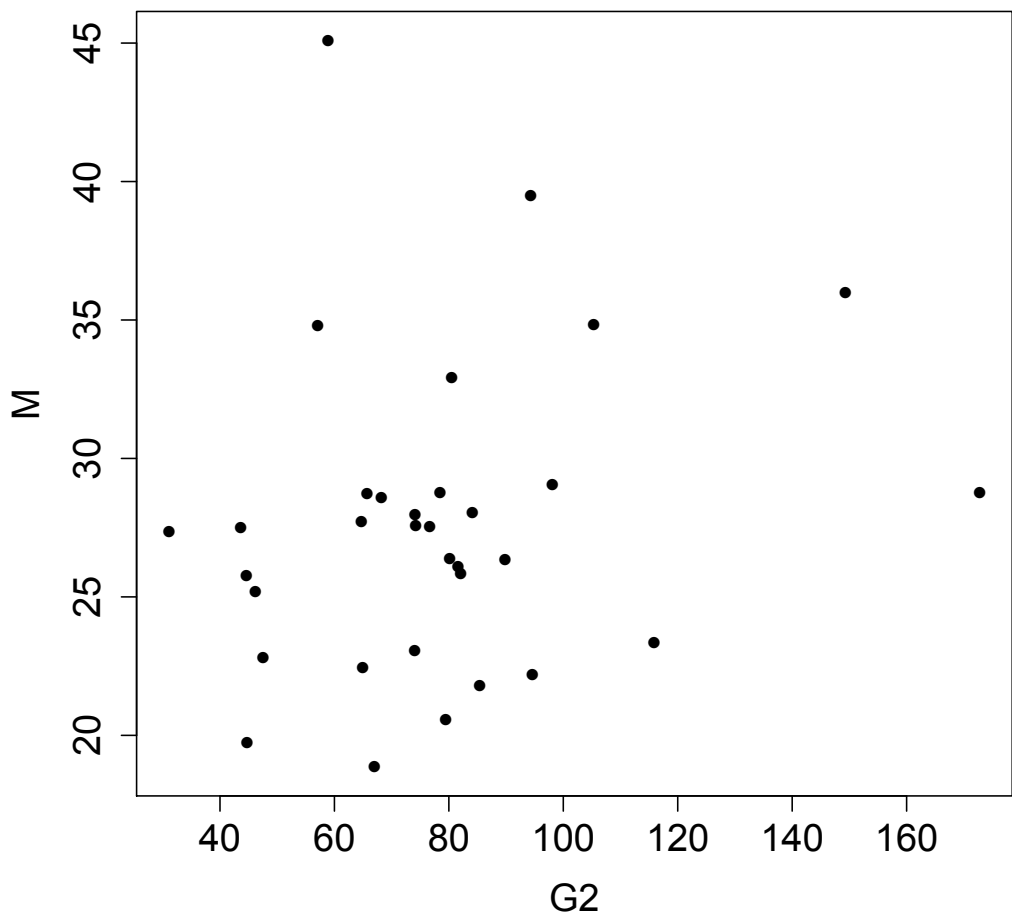
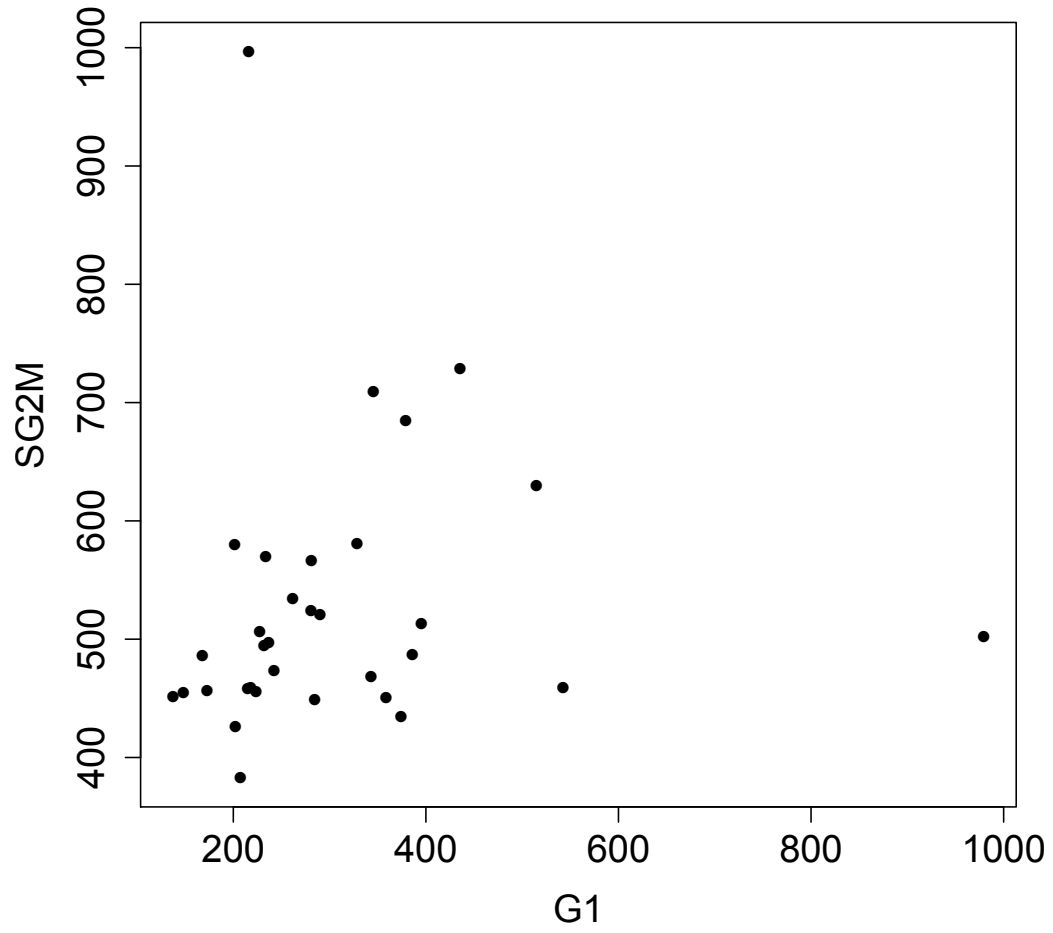**Fig. S13.** CTL : M duration vs. G2 duration

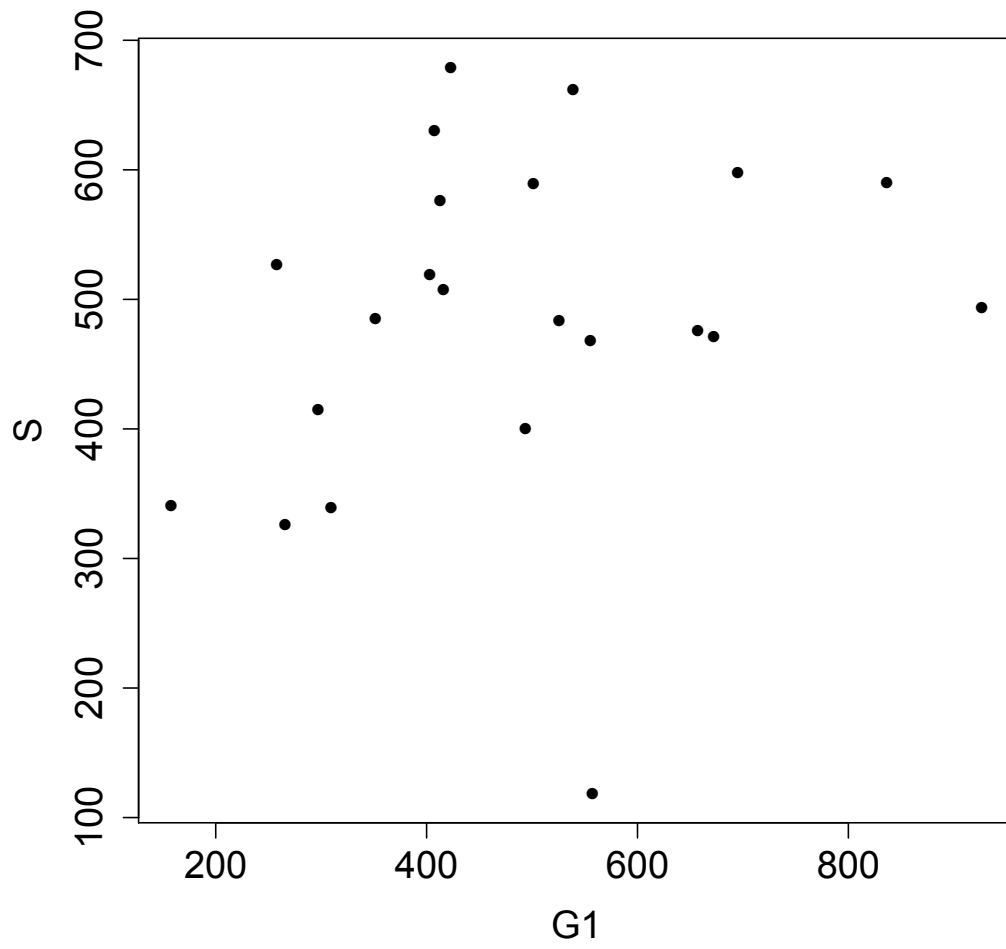**Fig. S14.** CTL : S+G2+M duration vs. G1 duration

2.3.3 Graphics for CDC25B
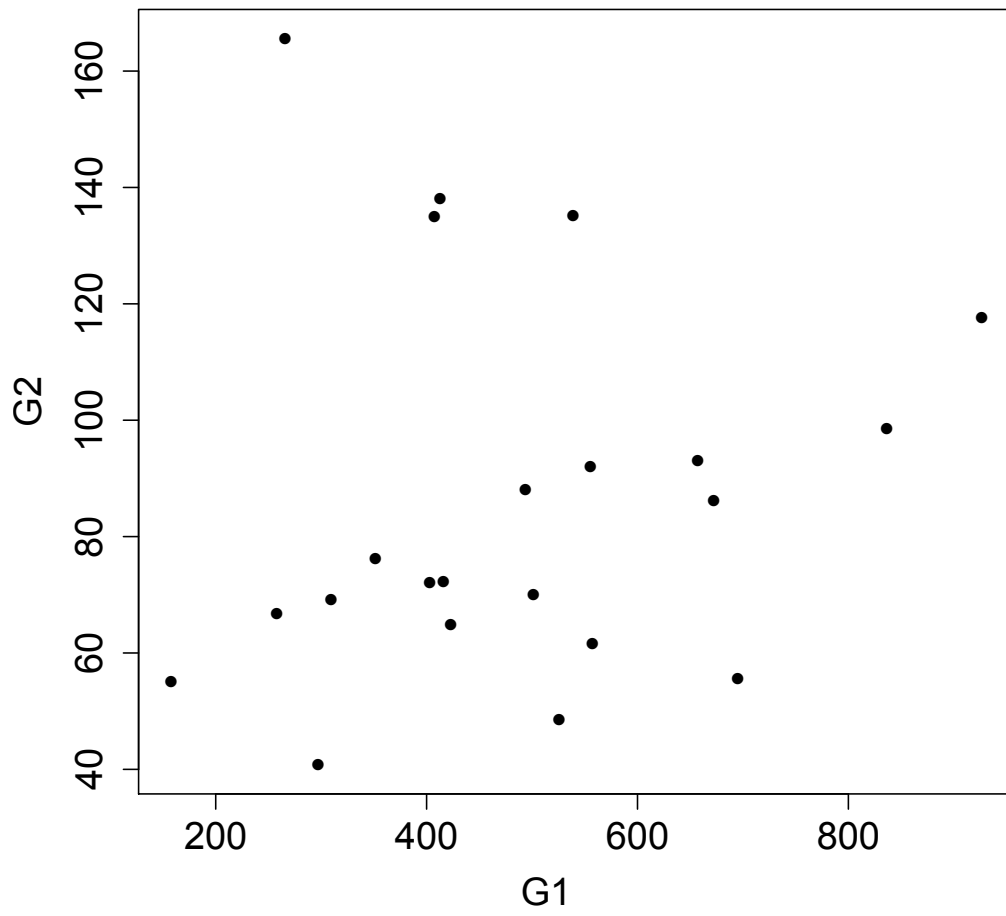

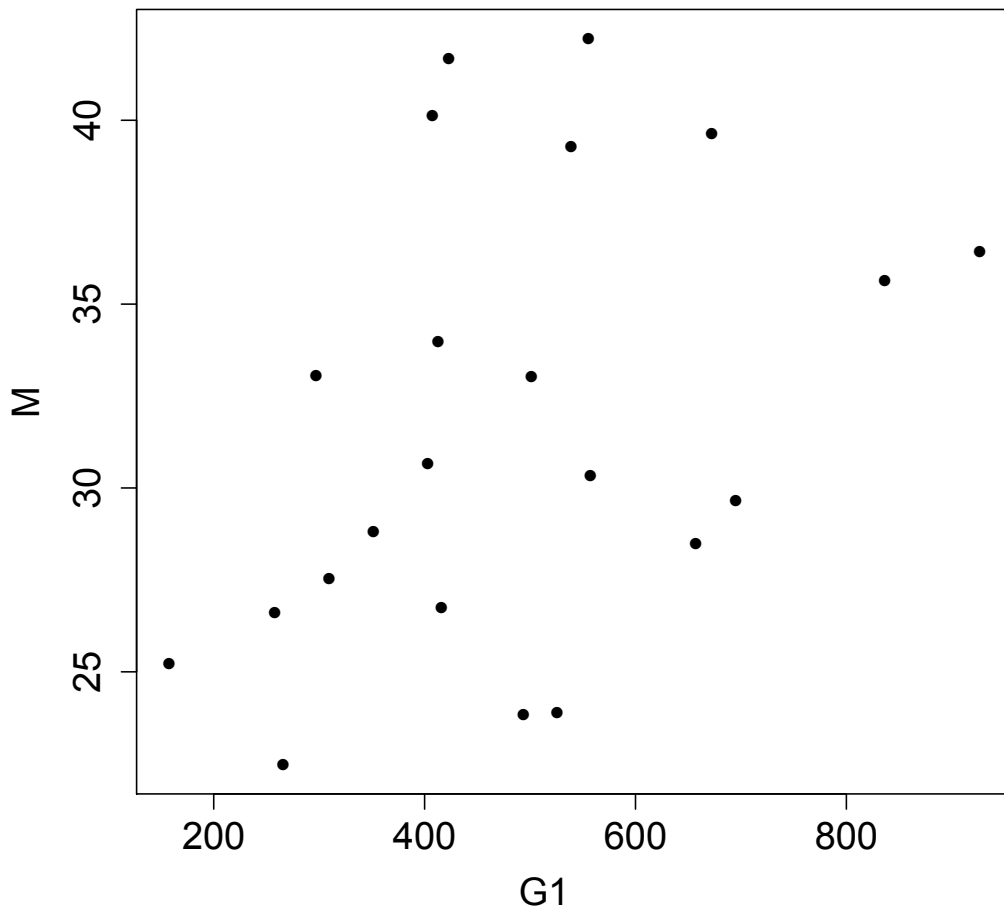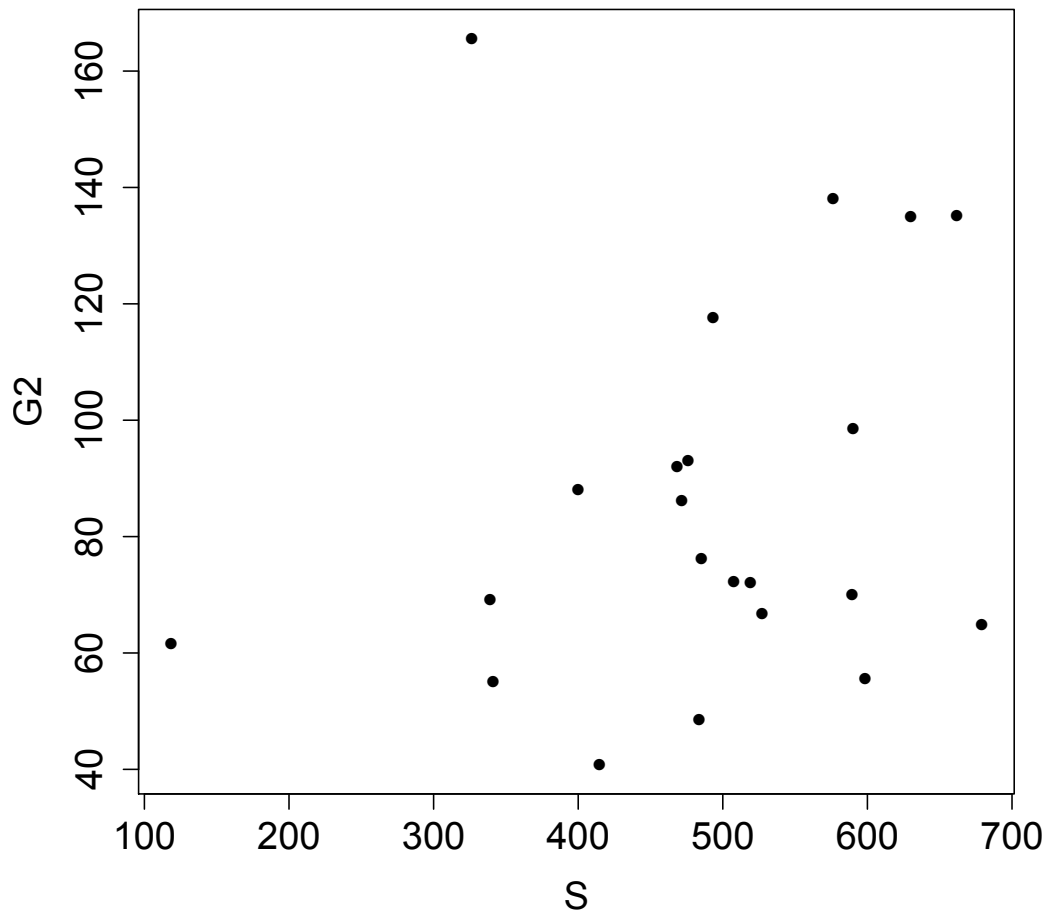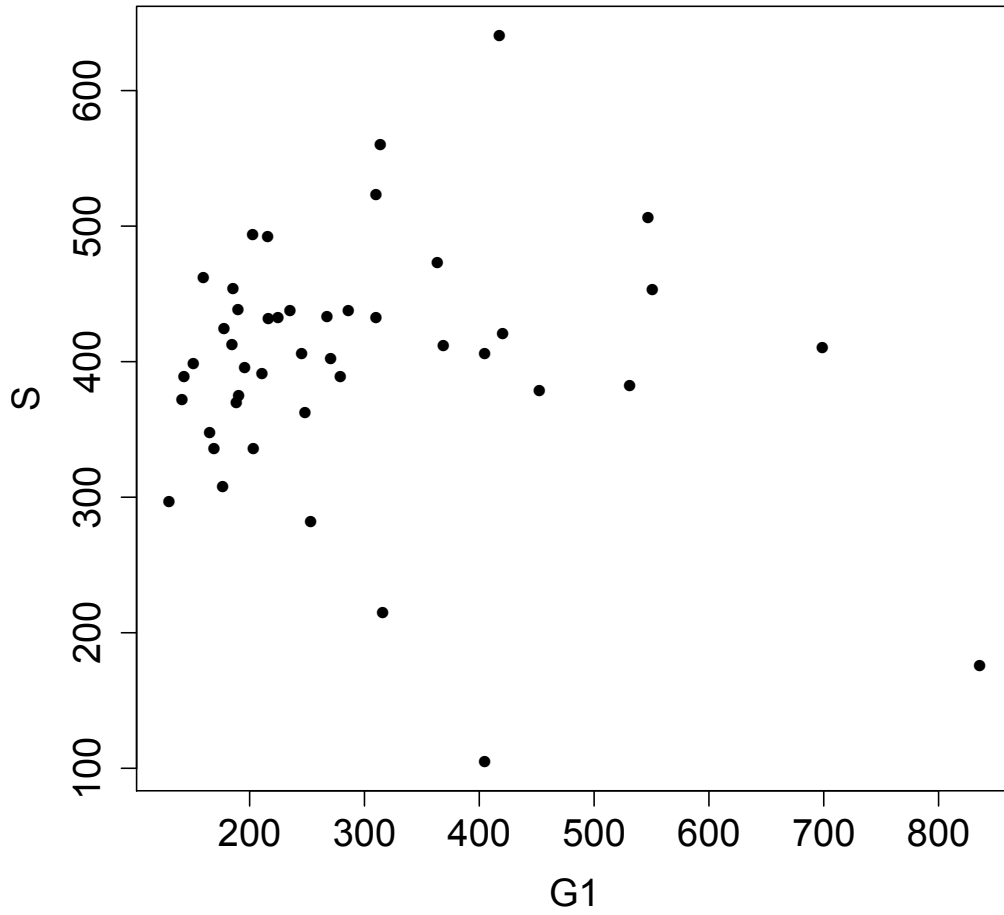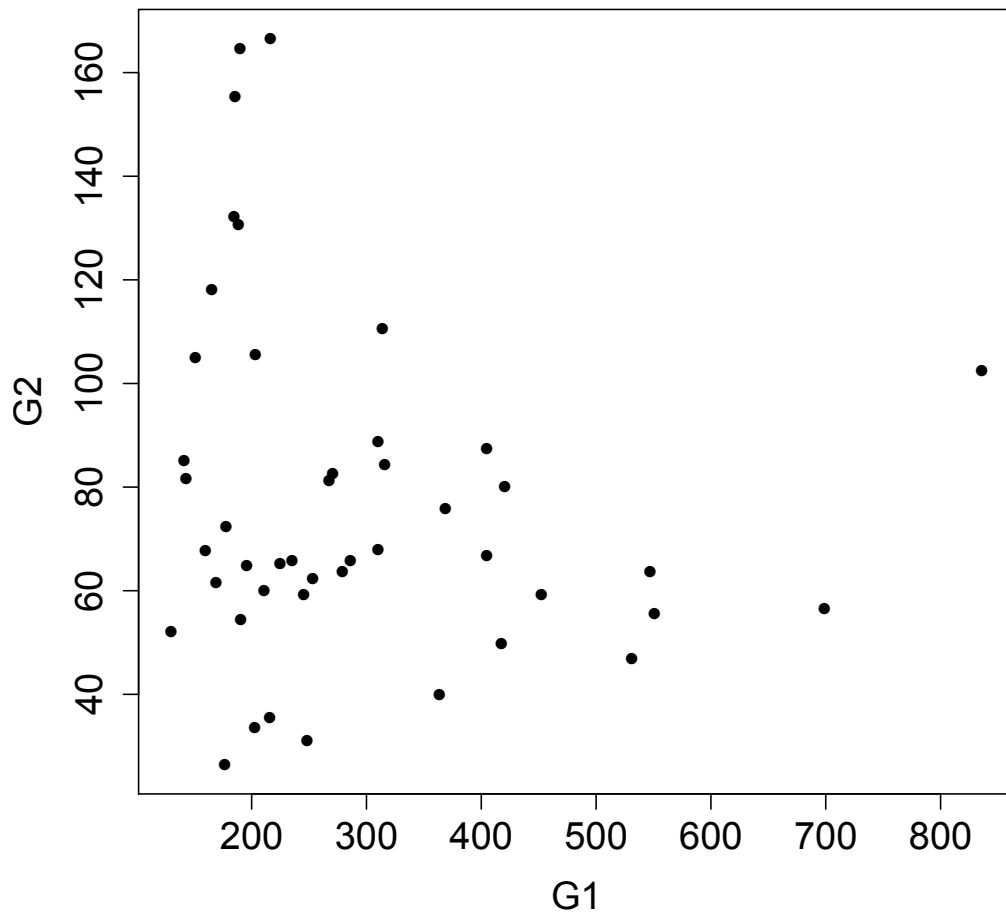**Fig. S15.** CDC25B : S duration vs. G1 duration

Fig. S16. CDC25B : G2 duration vs. G1 duration

Fig. S17. CDC25B : M duration vs. G1 duration

Fig. S18. CDC25B : G2 duration vs. S duration
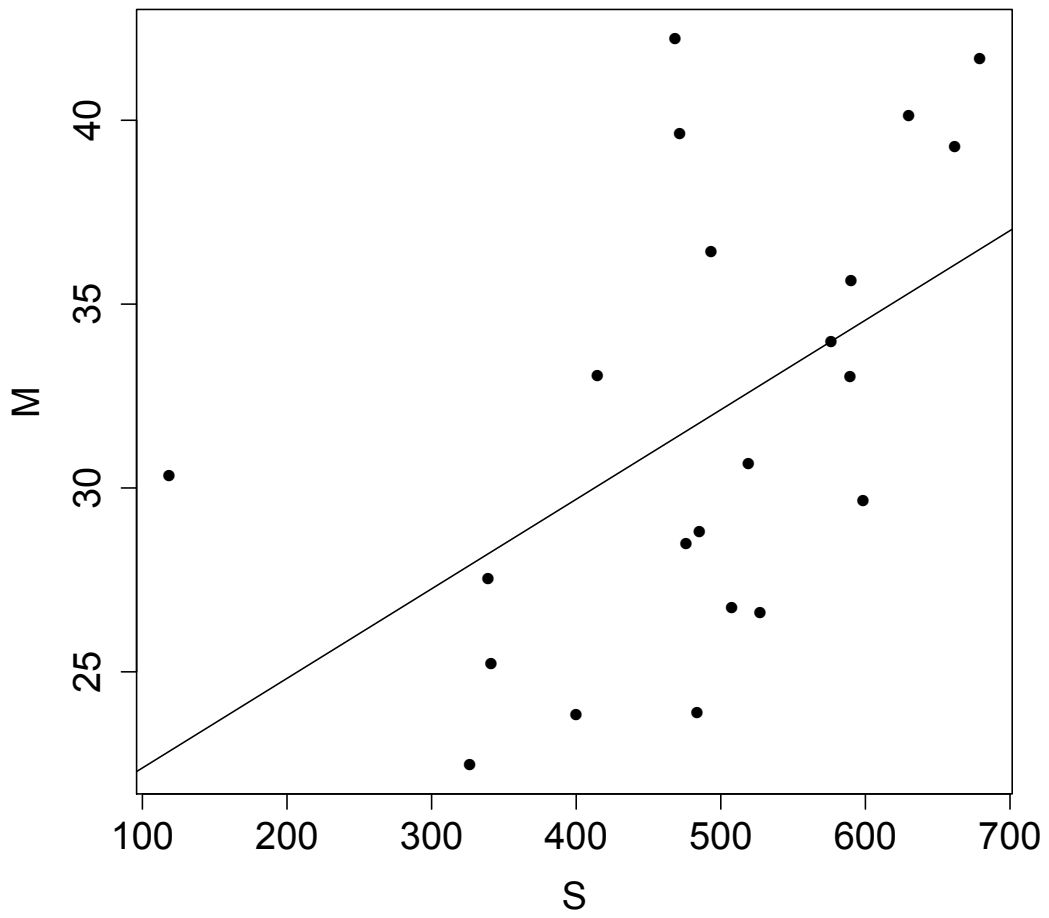
Fig. S19. CDC25B : M duration vs. S duration
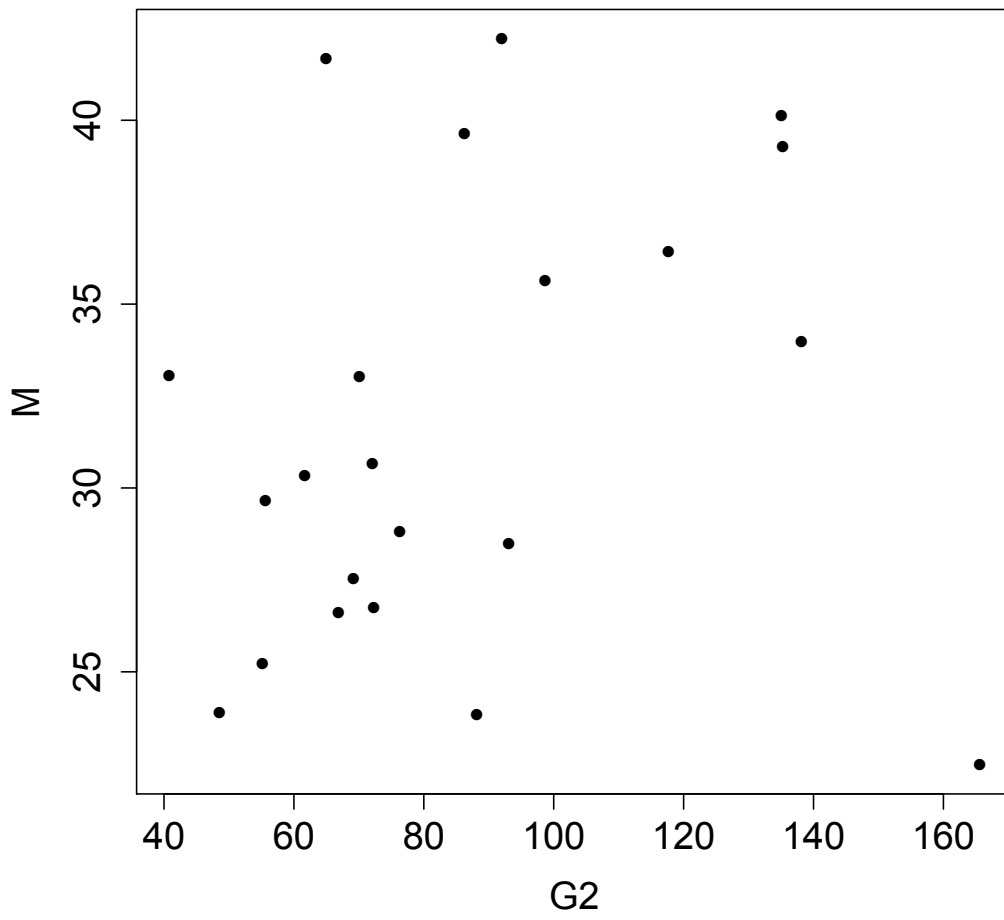
Fig. S20. CDC25B : M duration vs. G2 duration
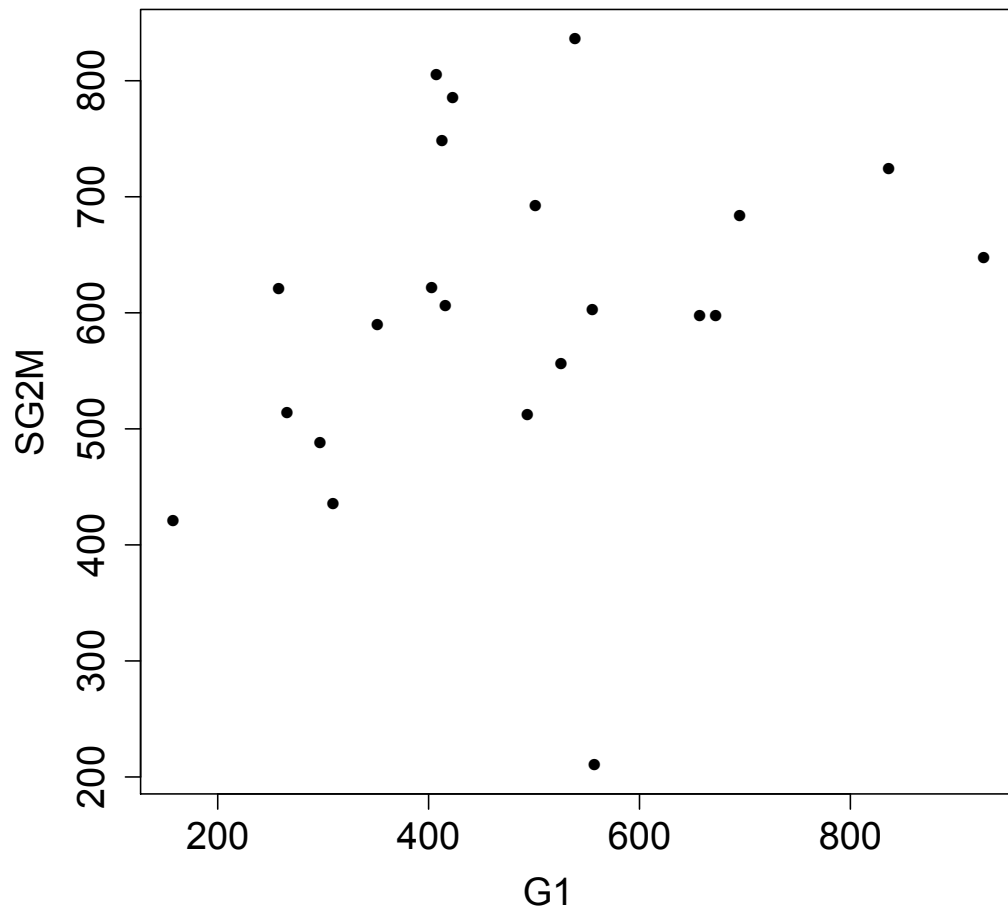
Fig. S21. CDC25B : S+G2+M duration vs. G1 duration

2.3.4 Graphics for $\mathrm{CDC25B}^{\Delta\mathrm{CDK}}$

Fig. S22. DeltaCDK : S duration vs. G1 duration

Fig. S23. DeltaCDK : G2 duration vs. G1 duration
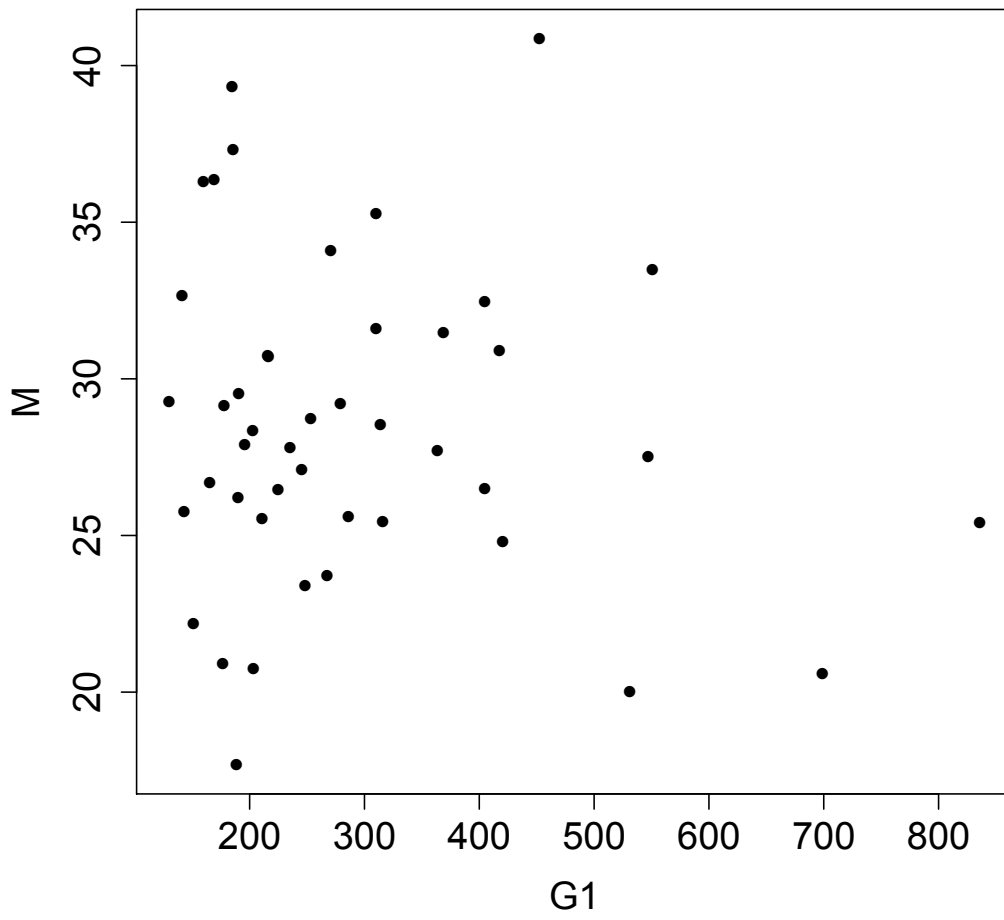
Fig. S24. DeltaCDK : M duration vs. G1 duration
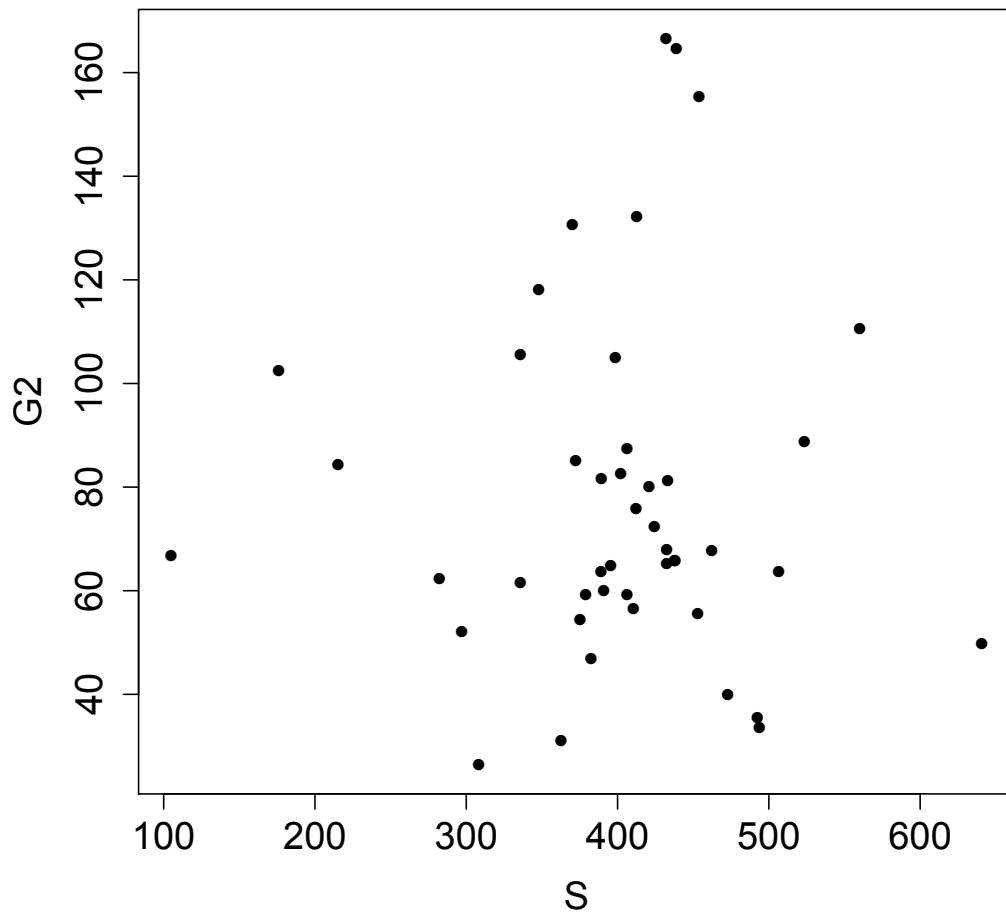
Fig. S25. DeltaCDK : G2 duration vs. S duration
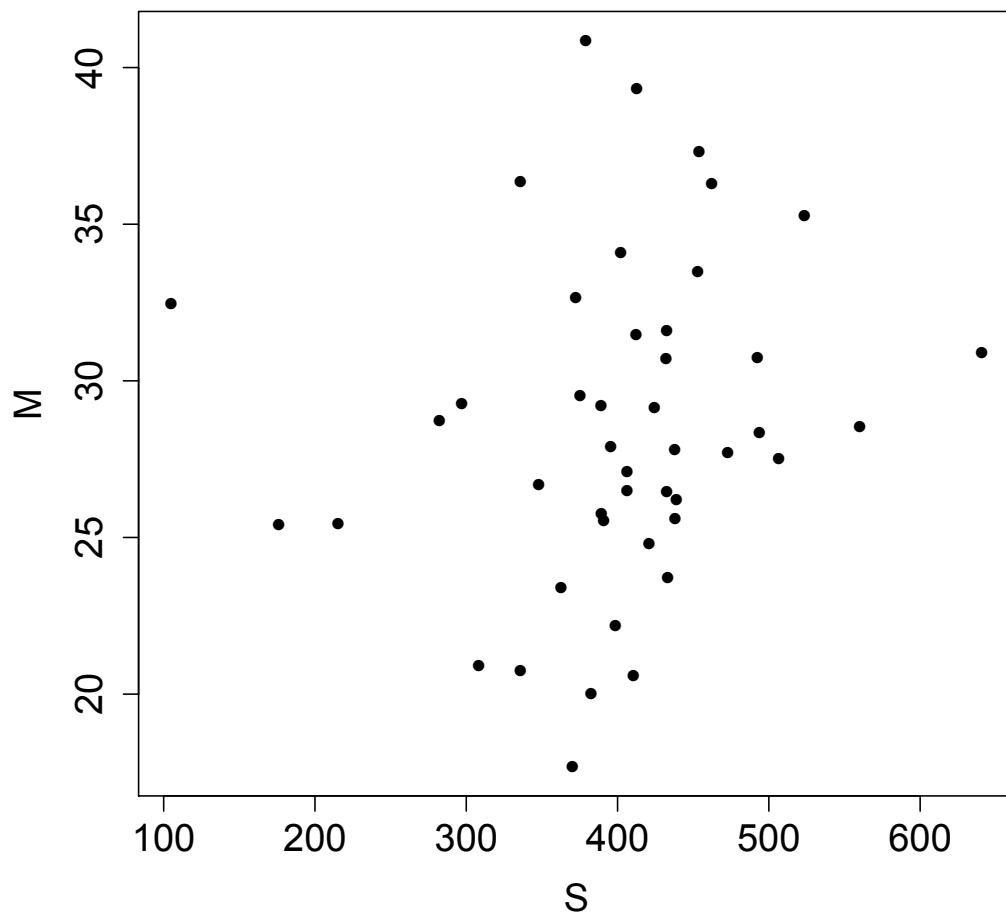
Fig. S26. DeltaCDK : M duration vs. S duration
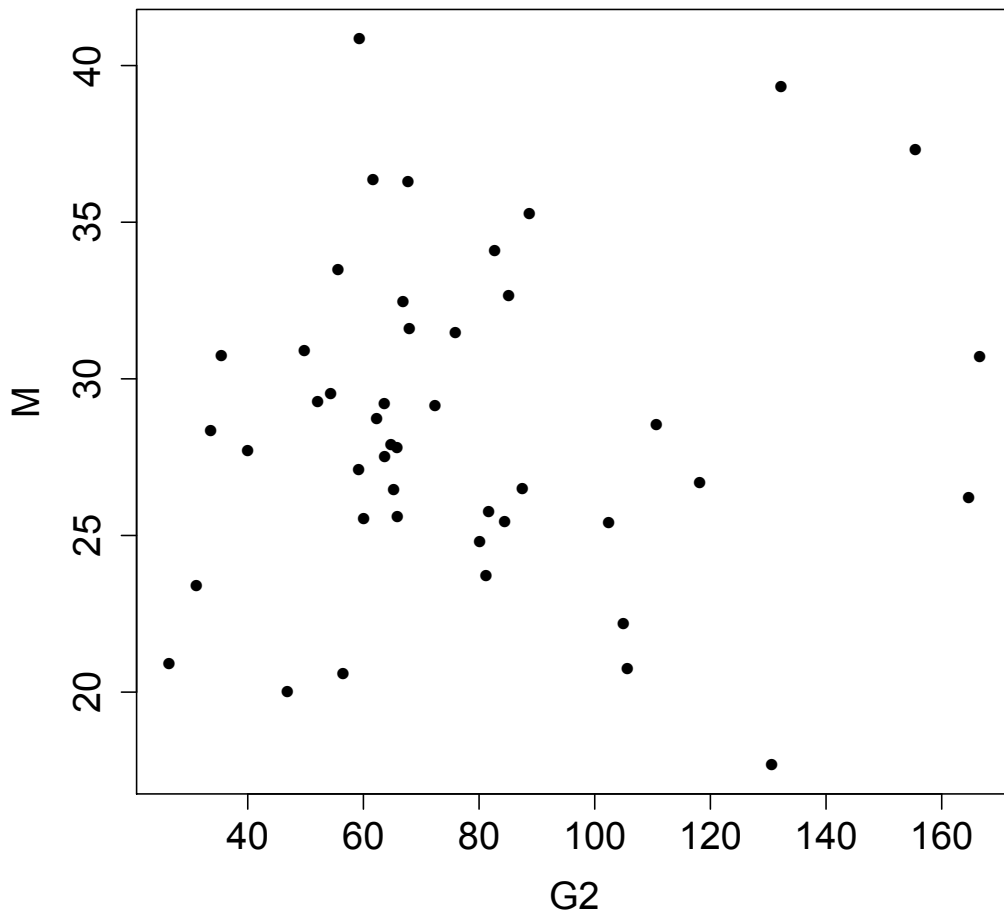
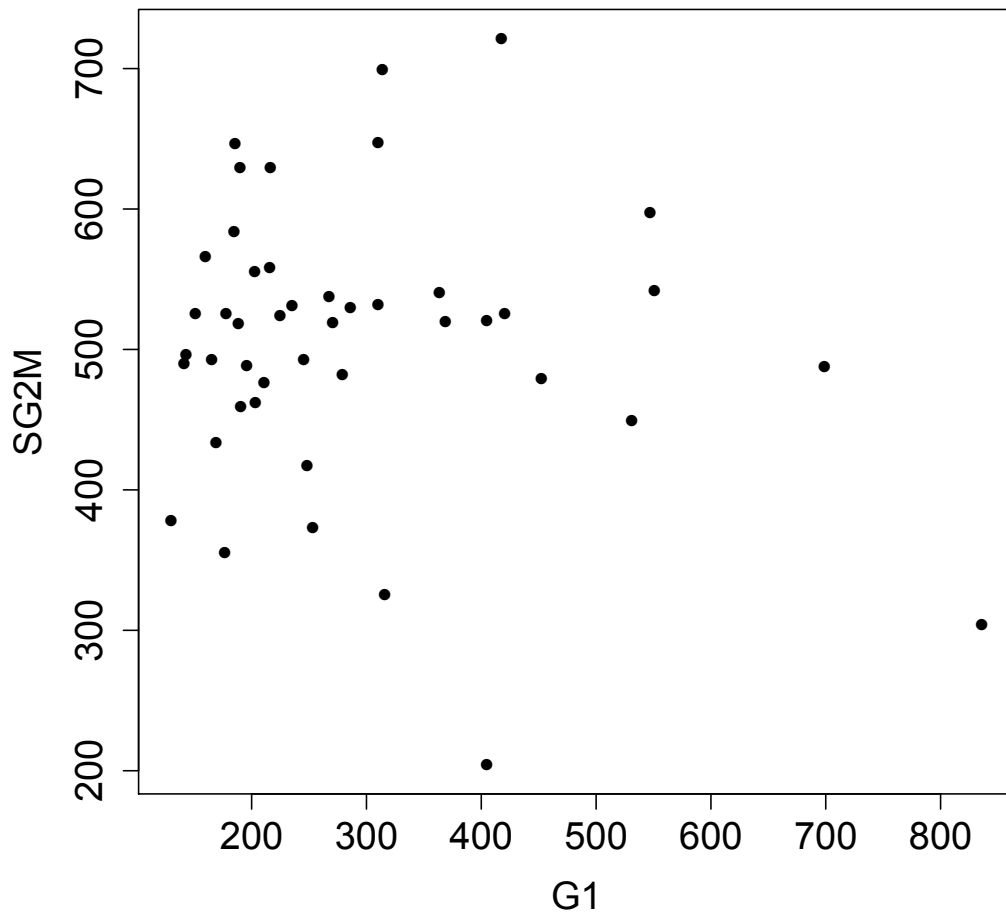**Fig. S27.** DeltaCDK : M duration vs. G2 duration

Fig. S28. DeltaCDK : S+G2+M duration vs. G1 duration

2.4 Predicted survival curves for total duration under independence hypothesis.

Survival curves for total duration Tc will be used to comfort the observation that phase durations are not correlated.

For this, we can compare the observed distribution of total durations to a theoretical model established under the null hypothesis of no correlation among phases duration.

However, such a theoretical model can be obtained only for restrictive condition and is used here only for CTL condition.

An alternative is to build a theoretical distribution using the data (Monte Carlo permutations).

2.4.1 Theoretical *null* model for total duration

Under the hypotheses that phase durations are independent from each other, and that exit time from each phase is a pure memoryless random process, we have a theoretical model for the statistical distribution of the total duration as a sum of four exponential distributions, each with its own parameter. Let denote R_i the *exit rates* (the inverse of the average exit time), then the survival function of total exit rate would follow:

$$S(t) = 1 - \left[\prod_{i=1}^{4} R_i \right] \sum_{i=1}^{4} \frac{e^{-R_i t}}{\prod_{k=1, \neq i}^{n} (R_k - R_i)}$$

See : Bibinger, M. (2013). Notes on the sum and maximum of independent exponentially distributed random variables with different scale parameters. https://arxiv.org/abs/1307.3945)

The expected distribution of Tc is obtained by adding the sum of the four minimal durations to this.

2.4.2 Null model by Monte Carlo permutation

Inspired from Monte Carlo permutation tests, the expected distribution of Tc under phase duration independence hypothesis can be built from data by random picking among observed values (mixing among the observed cycles). If there were some kind of compensation between phases within cycles to ensure some regulation of Tc, then the distribution of total duration would be more homogeneous that the one obtained by such random permutation : the slope of survival curve for observed data would be steeper than survival curve of random sampling.

2.4.3 Ordered permutations with full anti-correlation between G1 and S+G2+M

To illustrate how compensation of duration between G1 phase and the other phases would affect the survival curve and a more homogeneous series, we build the extreme case where the durations would be perfectly anti-correlated. To do this, we pair the G1 series sorted in ascending order with the S+G2+M series sorted in descending order.

2.5   Survival curves for phase exit time in each condition.

Here we check whether exponential decay could apply.
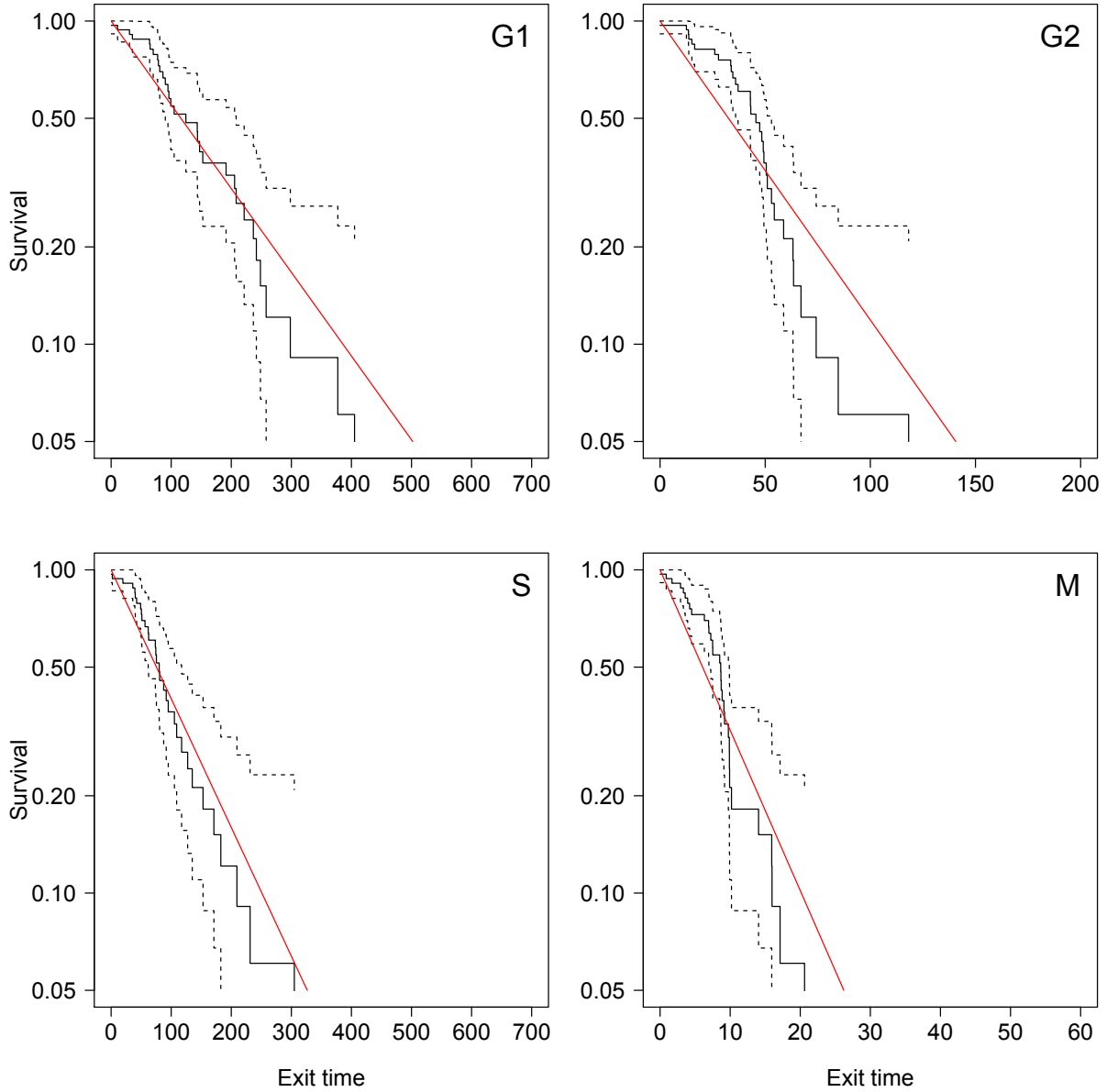
2.5.1   CONTROL

Fig. S29. Phases Survival curves for exit time. If we substract the minimal duration, the exit time process seems compatible with an exponential decay (pure random memoryless process)
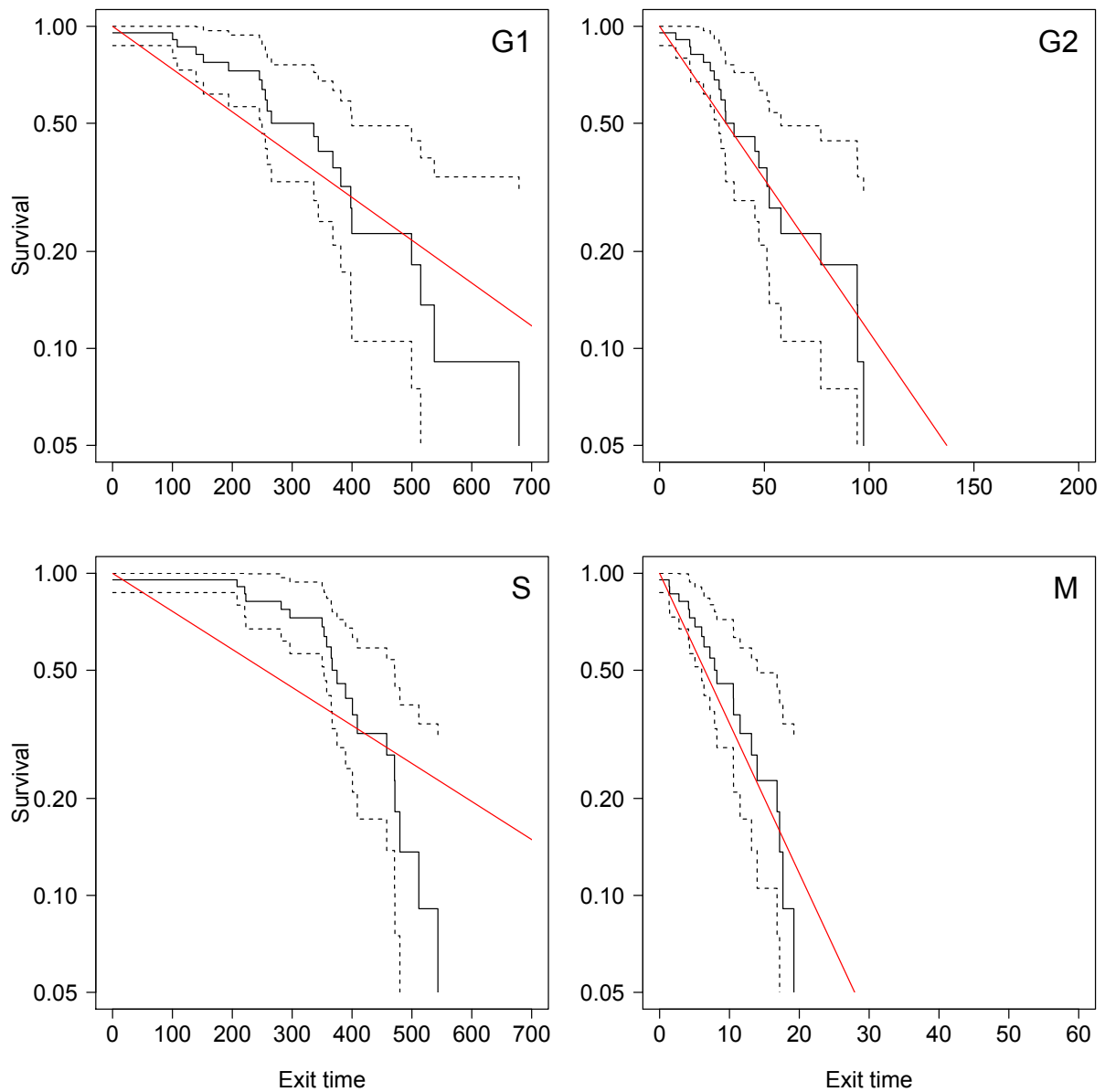
2.5.2 CDC25B

Fig. S30. Phases Survival curves. The exit time process for S phase does not fit an exponential decay (accelerated process)
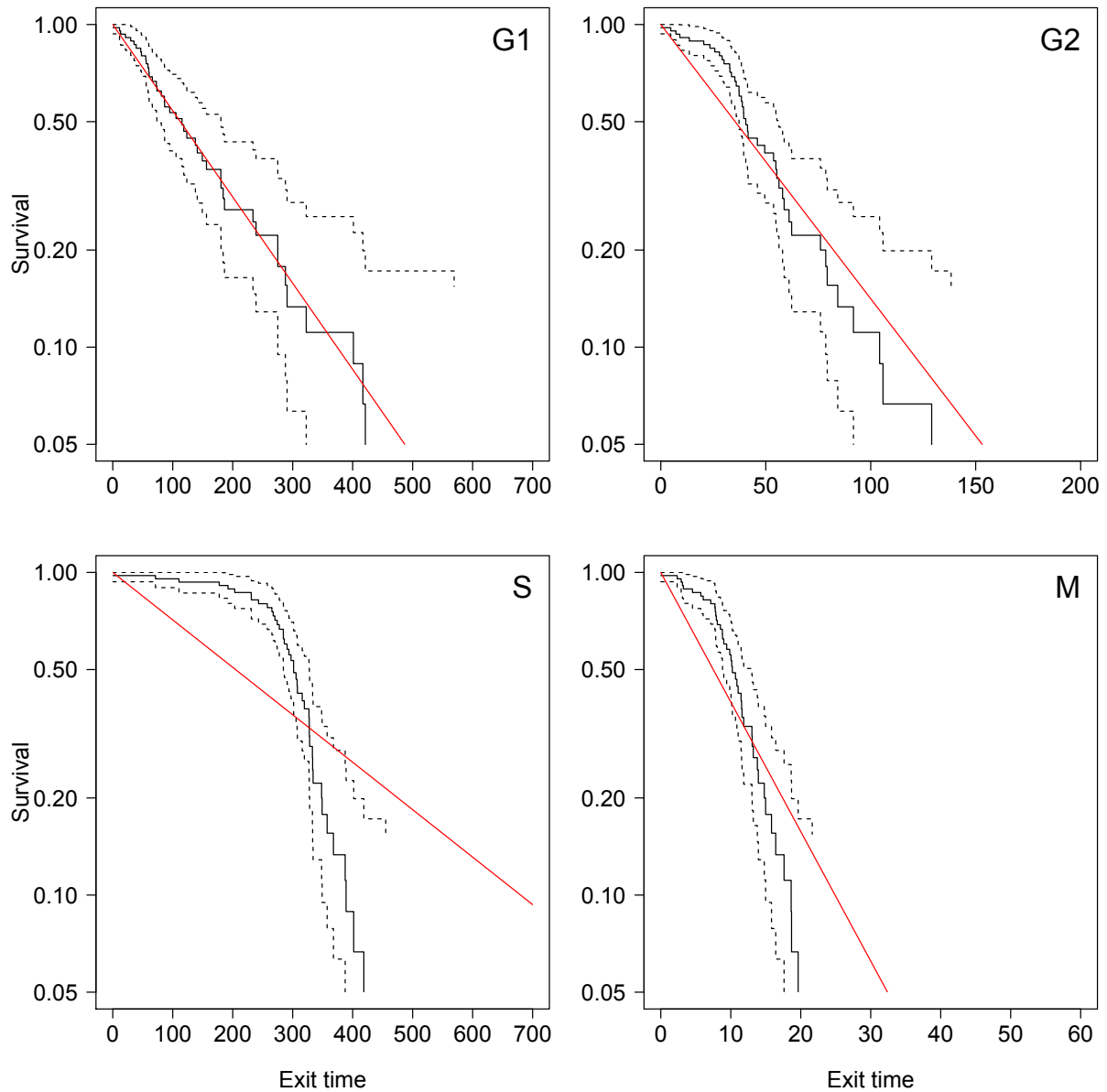
2.5.3 CDC25B$^{\Delta CDK}$

Fig. S31. Phases Survival curves. The exit time process for S phase does not fit an exponential decay (accelerated process)

34

2.6 Survival curves for Tc.

2.6.1 CONTROL

Data vs. Random sampling of phases

```
    Two-sample Kolmogorov-Smirnov test

data:  data and random
D = 0.10717, p-value = 0.8444
alternative hypothesis: two-sided
```
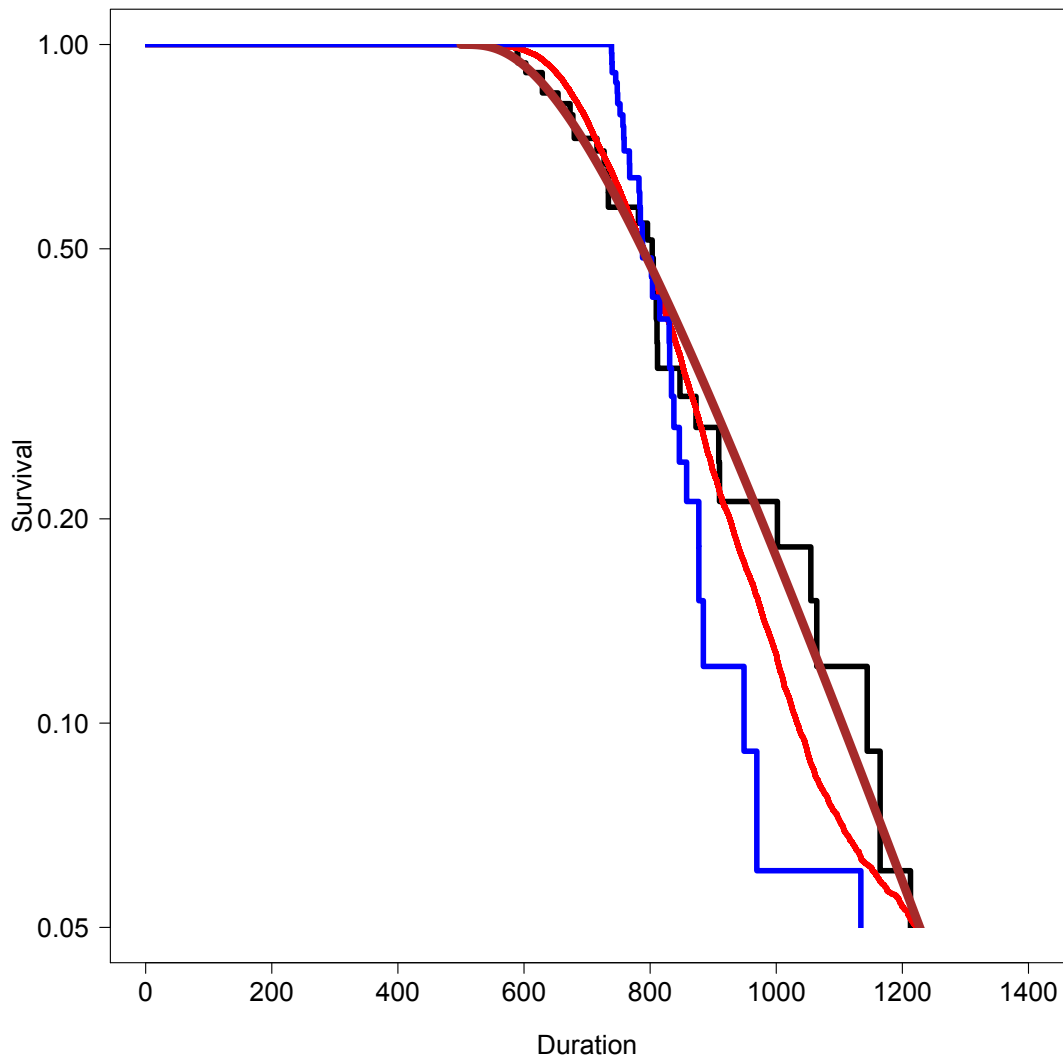
Data vs. anti-correlated

```
    Two-sample Kolmogorov-Smirnov test

data:  data and anticor
D = 0.42424, p-value = 0.004793
alternative hypothesis: two-sided
```


Supplemental Figure S32: Tc Survival curve. Brown curve indicates the theoretical prediction of the null model of phase duration independence. Red curve indicates the survival obtained by Monte Carlo permutations of phase durations from the data set (10^4 samples). Blue curve indicates the survival for the anti-correlated pairing.

2.6.2   CDC25B
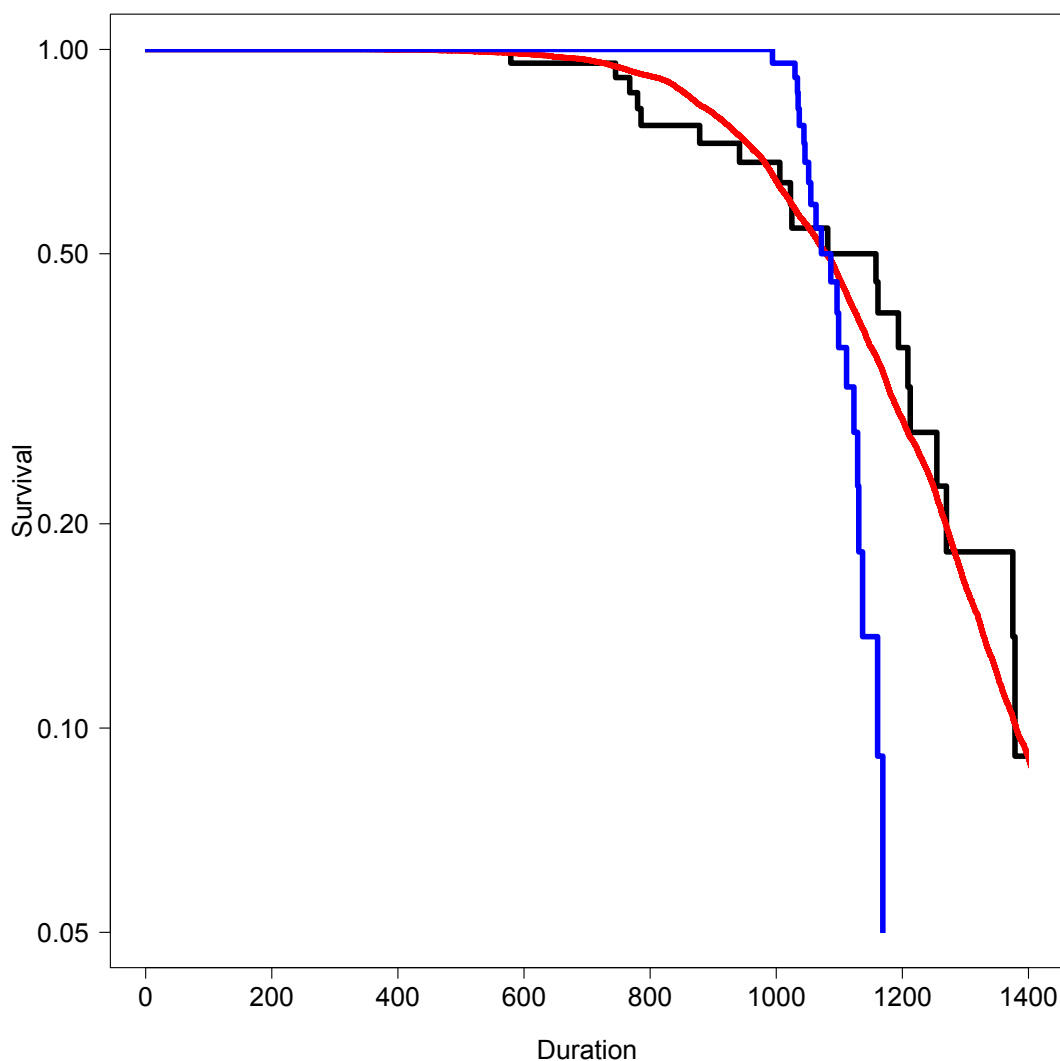
Data vs. Random sampling of phases

```
    Two-sample Kolmogorov-Smirnov test

data:  data and random
D = 0.10717, p-value = 0.8444
alternative hypothesis: two-sided
```

Data vs. anti-correlated

```
    Two-sample Kolmogorov-Smirnov test

data:  data and anticor
D = 0.42424, p-value = 0.004793
alternative hypothesis: two-sided
```


Supplemental Figure S33: Tc Survival curve. Since the survival curves for phase durations do not match exponential decay, the theoretical null model does not apply and is not shown. Red curve indicates the survival of total lengths obtained by Monte Carlo permutations of phase durations from the data set. Blue curve indicates the survival for the anti-correlated pairing.

2.6.3   CDC25B$^{\Delta\text{CDK}}$

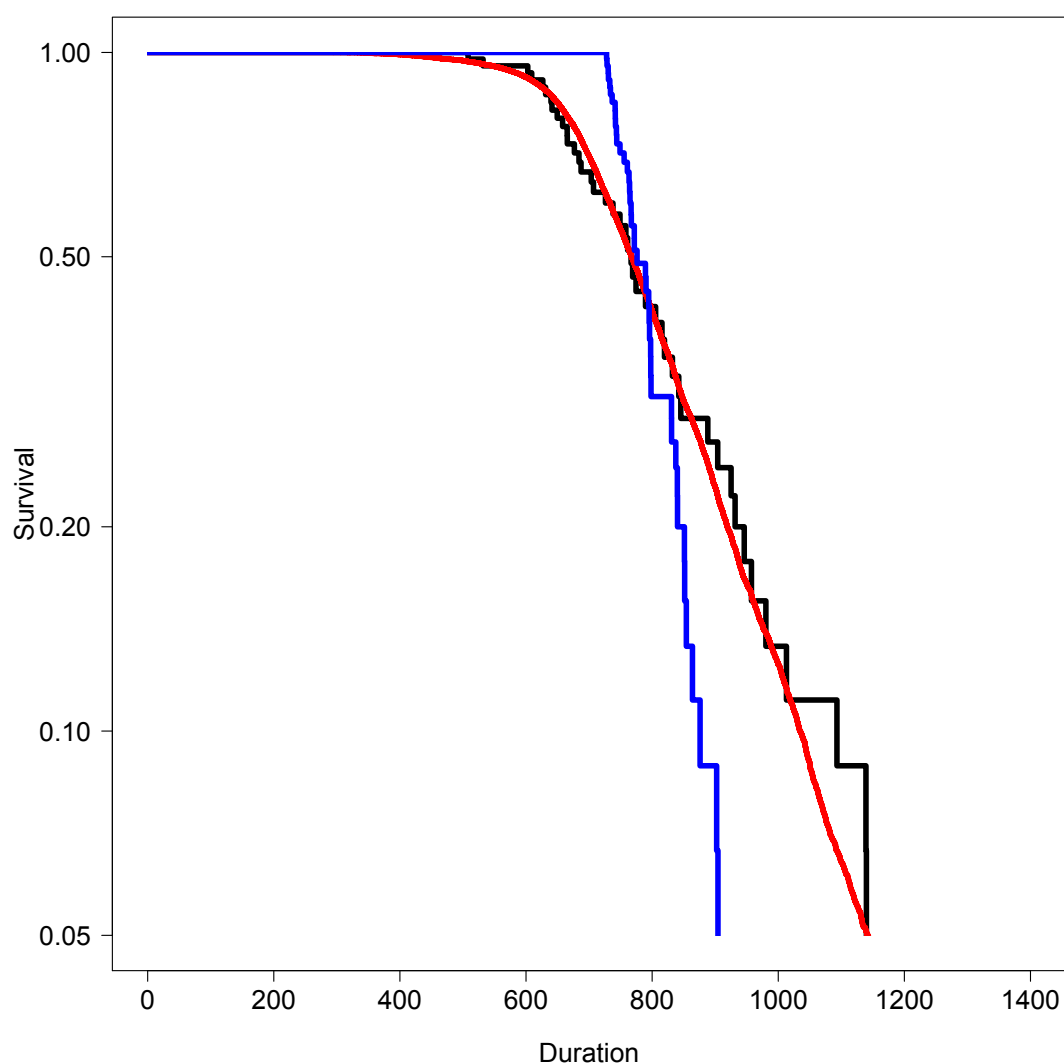Data vs. Random sampling of phases

 Two-sample Kolmogorov-Smirnov test

data: data and random
D = 0.10717, p-value = 0.8444
alternative hypothesis: two-sided

Data vs. anti-correlated

 Two-sample Kolmogorov-Smirnov test

data: data and anticor
D = 0.42424, p-value = 0.004793
alternative hypothesis: two-sided

Supplemental Figure S34: Tc Survival curve. Since the survival curves for phase durations do not match exponential decay, the theoretical null model does not apply and is not shown. Red curve indicates the survival of total lengths obtained by Monte Carlo permutations of phase durations from the data set. Blue curve indicates the survival for the anti-correlated pairing.

3 Survival Analysis for the experimental treatment

For each condition, we report two graphical representations : a histogram representation (vertical dotted line reports the average of the distribution) and the corresponding survival curves.

The p-value of the survival test is given by the Score (logrank) test.

The output of Cox Proportional Hazard test is given for information to indicate the order of ratio between rates (e.g. exp(coef)=0.5 for CDC25B factor indicates that the exit rate is twice as slow as the baserate (CONTROL)).

For the sake of graphical clarity, confidence intervals are not reported.

For survival analysis of Tc, only cells with fully tracked cycles are used.

3.1 Tc
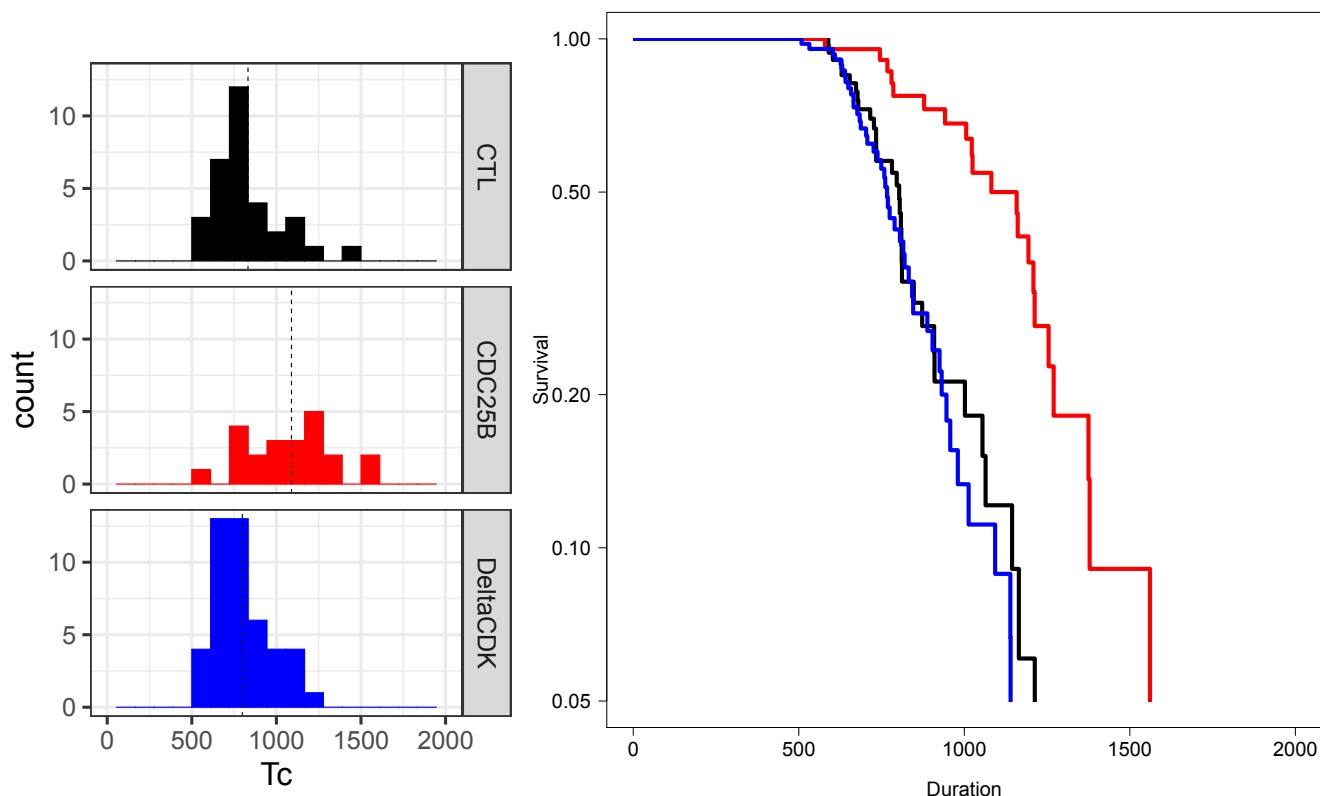

```
Call:
coxph(formula = Surv(dt$Tc, dt$sta) ~ dt$Condition)

  n= 100, number of events= 100
   (128 observations deleted due to missingness)


                     coef exp(coef) se(coef)       z Pr(>|z|)
dt$ConditionCDC25B  -1.0393    0.3537   0.2932 -3.544 0.000394 ***
dt$ConditionDeltaCDK 0.2690    1.3086   0.2352  1.144 0.252695
---
Signif. codes:  0 '***' 0.001 '**' 0.01 '*' 0.05 '.' 0.1 ' ' 1


                  exp(coef) exp(-coef) lower .95 upper .95
dt$ConditionCDC25B    0.3537     2.8273    0.1991    0.6284
dt$ConditionDeltaCDK  1.3086     0.7641    0.8254    2.0749

Concordance= 0.615  (se = 0.031 )
Likelihood ratio test= 23.66  on 2 df,   p=7e-06
Wald test            = 20.13  on 2 df,   p=4e-05
Score (logrank) test = 21.74  on 2 df,   p=2e-05
```
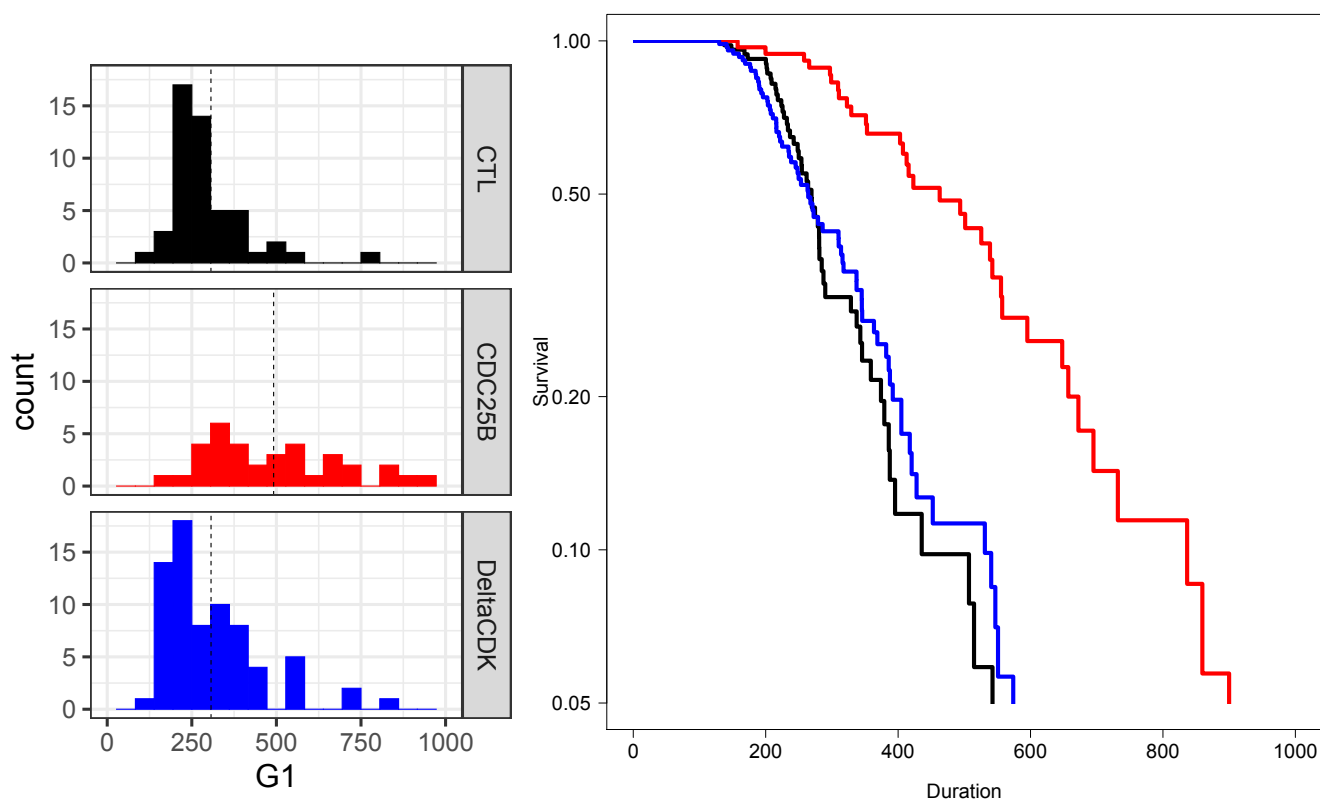
3.2   G1


```
Call:
coxph(formula = Surv(dt$G1, dt$sta) ~ dt$Condition)

  n= 157, number of events= 157
   (71 observations deleted due to missingness)


                      coef exp(coef) se(coef)      z Pr(>|z|)
dt$ConditionCDC25B  -0.88337   0.41339  0.22647 -3.901  9.6e-05 ***
dt$ConditionDeltaCDK 0.01138   1.01145  0.18672  0.061    0.951
---
Signif. codes:  0 '***' 0.001 '**' 0.01 '*' 0.05 '.' 0.1 ' ' 1


                  exp(coef) exp(-coef) lower .95 upper .95
dt$ConditionCDC25B     0.4134     2.4190    0.2652    0.6444
dt$ConditionDeltaCDK   1.0114     0.9887    0.7015    1.4584


Concordance= 0.608  (se = 0.025 )
Likelihood ratio test= 22.92  on 2 df,   p=1e-05
Wald test            = 20.17  on 2 df,   p=4e-05
Score (logrank) test = 21.29  on 2 df,   p=2e-05
```
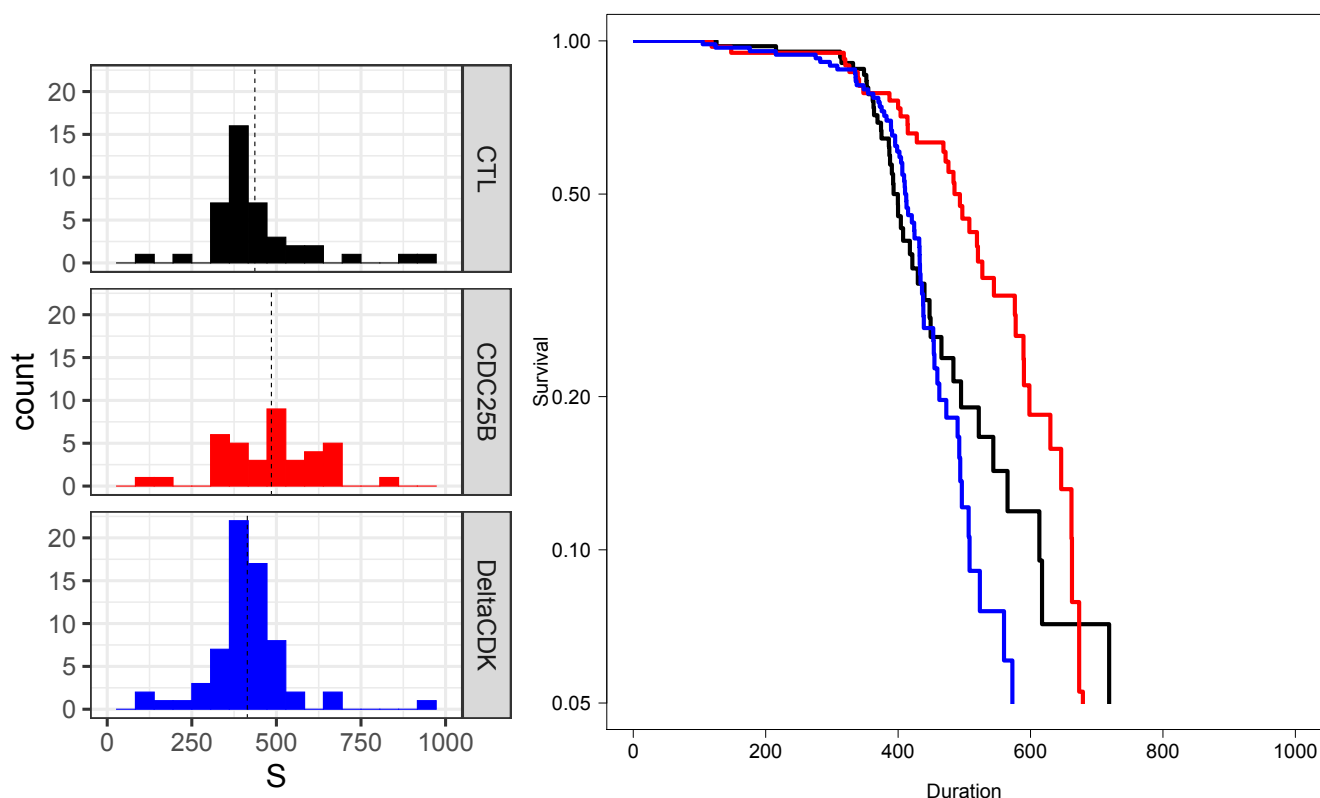
3.3 S


```
Call:
coxph(formula = Surv(dt$S, dt$sta) ~ dt$Condition)

  n= 146, number of events= 146
   (82 observations deleted due to missingness)


                      coef exp(coef) se(coef)       z Pr(>|z|)
dt$ConditionCDC25B   -0.4198    0.6572   0.2284 -1.838   0.0661 .
dt$ConditionDeltaCDK  0.1809    1.1983   0.2021  0.895   0.3706
---
Signif. codes:  0 '***' 0.001 '**' 0.01 '*' 0.05 '.' 0.1 ' ' 1


                   exp(coef) exp(-coef) lower .95 upper .95
dt$ConditionCDC25B    0.6572     1.5217    0.4200     1.028
dt$ConditionDeltaCDK  1.1983     0.8345    0.8065     1.781


Concordance= 0.559  (se = 0.027 )
Likelihood ratio test= 8.69  on 2 df,   p=0.01
Wald test            = 8.25  on 2 df,   p=0.02
Score (logrank) test = 8.43  on 2 df,   p=0.01
```
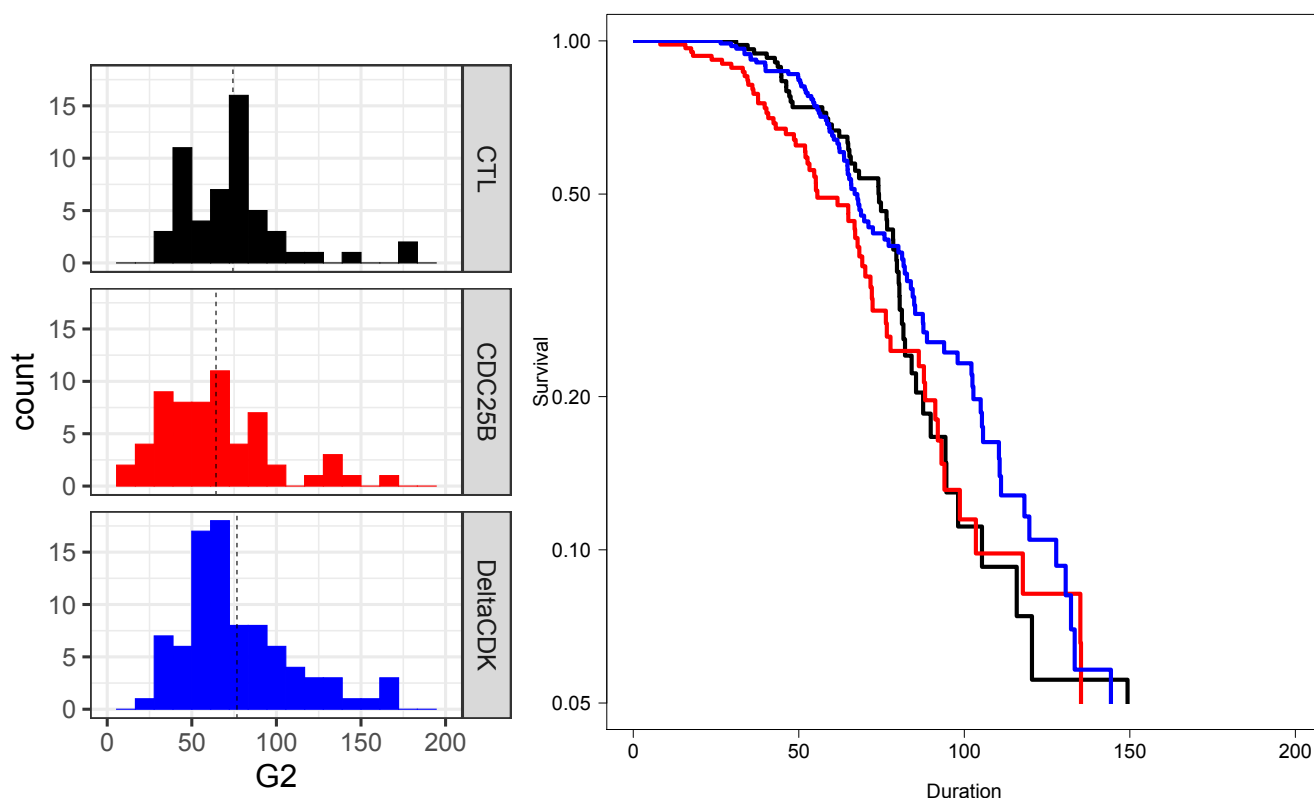
3.4 G2


```
Call:
coxph(formula = Surv(dt$G2, dt$sta) ~ dt$Condition)

  n= 201, number of events= 201
   (27 observations deleted due to missingness)


                         coef exp(coef) se(coef)       z Pr(>|z|)
dt$ConditionCDC25B    0.26603   1.30478  0.18989  1.401    0.161
dt$ConditionDeltaCDK -0.02233   0.97792  0.17675 -0.126    0.899

                  exp(coef) exp(-coef) lower .95 upper .95
dt$ConditionCDC25B    1.3048     0.7664    0.8993     1.893
dt$ConditionDeltaCDK  0.9779     1.0226    0.6916     1.383


Concordance= 0.55  (se = 0.023 )
Likelihood ratio test= 3.19  on 2 df,   p=0.2
Wald test            = 3.31  on 2 df,   p=0.2
Score (logrank) test = 3.33  on 2 df,   p=0.2
```
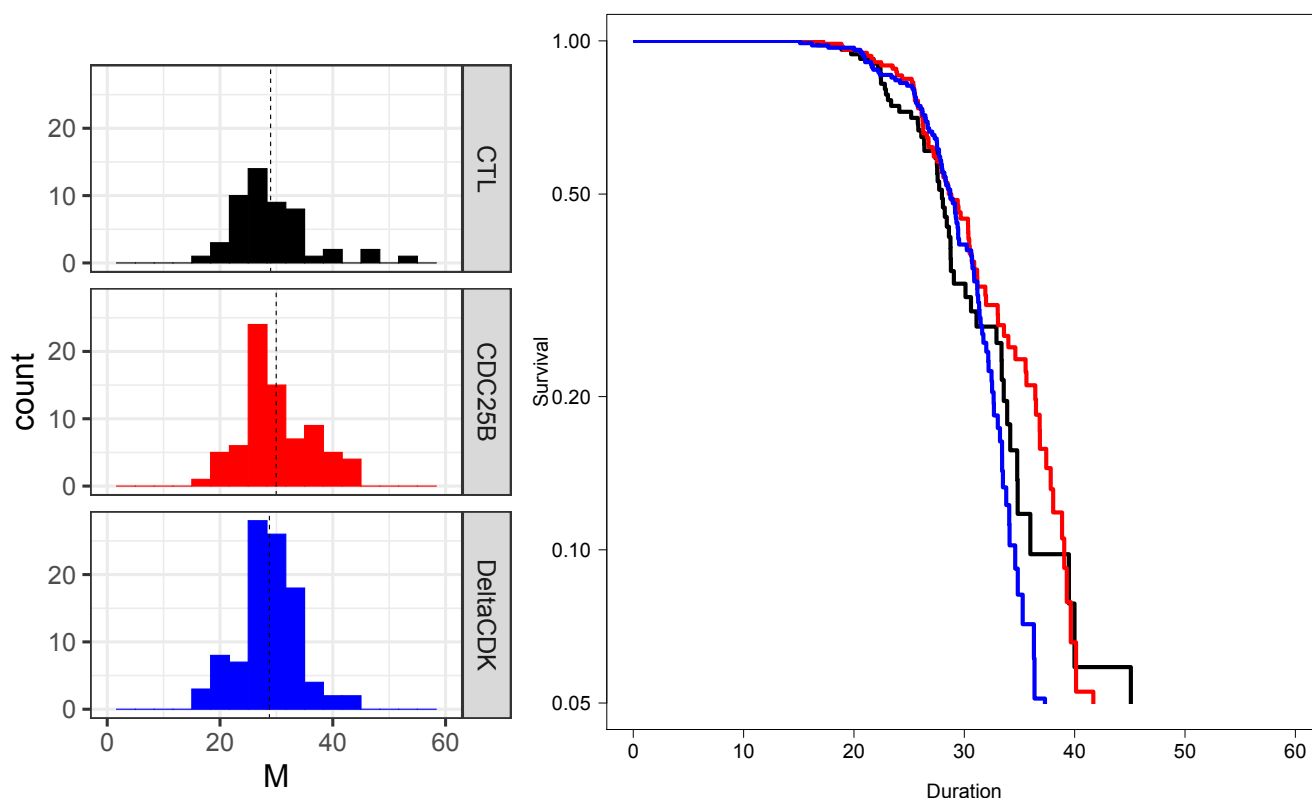
3.5 M


```
Call:
coxph(formula = Surv(dt$M, dt$sta) ~ dt$Condition)

  n= 225, number of events= 225
   (3 observations deleted due to missingness)


                     coef exp(coef) se(coef)      z Pr(>|z|)
dt$ConditionCDC25B  -0.07976   0.92334  0.18570 -0.430    0.668
dt$ConditionDeltaCDK 0.13998   1.15025  0.17888  0.783    0.434


                  exp(coef) exp(-coef) lower .95 upper .95
dt$ConditionCDC25B    0.9233    1.0830    0.6416    1.329
dt$ConditionDeltaCDK  1.1502    0.8694    0.8101    1.633


Concordance= 0.513  (se = 0.021 )
Likelihood ratio test= 2.07  on 2 df,   p=0.4
Wald test            = 2.07  on 2 df,   p=0.4
Score (logrank) test = 2.08  on 2 df,   p=0.4
```